

Discrete Robotic Construction

by

William Kai Langford

B.S., Tufts University (2012)

M.S., Massachusetts Institute of Technology (2014)

Submitted to the Program in Media Arts and Sciences,
School of Architecture and Planning
in partial fulfillment of the requirements for the degree of

Doctor of Philosophy

at the

MASSACHUSETTS INSTITUTE OF TECHNOLOGY

September 2019

© Massachusetts Institute of Technology 2019. All rights reserved.

Author
Program in Media Arts and Sciences,
School of Architecture and Planning
August 9, 2019

Certified by
Neil Gershenfeld
Director, MIT Center for Bits and Atoms
Thesis Supervisor

Accepted by
Tod Machover
Academic Head, Program in Media Arts and Sciences

Discrete Robotic Construction

by

William Kai Langford

Submitted to the Program in Media Arts and Sciences,
School of Architecture and Planning
on August 9, 2019, in partial fulfillment of the
requirements for the degree of
Doctor of Philosophy

Abstract

Robots, which require the integration of a wide variety of mechanical and electrical functionality, are seldom built in a single process, but are instead assembled from parts created using a variety of different processes. While fabrication has advanced significantly to enable the routine fabrication of complex and precise objects from computer designs, the assembly processes used to integrate these parts are still largely manual and are notoriously difficult to automate. Recent research in digital fabrication has looked for ways to avoid assembly altogether by manufacturing integrated devices in a single process but has often struggled to integrate more than a few materials or functionalities. Instead of avoiding assembly, this work embraces it. Inspired by the universality of amino acids that are the basis of molecular biology, I demonstrate an interchangeable set of building blocks that enable the construction of a wide variety of robotic capabilities, including machines that can assemble themselves. In this thesis I introduce a discrete approach to robotic construction that enables the fabrication of structure, mechanism, actuation, circuitry, and computation in a single process through the assembly of a small set of building blocks. This work is based on discretely assembled “digital” materials, in which parts are reversibly joined with a discrete set of relative positions and orientations, allowing for global geometries to be determined from local constraints, assembly errors to be detected and corrected, heterogeneous materials to be joined, and disassembly and reuse rather than disposal. This approach simplifies the fabrication of integrated electromechanical machines and points to the possibility of building technology that is able to grow (exponential self-assembly) and self-repair. Furthermore, this approach discretizes robotic systems at a finer granularity than prior work in modular robotics, offering benefits including the flexibility to integrate heterogeneous functions, agility to rapidly construct and modify designs, and incremental extensibility in both system size and performance. These benefits help lower barriers in the rapid prototyping of electromechanical machines, make designs more reusable by providing a physical representation that facilitates design automation and abstraction, and enable machines that are more integrated than would be practical with alternative methods.

Thesis Supervisor: Neil Gershenfeld

Title: Director, MIT Center for Bits and Atoms

Discrete Robotic Construction

by

William Kai Langford

This dissertation/thesis has been reviewed and approved by the following committee members

Sangbae Kim

Associate Professor of Mechanical Engineering
Massachusetts Institute of Technology

Discrete Robotic Construction

by

William Kai Langford

This dissertation/thesis has been reviewed and approved by the following committee members

Jennifer Lewis.....

Hansjorg Wyss Professor of Biologically Inspired Engineering
Harvard University

Acknowledgements

I'd like to acknowledge of the people who helped and supported me in this work. I wouldn't have been able to do it without you all.

Thank you to my committee members – Sangbae Kim and Jennifer Lewis – for taking time out of your very busy schedules to meet with me and to help me think through outcomes of this work beyond CBA's research roadmap.

I'd like to thank my advisor, Neil Gershenfeld. I certainly could not have done this work anywhere else. You're unwavering vision for the work we do is inspiring. Thank you for showing me a new way to look at the world. I'm certain that I will never again have access to quite the same level of resources again. Being able to design something in the morning, go to the shop in the afternoon, run jobs on the wire-EDM, precision CNC mill, and multiple 3D printers (all simultaneously), and then have a first prototype by dinner is a very special kind of power that I know I'll miss.

However, the tools are not nearly CBA's greatest feature. It is it's people. In the seven years that I've been here I've made great friends and had the opportunity to work with amazing collaborators.

I first want to thank the CBA staff – Joe, James, Kara, Jamie, John, Tom, and Ryan – not just for their support in managing projects, putting in orders, and doing all the behind-the-scenes work that makes our research work possible, but also for getting lunch, hanging out, and creating a sense of community.

I'd like to thank all of the CBA students – Sam, Prashant, Ben, Amanda, Grace, Jake, Sara, Erik, Amira, Filippas, Patricia, Noah, James, Nadya, Eric, Matt C., Matt K., and Kenny. I've learned so much just from being around you all for these years. Sam, in particular, thanks for our coffee-talks and whiteboard sessions.

I'd like to thank my friends and collaborators outside of CBA – Carlos, Jifei, Lining, Guillermo, and Sophia. In particular, Carlos, thank you for always making sure my priorities are straight with our weekly call (even when I'm "too stressed").

Thank you Sherry and Neil for taking me on Fablab trips all over the world. It's an amazing privilege to be able to travel to some of the coolest places in the world to help teach people about digital fabrication.

Thank you to the CBA UROPs – Uyen, Soma, Jason, Steven – for helping me experiment with ideas and being guinea pigs for my developing leadership and mentoring skills.

Thank you to my family – Mom, Dad, Ben, Grandma, and Oscar – for making me who I am today.

Thank you Iris for always believing in me and encouraging me to be my best self.

Contents

1	Introduction	15
1.1	Motivation	15
1.2	Background	18
1.2.1	On-Demand Fabrication of Robotic Systems	18
1.2.2	Self Replicating Machines	20
1.2.3	Biology	21
1.3	Approach	24
1.3.1	Implications	24
1.3.2	Goals and Metrics	25
2	Joints	27
2.1	Design Guidelines	27
2.2	Interlocking Press-Fit Slots	28
2.2.1	Electrical Characterization	29
2.3	Alternative Joint Systems	31
3	Structure	33
3.1	Lattice Structures	33
3.2	Digital Materials	34
3.3	A New Geometry	35
3.4	Sizing	36
3.5	Production	37
4	Mechanism	39
4.1	Compliant Mechanisms	39
4.2	Part Types	40
4.3	Modeling	40
4.3.1	Kinematics	40
4.3.2	Quantization of a continuous range of transmission ratios	42
4.3.3	Dynamics	44
4.4	Production Methods	45
4.5	Discussion	47

5	Actuation	51
5.1	Actuation at the millimeter scale	51
5.2	Electromagnetic Lorentz Force Actuators	53
5.2.1	Modeling	54
5.2.2	Experimental Characterization	57
5.2.3	Production	60
5.2.4	Discussion	61
6	Walking Motor	63
6.1	Design	63
6.2	Characterization	63
6.2.1	Speed and Repeatability	64
6.2.2	Force Additivity	66
6.3	Discussion	67
7	Walkers	69
7.1	Electropermanent Feet	69
7.2	MOTILE – Modular Tiny Locomotion Element	71
7.3	Discussion	73
8	Positioning and Manipulation	75
8.1	Positioning	75
8.2	Manipulation	75
8.3	Discussion	76
9	Circuitry	79
9.1	Background	79
9.2	Routing	80
9.3	Logic	82
9.4	Control	84
9.4.1	Control in struts	84
9.4.2	Control between struts	84
9.4.3	Redefining struts for greater routing density	86
9.4.4	Tiles – Decoupling mechanical and electrical routing	87
9.5	Production Methods	88
9.6	Discussion	91
10	Automation	93
10.1	Electronic Digital Material Stapler Assembler	93
10.2	Design Overview	93
10.2.1	Detailed Design	94
10.2.2	Workflow and Characterization	94
10.3	FABBR – Functional Assembler of Building Block Robots	96
10.3.1	Design Overview	96
10.3.2	Detailed Design	97

10.3.3	Characterization	99
10.3.4	Extensions	101
10.4	Assembling Assemblers	102
10.4.1	Current Limitations	105
11	Scaling	107
11.1	Part Production	107
11.2	Actuation	108
11.3	Assembly	110
12	Modeling	113
12.1	Modeling Approaches	113
12.2	Optimization Approaches	114
12.3	Compliant Mechanism Simulation and Optimization	114
13	Applications and Extensions	117
13.1	Discrete Integrated Circuit Electronics (DICE)	117
13.2	Relaxing Constraints	119
14	Conclusion	123
A	Lessons Learned	125

Chapter 1

Introduction

1.1 Motivation

The design and fabrication of robots today can be expensive, time consuming, and inflexible. It often involves the integration of a wide variety of unique parts, each of which may be made using separate and unrelated processes. This assembly and integration step often represents the bottleneck in the time and flexibility in the development of a new robotic system [1] [2]. Achieving high performance often means designing from the ground up and fabricating a bespoke, application specific robot.

Researchers have looked at modularity as a way to increase the flexibility in the configuration of new robotic systems. By abstracting robotic capabilities to a small number of unique modules, a new robotic system can be configured and reconfigured to suit a particular task through the (relatively) simple arrangement of the modular parts. These modular parts, however, often end up needing to integrate actuation, sensing, communication, computation, and structure, and do so in a physically small volume. This results in modules that are expensive and difficult to manufacture, and ultimately limits the performance of the resulting robots made this way [3]. In doing so, the difficulty to develop a new robotic system has been reduced but at the expense of a simultaneous reduction in performance (Figure 1-1).

As a result, recent research in digital fabrication has looked to avoid the assembly and integration step altogether by fabricating devices in a single monolithic process. This includes processes that assemble intricate mechanisms through the lamination of various pre-machined layers [8], the integration of hydraulic channels in additively manufactured robot limbs [9], and even the direct printing of entirely soft robots [10]. However, each of these processes still has inherent limitations including the kinds of materials it can work with, the dimensionality of the end-product (2D vs 2.5D vs 3D), and the dynamic range it can support (maximum size per minimum feature size). As a result, I argue that no one process will be able to span the full range of desired robotic capabilities.

Biology offers an alternative inspiration. Rather than trying to integrate all of the desired functionality in a common process, it builds from a standardized set of building blocks that share a common interface. All of life is assembled from 20 standardized building blocks, amino acids (Figure 1-2). These building blocks are assembled one part at a time by a machine, the ribosome, which itself is made from the same building blocks. These biological assemblies are truly complex and integrated. They sense, actuate, move, flex, and act as structure and do so at a resolution

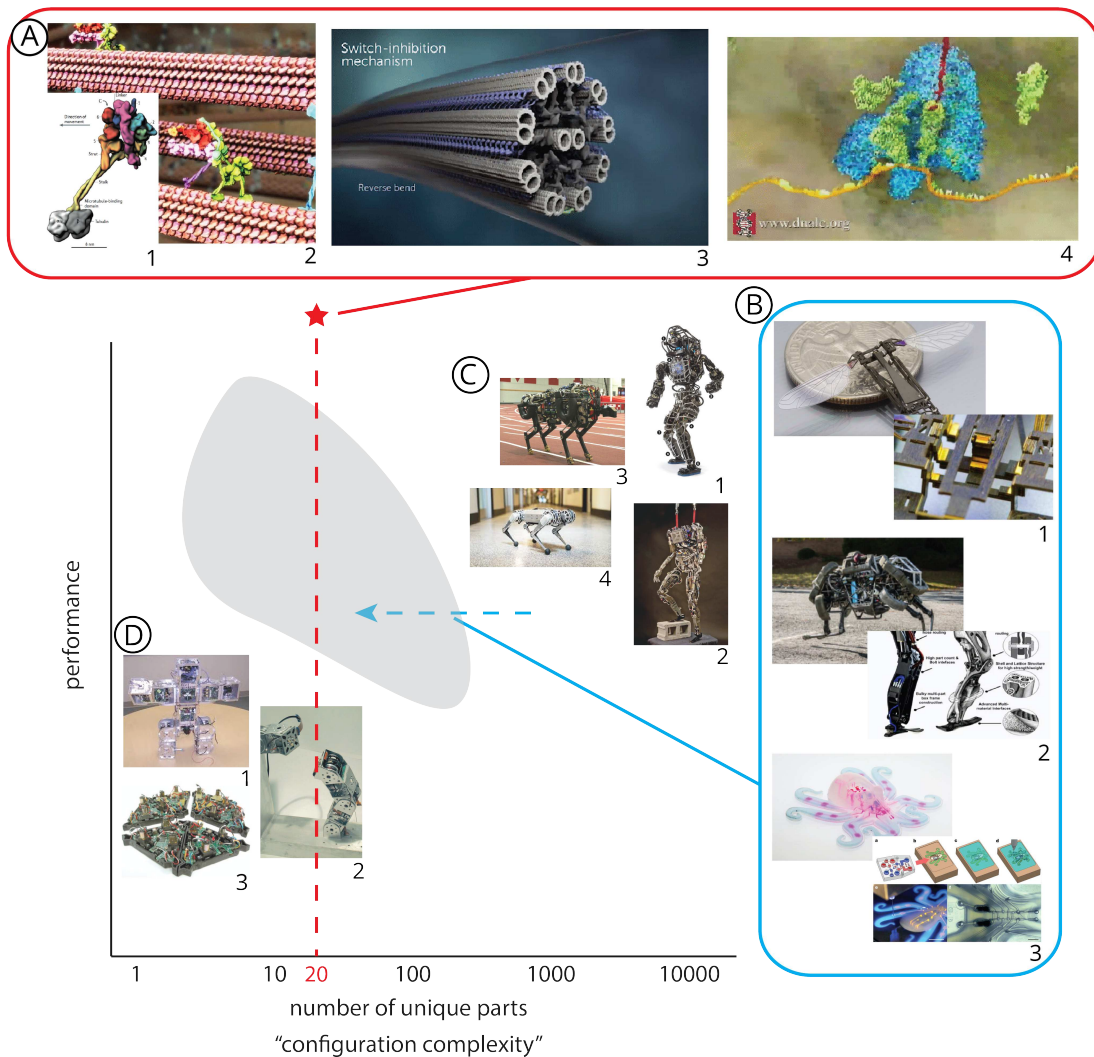


Figure 1-1: The robot design and fabrication space in terms of "configuration complexity" (number of unique parts) vs performance. Highly performant robots (C) are often bespoke and require ground-up design and development (1-4) [4] [5] [6] [7]. Modular robots (D) tend to tradeoff performance for versatility (1-3) [3]. Digital fabrication research (B) has looked for ways to avoid assembly by integrating functionality in monolithic processes (1-3) [8] [9] [10]. Biology (A) offers an inspiring alternative as it assembles all of life from (essentially) 20 building block parts (amino acids) (1-4) [11] [12] [13] [14].

and performance that far exceeds what we are currently capable of producing with human-made technology [15] [16].

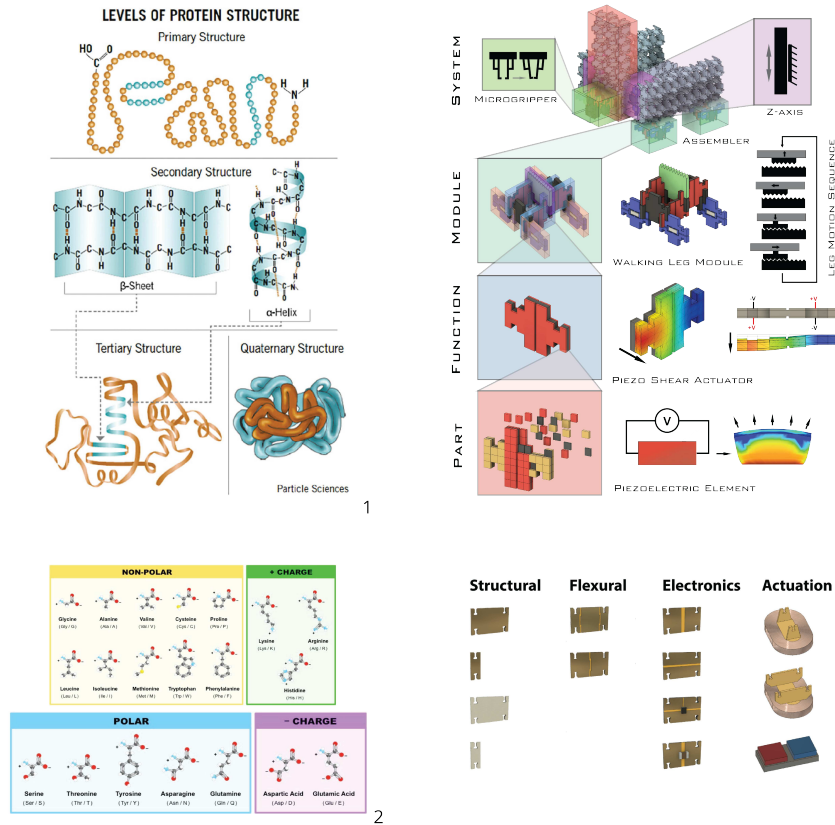


Figure 1-2: The twenty amino acids that enable the assembly of biological systems do so through levels of hierarchy: primary, secondary, tertiary, and quaternary structure. The “engineering amino acids” should likely exhibit a similar structural hierarchy. Individual bulk-material building blocks assemble functional parts, functional parts assemble into modules, and modules then assemble into systems (1-2) [16] [17].

This leads to the question that prompted the work developed in this thesis: **Can we develop a set of simple, functional parts that enable the assembly of a wide range of integrated machines?** In this thesis I introduce a discrete approach to robotic construction that enables the fabrication of structure, mechanism, actuation, circuitry, and computation in a single process through the assembly of a small set of building blocks. This approach takes inspiration from the amino acid building blocks that are the basis of molecular biology and offers benefits in the integration of heterogeneous functionality, agility in creating and modifying designs, and points towards the capability for technology to grow (self-assemble) and self-repair. Rather than avoiding assembly in pursuit of integrated manufacturing, this approach embraces it, and demonstrates that the interchangeability of building blocks enables the assembly of a wide variety of capabilities from a small set of part types.

The approach I introduce is based on prior work in discretely assembled “digital” material systems. Digital materials are based on a discrete set of parts, which are reversibly joined with a discrete set

of relative positions and orientations [18]. These properties allow global geometries to be determined from local constraints, assembly errors to be detected and corrected, heterogeneous materials to be joined, and disassembly and reuse rather than disposal [19]. Digital materials have been used to produce the highest reported modulus ultralight materials [20], shape morphing structures with the use of rigid and flexural parts [21], as well as electronic structures with the addition of conductive and insulating parts [22] [23].

This approach builds systems with integrated structure, mechanisms, and actuation in a way that can be incrementally extended and modified. Standardizing the assembly interfaces between parts and simplifying the assembly process, to require just a single vertical motion, means the assembly process can more closely resemble a digital fabrication workflow and represents a significant step towards enabling on-demand fabrication of a wide-range of robotic systems.

1.2 Background

The approach introduced in this thesis works towards two active goals in the areas of digital fabrication and modular robotics: (1) on-demand fabrication of robotic systems and (2) self-replicating machines. Additionally, this approach takes inspiration from the way that biological system manufacture across scales (grow).

1.2.1 On-Demand Fabrication of Robotic Systems

The goal of simplifying the manufacturing of highly integrated machines and robots to enable on-demand fabrication of robotic systems has been explored from a number of different perspectives. These include folded and origami-based manufacturing methods, additive manufacturing and soft-robotics, as well as digital material assembly.

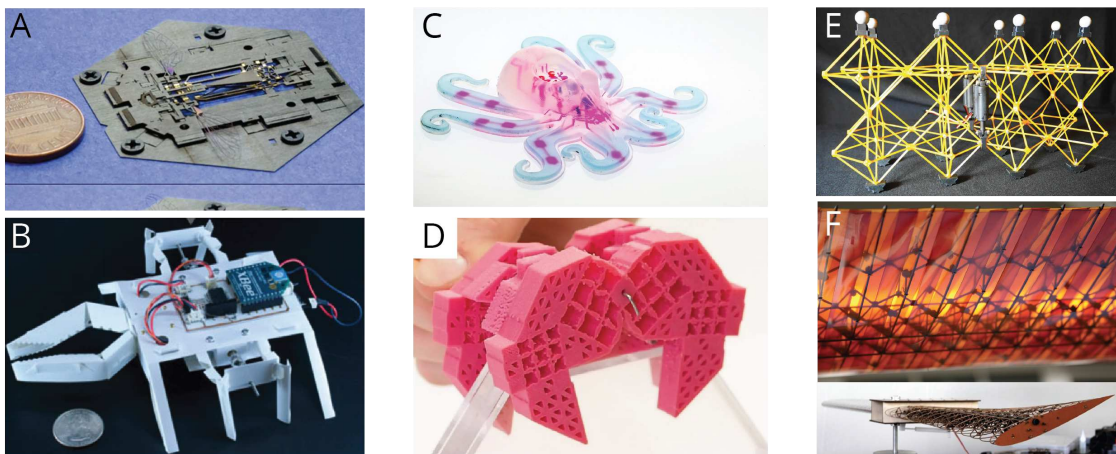


Figure 1-3: The goal of enabling on-demand robot fabrication has been approached by ways including: folding-based methods (A,B) [8] [24], soft robotics (C,D) [10] [25], and digital material (E,F) [26] [21].

Folding-Based Processes

Folding based processes look for ways to pattern functionality in a two-dimensional sheet and then fold to create a three-dimensional structure (Figure 1-3 A,B). These kinds of processes are well suited for on-demand robot fabrication because patterning and structuring two-dimensional sheets can be done quickly, precisely, and at a high resolution. These processes are often able to incorporate multiple materials to achieve various kinds of functionality within a single device. Whitney et al. demonstrated the assembly of complex mechanical linkages through the lamination of rigid and flexible layers [8]. Furthermore, an assembly scaffold, patterned along with the robot, was then used to coordinate the folding of the two-dimensionally patterned sheets into a three-dimensional robot, the Robobee. This approach has enabled the batch production of devices with a broad material set and a design flexibility that was previously inaccessible in millimeter-scale robotics. While these robots are still typically designed by hand, others have looked at the possibility of automating the design of folded robots [27]. The work of Onal et al. demonstrates how a library of design templates with parametric dimensions may be used to lower the barriers in the design and development of these robots [24]. Furthermore, these machines show the extent to which a single laser-cut shape can define complex three-dimensional body shapes and mechanisms.

While these folding processes are often able to incorporate both mechanical linkages and circuitry in a single process, actuation is typically integrated in a separate step. Onal et al., for example, attach off the shelf DC motors to the robot after it has been folded. In millimeter-scale laminate devices actuation often takes the form of a piezoelectric actuator that is made using a separate laminate process and assembled manually [28]. As these devices become more complex and integrate more functionality, the number of layers and process steps increases. Given the monolithic nature of these devices, an error in any single layer can ruin a whole device. As such, it is common for the designer to invest significant time upfront in the design of the device to ensure there are no errors, limiting the resulting turn-time and agility of the fabrication approach [27]. As a result, while monolithic designs could ultimately enable on-demand robot fabrication, practically, it often makes more sense to split a complex design into subsystems which are laminated and then integrated separately [28].

Additive Manufacturing and Soft Robotics

Recent efforts to integrate actuation into 3D printing workflows have seen promise in the direct printing of soft robots and actuators (Figure 1-3 C,D). By structuring geometry, hydraulic or pneumatic forces can be converted into motion [29] [30]. These processes are able to produce devices with useful forces and motions in a nearly monolithic process. While these robots have been traditionally made with molding processes, more recent research has demonstrated the possibility of directly printing these kinds of soft robots and machines [10] [25]. These soft machines have a range of useful applications and are often applicable in scenarios that are not well served by traditional “hard” robots.

While these processes greatly extend the capabilities of robotic fabrication, they are still limited in the kinds of materials and functionalities that they can integrate. The material set is often limited by the requirements of the deposition processes, which constrains the range of functionality and, as a result, the potential applications. Furthermore, the scarcity and properties of compatible soft-materials limits the available functionality below the millimeter scale [31] [32].

Other research has looked at ways to directly print hydraulic actuators for use in high-performance robots such as Boston Dynamic’s Atlas robot [9]. These actuators are able to unify what used to be several separate components. But beyond hydraulic actuators, this process doesn’t likely scale to include other kinds of functionality like electronics or large displacement compliant joints.

Digital Materials

Discretely assembled “digital” material systems are another avenue that has been explored towards the goal of enabling on-demand robot fabrication. Digital materials are a discrete set of parts, which are reversibly joined with a discrete set of relative positions and orientations [18]. These properties allow global geometries to be determined from local constraints, assembly errors to be detected and corrected, heterogeneous materials to be joined, and disassembly and reuse rather than disposal. The building block parts that compose a digital material can be produced using a range of different processes and in a range of different materials. This enables the integration of diverse functionalities including structure [20], mechanisms [21], and electronics [22] [23] within a single assembly framework.

The prospect of using digital materials to enable on-demand robot fabrication has been explored in theory [33] [34] but physical implementations have largely relied on either slow global thermal actuation [33] or on off-the-shelf actuation components [23]. In a more recent study, Cramer et al. demonstrated very simple locomoting robots made through the actuation of deformation modes of a discretely assembled lattice using commercially available linear servo motors [26] (Figure 1-3 E).

1.2.2 Self Replicating Machines

The idea that modular building blocks can be used to assemble self-replicating systems is not a new one and has been explored computationally since at least the 1940’s. At that time Von Neumann developed the concept of a universal constructor, built around a set of cellular automata rules, that can construct itself and pass on a blueprint for further self-replication [35]. For a number of reasons, Von Neumann’s concept is not particularly physically realistic. For example, blocks are not translated but rather destroyed at one location and created at another. However, others have built on Von Neumann’s original idea and developed versions of the universal constructor that are more physically-based [36]. These ideas are still very far from a physical embodiment but demonstrate that a self-replicating machine is kinematically feasible. Researchers as recently as 2016 have written papers entitled, “Are Self-Replicating Machines Feasible?” [37], clearly showing the disparity between theory and practice. This more recent research still concludes that self-replicating machines are feasible, but notes that there are a number of practical barriers that must be overcome first.

Modular Robotics

Work in the field of modular and reconfigurable robotics has looked to address the challenges of self-replication by simplifying the feedstock to a set a of modular building blocks [42] [43] [40]. These systems typically integrate actuation, controls, communications, and structural connections within modular units, which are then configured (and reconfigured) to suit a particular task. While these systems illustrate the universality of a small number of modular building blocks, the resulting modules are relatively complex, involve dense integration of the various functions, and tend to be

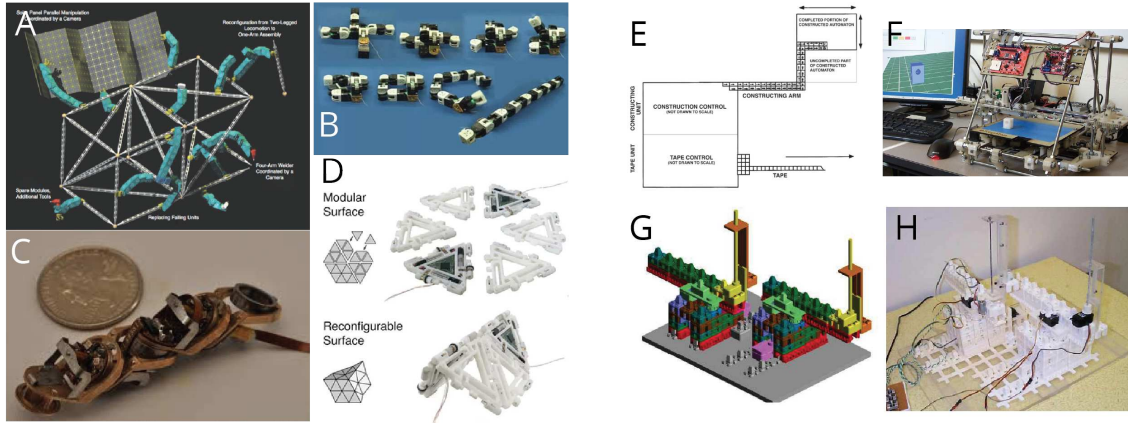


Figure 1-4: Modular robotic systems are configurable and capable of adapting to a variety of different applications. They may be used as manipulators to assemble truss structures [38]. Modular chain robots [39] [40] and surfaces [41] can be contorted and twisted to form a variety of shapes and structures.

expensive to fabricate in volume. As a result, they have typically found limited utility outside of the research lab.

In-Situ Resource Utilization (ISRU) Approaches

These self replicating machines are being pursued for a number of different applications, one of which is space exploration and development. The development of in-space manufacturing capabilities and modular robotics architectures are important steps towards self-replicating systems. Research in self-replicating hardware is in early stages and most prior work addresses high-level system design challenges including hierarchy and scale [44] as well as required ISRU capabilities and launch requirements for self-sustaining factories [45]. Other prior work has looked at lower-level implementation details and established methods of creating self-replicating systems with macroscale building blocks. Moses et al. built a universal constructor system, for example, using 18 part-types that is capable of assembling some of its own subsystems [46]. However, the parts have a high-degree of embedded complexity, including conventional actuators and processors, which limits the potential scalability of such a system.

1.2.3 Biology

Ribosomal Assembly (Growth)

Ribosomal assembly, or growth, is able to achieve a wide dynamic range between the size of the parts and the size of the assemblies because of error correcting processes during part assembly and because of its self-replicating machinery that enables an exponential ring-up in manufacturing capacity (ribosomes assemble ribosomes).

Amino acids are often referred to as the building blocks of life [15] and make up, when assembled as proteins, approximately 60% of the dry mass of mammalian cells. They are made up of a common backbone, which allow them to bond to form a string, and a side chain, which confers simple chemical, structural, or functional properties to the part such as hydrophobic/hydrophilic or basic/acidic.

These twenty standard L- α amino acids, each with unremarkable properties on their own, are the building blocks that enable the assembly of all biological machinery, including a machine that can make itself, the ribosome. Ribosomes assemble amino acids at relatively unremarkable rates, ranging from 0.6 Hz to 20 Hz [47], but each cell may contain upwards of 72,000 ribosomes (in fast growing *E. Coli*), representing one third of the cell's dry mass and a volumetric density of approximately 50,000 per cubic micrometer [15]. The tens of trillions (10^{13}) of cells in the human body, each containing, on average, a few billion proteins (10^9), which are themselves made up of a couple hundred amino acids (10^2), means we are made up of approximately 10^{26} parts [15]. In comparison, the largest dynamic range (minimum feature size to build area) of our most advanced manufacturing techniques is only about 10^{13} (Nanoscribe [48]). This kind of complexity is made possible in reasonable time-scales not because ribosomes are fast (they assemble at approximately 1 Hz), but because ribosomes can assemble ribosomes, enabling massively parallel assembly.

Beyond the ability of ribosomes to assemble ribosomes, another critical aspect in being able to span large dynamic ranges in a single process is error correction. Before the mRNA instruction set reaches the ribosome, it has already gone through multiple stages of error correction and proofreading through the transcription process. During and after translation of the mRNA into the peptide chain, another set of error correcting steps is taken to discard, degrade, and recycle incorrectly translated proteins. Transcription has been reported to have error rates on the order of 10^{-5} while translation error rates are an order of magnitude more, or 10^{-4} [49] [15] [50].

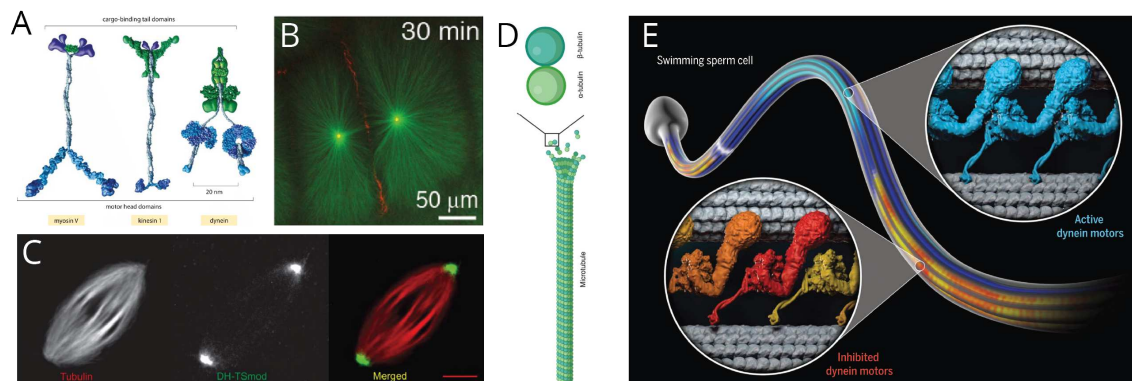


Figure 1-5: Biological machines exhibit modularity and reusability. The same motor proteins (A) [15] and microtubules (D) [51] that help organize the cell (B,C) [52] [53] are also used to actuate flagella mechanisms of swimming sperm (E) [13]

Amino acids enable the assembly of highly capable machines and behaviors. The proteins assembled from amino acids are present in a wide range of sizes but have an average length of approximately 400 amino acids in eukaryotic cells [15]. As the protein's primary structure is being formed through translation of mRNA by ribosomes, it folds into a three-dimensional structure based on hydrophobic/hydrophilic interactions, molecular chaperones, and environmental conditions such as pH. The structure of the protein exhibits hierarchy and its functionality and geometric motifs can be grouped into primary, secondary, tertiary, and quaternary levels [16]. These proteins are then used as building blocks for a wide variety of cellular mechanisms and behaviors including structure, elasticity, transport, and signaling [54]. Furthermore, as a result of assembling all of life from the

same twenty building blocks, biological assemblies end up having a great deal of modularity and reusability across a number of different applications. The same kinds of microtubules and motor proteins that organize cells and give them their structure are also used to actuate flagella to propel swimming organisms like sperm [13] (Figure 1-5).

Manufacturing Across Scales

Treating ribosomal assembly like a manufacturing process, it is possible to compare our existing manufacturing methods and see that all fall short of the precision, resolution, and complexity of biological assembly. In Figure 1-6 I present estimates of the resolution and throughput of ribosomal assembly in biological systems. These estimates should be viewed as establishing orders of magnitude rather than precise measured quantities. For each biological system I estimate the number of amino acids that compose all of the proteins that make up that specimen. For the three mammals presented (Mouse, Human, Blue Whale), I estimate amino acid content based on a protein fraction of their dry mass (60%) and assume a dry mass fraction (30%) of their total mass. I do the same for C. Elegans noting that the protein fraction is closer to 55% of their dry mass. HeLa cell, E. Coli, and Eukaryotic protein estimates are based on protein counts reported in literature combined with average protein length in Eukaryotes (400aa) [15]. In all of the above I assume that growth rate is linear with time, which will both overestimate and underestimate growth at certain development stages but therefore represents a reasonable average.

I do the same for manufacturing techniques including discrete assembly, additive manufacturing, and state of the art conventional assembly, estimating the effective number of resolvable elements and the throughput at which those elements can be assembled.

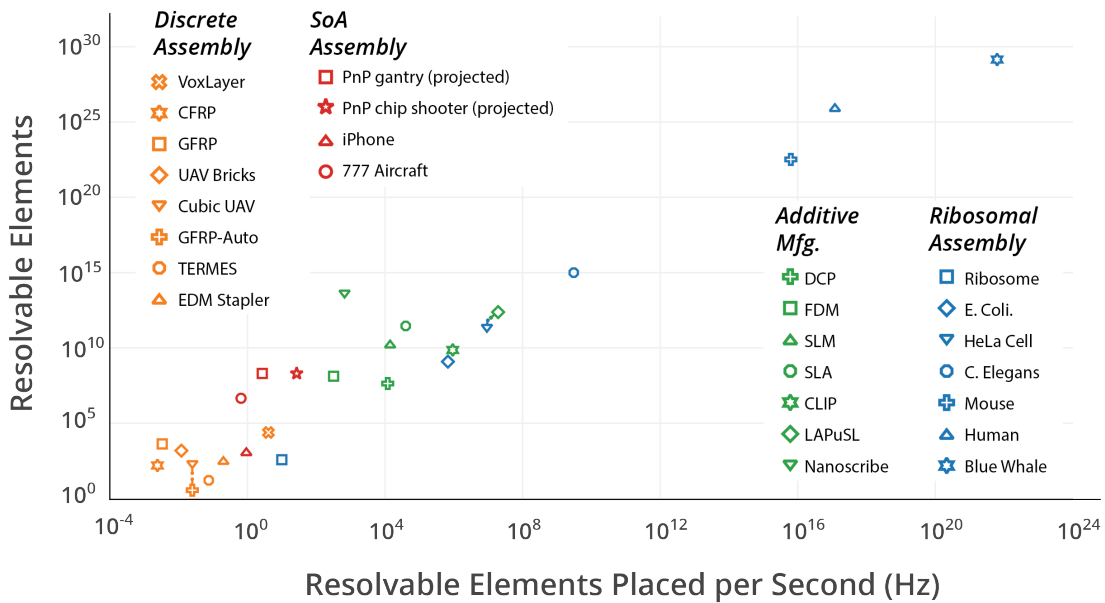


Figure 1-6: Manufacturing throughput vs dynamic range for across manufacturing processes. Biology's throughput scales with the size of the manufacturing problem and enables the fabrication of organisms with far more fabrication complexity than any state-of-the-art technological process.

From the plot, it's clear that the state of the art in digital fabrication roughly matches the

throughput and complexity of a human cell. Beyond that, there is no technological fabrication process that can extend into the space that biology occupies. We (humans) are made from on the order of 10^{26} amino acid parts. While our fabrication capabilities let us span from tens of nanometer silicon chips to hundreds of meter long aircraft, we do so in discontinuous processes with no shared representation. And it is the discontinuities in this approach that I argue largely limit the flexibility of manufacturing.

1.3 Approach

This thesis attempts to address the question: **can we develop a set of simple functional parts that enable the assembly of a wide variety of integrated machines?**

The hypothesis is that by standardizing the interfaces between parts, the assembly process can be treated like a digital fabrication process. Furthermore, by discretizing functionality at such a fine level, we can enable much tighter integration and coupling between functionality that is typically separate in conventionally made robotics. This merging of functionality represents a unified approach to robotic construction that could also help lower the barrier to things that are not yet possible, like machine self-replication.

In this thesis I focus on the development of capabilities necessary to build assemblers that can assemble assemblers. This application serves both as a case study for integrating various robotic functionalities within a machine, and represents the direction toward massively-parallel high-throughput assembly. In order to build assemblers that can assemble assemblers there are a number of capabilities that are needed and steps to achieve. The assembler will need to integrate structure, mechanism, actuation, circuitry, and computation. The following chapters will describe the design of the building block parts and how their arrangement enables the assembly of these various capabilities.

1.3.1 Implications

This work impacts the way in which robotic systems are designed and fabricated today and helps pave the way towards future goals such as high-resolution on-demand fabrication of robotic systems and self-replicating machinery. Specific implications of this work include:

- **Treating assembly like a digital fabrication process.** This work shows that by standardizing assembly interfaces, the assembly and configuration of functional systems can be treated like a digital fabrication process, enabling on-demand fabrication of robotic systems.
- **A unified approach to robotic construction enables a tighter coupling between structure, mechanism, actuation, circuitry, and computation.** By discretizing at a fine-grained functional level, capabilities that are typically distinct can be merged much more densely in this approach. Circuits can be routed through structural volumes, actuated degrees of freedom can be distributed rather than centralized, and computation and control elements can be spatially distributed closer to the components they drive.
- **A new way of digitally fabricating integrated machines and robots with a unmatched range of functionality.** Rather than trying to integrate multiple functionalities in

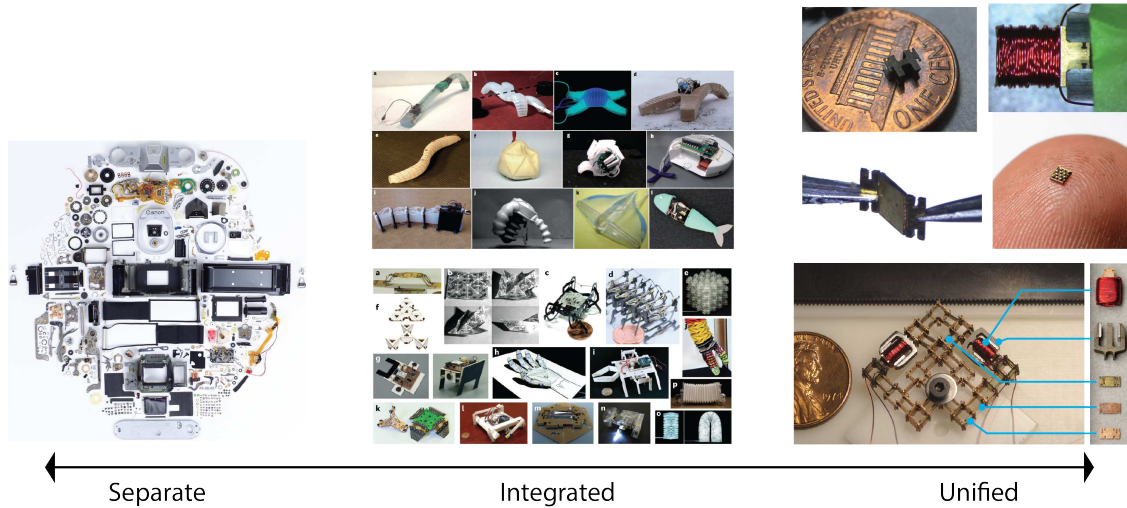


Figure 1-7: The approach explored in this work represents a unified approach to robotic construction. Conventional machines integrate diverse functionalities without any standardization and are often bottlenecked by boundaries between functionality. Rather than integrating the fabrication of functionality within a single process [55] [56], this approach enables the assembly and integration of wide variety of parts, each of which can be made using separate and dedicated processes. “Separate” image from [57].

a single process, this approach is able to achieve an unmatched range of integrated functionality through the integration of parts made in a wide range of different processes.

- **A viable way to close the fabrication complexity gap.** This approach helps lower barriers to assembling assemblers and provides a viable way to increase the resolution and complexity of technological systems through recursive assembly.

1.3.2 Goals and Metrics

This work is guided by the following metrics:

Complexity The aim of this work is to enable the assembly of relatively complex devices from relatively simple parts. For this assembly approach to be interesting, the dynamic range between the complexity of the parts and the whole should be larger than existing work in modular robotics and much closer to the dynamic range (minimum feature size to work envelope) of an additive manufacturing process.

Universality An additional aim of this work is to show how a small number of building blocks can be combined to form a large variety of assemblies. This metric discourages special-purpose parts and emphasizes finding part types that play a number of useful roles in a system.

Performance Finally, the assemblies fabricated using this process should be useful and competitive with existing techniques for on-demand robot fabrication. Power density, specific stiffness, and fabrication time are criteria that are particularly relevant to this work.

In the following chapters I will discuss the components of this assembly framework: starting with an individual structural joint, and demonstrating the assembly of structure, mechanism, and actuation. Following that, I will demonstrate the assembly of machines that integrate these capabilities. From there, I will discuss how circuitry and computation can be added to these assemblies, look at the automation and scaling of this work, and finally discuss future applications and promising results that are being explored.

Chapter 2

Joints

2.1 Design Guidelines

One of the most fundamental aspects of this work is the identification of interlocking joint systems that can be used to reliably and robustly join parts in this assembly framework. This is also one of the most challenging aspects of this work: finding functionally compelling joints that are simple and small enough to “disappear” in the structure. The assembly framework presented in this work does not presuppose any particular joint type but does seek a number of desirable traits:

- **The parts should interlock mechanically.** One of the fundamental takeaways in [58] was the observation that “To build strong structure from bricks, they should be interlocked. This gives the structure the strength of covalent bonding in at least some directions.”
- **The joints should function both as a mechanical connection and electrical connection.** This work hinges on the idea that parts can serve a dual purpose, providing structure as well as electronic functionality simultaneously.
- **The joints should be reversible.** They should be capable of being removed and rejoined a number of times before failing. Generally electronic connectors are rated to maintain a certain connection resistance over a certain number of cycles [59]. The challenge is in designing the connector to not wear significantly with use but still achieve a reliable contact that is able to circumvent insulating surface oxides [60].
- **The joints should be geometrically small and simple.** Because each part will feature at least two (and likely more) joints, the volumetric overhead of the joints adds up very quickly.
- **The joint should have some degree of error correction or self-aligning features.** Features that help guide the assembly reduce the precision required by the assembly machine (or person).
- **The joint should be easily “automatable.”** For example, joining with only a single degree-of-freedom motion and not requiring the coordination of multiple end-effectors.

2.2 Interlocking Press-Fit Slots

Based on these desirable traits, I selected a simple interlocking press-fit slot as the best suited joint system (Figure 2-1). The connection between parts is made with two orthogonal interlocking slots that are toleranced to be a tight fit with one another. This joint works well for this application first and foremost because it is geometrically small and simple. The geometry takes up a volume of $3t \times h/2.1 \times t$ given part thickness, t , and part height, h .

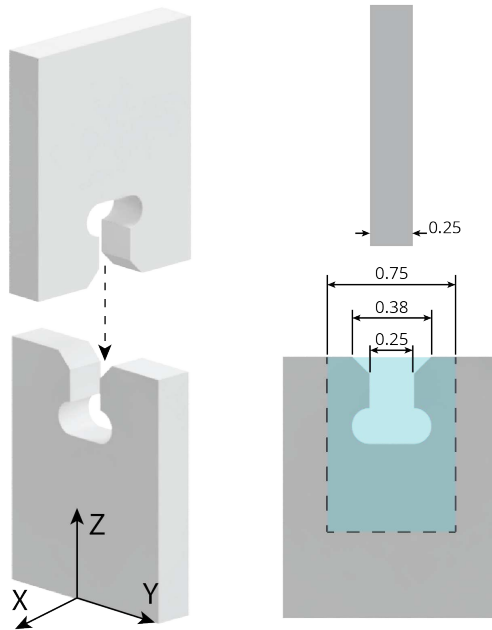


Figure 2-1: Interlocking Press-Fit Slot Design. The blue region indicates the area taken up by the single joint.

Cutouts at the bottom of the slots (often referred to as “dog-bone cutouts”) are required to ensure that the parts can fully seat. Without the cutouts the radiused cutting tool (in this case the 0.23 mm kerf width of the Wire-EDM) will leave a radius in the corner of the slot and not allow the full insertion of the parts.

The length of the slot is chosen to be as long as possible with respect to the part geometry. In this case that length is slightly less than one quarter of the part-height, h . The length of the slot provides rigidity against torques about the X and Y axes. Rigidity against torques in the Z-axis is improved with an increase in the thickness of the parts.

The joints feature chamfers on the edge of the part geometry to aid in the relative alignment between mating parts. The chamfers are dimensioned to accommodate translational errors in X or Y assembly axes of up to $\pm 190 \mu\text{m}$.

The force required to insert a part scales with the number of simultaneous interlocking interfaces. For the parts used in this work, which are $250 \mu\text{m}$ thick and made of phosphor bronze, approximately 15 N of force is required per joint interface to insert (Figure 2-2). Because of the symmetry in the interlocking slots, the joint requires approximately the same amount of force to remove as it does to attach. This means these joints can resist tensile forces up to this insertion force.

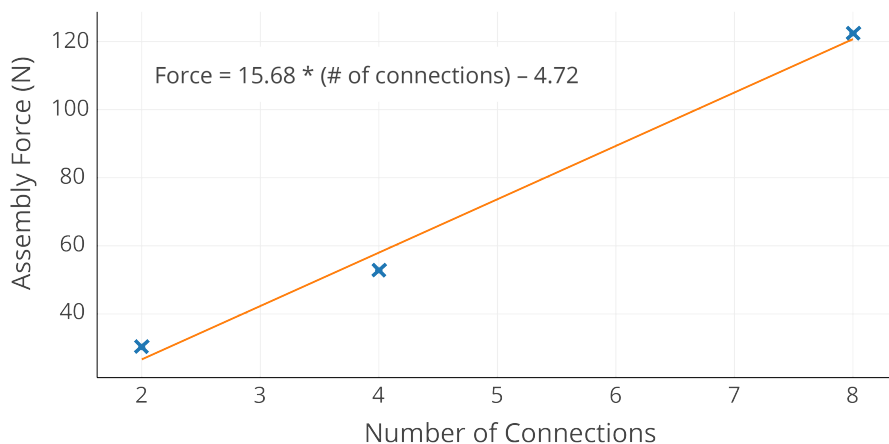


Figure 2-2: Assembly force is proportional to the number of simultaneous joints being made (15.7 N per joint).

2.2.1 Electrical Characterization

In my Master’s thesis I characterized the electrical conductivity of these kinds of press-fit joints [61] (Figure 2-3). I’m including a summary here for completeness and convenience.

The joints are reversible meaning that the parts can be joined and unjoined a number of times while still maintaining a low contact resistance. To measure this, I constructed a machine that can join and un-join the parts rapidly and measure the resistance across the joint using a sensitive four-wire measurement. In their joined state, the parts are preloaded with a constant force spring. What I found is that the contact resistance is initially somewhat variable and then settles after a few cycles to a low ($\approx 1 \text{ m}\Omega$) contact resistance.

Load cycling of a sample containing many joints led to an overall increase in conductivity. An electron micrograph of the surface revealed the likely cause of this conductivity increase was the flattening of surface asperities, effectively increasing the contact area.

Surface Preparation

Surface quality and preparation plays an important role in the development of good electrical contacts. It’s common practice in the design and manufacturing of electrical contacts to plate the contacts with metals that form good electrical contacts. These metals are often soft (have low hardness), have high conductivity, and do not form hard oxide layers.

I tested an assembled sample before and after copper electroplating to determine its impact on the electrical conductivity of the sample. The assembled sample is composed of two nodes and three struts. The sample measures $20 \text{ m}\Omega$ using a 4-wire resistance measurement (measuring from outer strut to outer strut). This resistance is composed of two components: bulk resistivity of the bronze parts and the contact resistances of the joints. I can very roughly approximate the resistance due to the bulk resistivity of the parts by integrating the resistivity over the volume of the parts with the equation: $R = \rho L/A$. Based on this, I should expect the contribution of the bulk resistivity to be approximately $1 \text{ m}\Omega$, much less than the $20 \text{ m}\Omega$ that I measured. This indicates that, unsurprisingly,

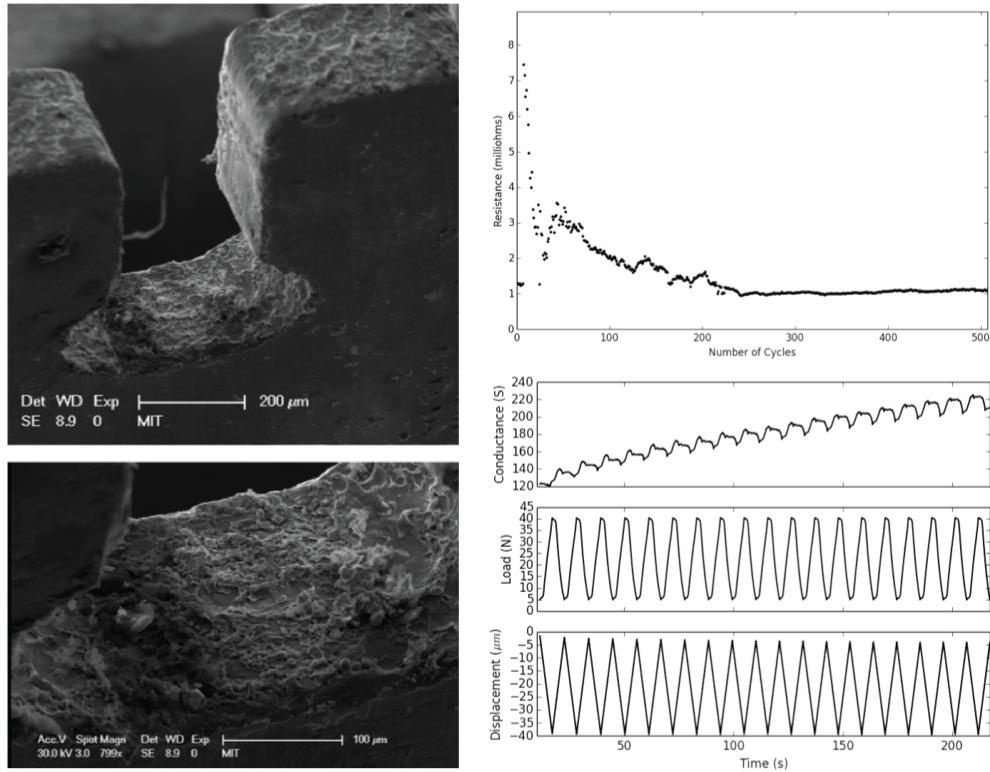


Figure 2-3: (Left) A scanning electron micrograph of an interlocking slot after having been used. Flattening of surface asperities is visible on the side of the slot walls. (Right-Top) The joint is reversible and has a $1 \text{ m}\Omega$ contact resistance even after 500 cycles. (Right-Bottom) Load cycling a structure composed of joints works to increase the conductivity of the bulk specimen.

the contact resistances contributes significantly to the resistance of the sample.

To account for the individual contact resistances within the sample it's important to have an idea of which resistances are in parallel and which are in series. Imagining the path of an electron through the the sample, I constructed an equivalent circuit to determine how the overall resistance is summed from the individual contact types (strut-node and node-node).

To determine the contribution of contact resistance on the overall resistance, I electroplated the specimen with copper (10 minutes at 200 mA). The idea being that the thin layer of extra copper has a negligible effect on the bulk resistivity but bridges the small gaps at the joints between parts, drastically reducing contact resistance. In fact, after electroplating, the resistance across the structure measures $1 \text{ m}\Omega (\pm 1 \text{ m}\Omega)$.

Using electroplating to post-process assemblies is potentially possible but not ideal since it does not align well with the idea that discrete assembly can be a digital fabrication workflow. Instead, it is possible to just electroplate node parts prior to assembly and achieve many of the same benefits. Electroplating just the nodes (for 12 minutes at 50 mA) reduces the resistance of the assembled test structure to $1.5 \text{ m}\Omega (\pm 1 \text{ m}\Omega)$, roughly same as the fully electroplated sample.

2.3 Alternative Joint Systems

While I selected the interlocking slot joint system as the most suitable to develop the functionality that I sought in this assembly framework, other joint types could certainly be worth exploring in more depth. Here, I'll give a cursory overview of some of the other joint types I've considered and their relative merits.

“Snap-lock” This joint is very similar to the press-fit slot but includes cutouts on either side of the slot to allow for the creation of flexural “snap-lock” features. This joint system allows for the possibility of tuning the insertion and removal force separately, potentially enabling a very low force insertion but high force removal. This joint suffers two primary downsides. For one, the cutouts on either side of the slot increase the size of the joint, certainly increasing the width of the joint by more than four times the minimum feature size of the manufacturing process (since a slot needs to be cut on either side of the flexure). For parts already produced at the minimum feature size of a process (where $\delta_{kerf} \approx t$), this increases the width of the joint by more than 2 times ($3t + 4\delta_{kerf} \approx 7t, 7/3 = 2.33$). The second major downside is that these flexural cutouts greatly reduce the torsional stiffness of the joint. While it may be possible to include geometric features that help address this concern, they will certainly increase the size of the joint greatly or else negate the potentially low insertion force.

Directional Locking Features Joints don't necessarily have to be made in a single motion, but can leverage a sequence of motions to insert and lock a part in place. This could be done, for example, with parts that slide in place (in the plane of the build front) and then are locked in place by a keystone element on the subsequent layer [62]. This kind of joint is attractive because it decouples assembly force from the ultimate strength of the joint. It is also a reversible joint; the assembly just needs to be disassembled in the right order to extract one part at a time. Another variant of this joint type uses micro-structured features (e.g. velcro) in order to attach parts in a controllable way [63].

Clip This kind of joint involves features for alignment and relative positioning (like loose interlocking slots) and an orthogonal clip that binds the two parts together. These have been shown to be capable of achieving high performance material properties at relatively small scales (≈ 5 mm) [64]. A main advantage of this method is the decoupling of the force required for assembly from the ultimate joint strength because the clip can be designed to be inserted with very little force in the orthogonal direction but exhibit high strength otherwise. The challenge with this joining method is two fold: the size of the joint area can very easily increase dramatically with the introduction of this orthogonal clip and the clip itself represents an extra (often very small) part that needs to be picked up and manipulated, often greatly complicating assembly.

Nut and Bolt Nuts and bolts represent another way to join parts. The main advantage of this approach is that it is capable of making very strong joints [65]. The screw mechanism represents a mechanical advantage that transforms the relatively light installation torque into a large compressive force between the parts. While it has been shown that automated assembly of nut and bolt joints is possible ([66]), it is greatly complicated by the need to manipulate multiple small parts and often

necessitates complex toolheads or multiple end-effectors. This joint method is limited in its ability to scale down in size as the smallest commercially available nuts and bolts tend to be no smaller than 0.86mm (#000-120).

Adhesive Adhesive joints usually take the form of a liquid glue or tape. Liquid glues have the advantage of not requiring any assembly force and are able to join a wide range of different materials including plastics and metals. But they often need time to cure. Dispensing and applying liquid adhesives can be a challenge to do precisely at small small scales but has been shown to be possible, at least with some part geometries (e.g. [67]). For this reason, adhesive tapes may be a more attractive solution. Pressure sensitive adhesives require large assembly forces and may not provide the desired joint strength. B-staged thermoset adhesive tapes can provide a much larger joint strength but require a high temperature (200 °C) and long duration (\approx 2hrs) post-processing step [68]. Adhesives are less well suited for making conductive joints. While conductive epoxies, which include conductive fillers, can be used, they greatly limit the available options. Conductive Z-axis tape, which is only conductive through its thickness, may be used for the assembly of higher density electronic interconnect but suffers from the same problems as pressure sensitive adhesive, namely large assembly forces and low resulting strength [69].

Solder Solder is a joint method that's potentially capable of achieving high strength and high conductivity while still enabling disassembly. It has been used in modular robotics and controlled with embedded resistive heaters to activate and deactivate the joint [70]. It is also capable of scaling to relatively small sizes as it has been used with parts as small as 3 mm on a side [71]. However, solder requires the presence of flux to properly wet contact points and because this flux is often corrosive and in liquid form, it would likely need to be applied very soon before part placement and attachment, and may need a post-processing step to remove any excess flux. To activate the joint requires the application of heat. While low temperature solders exist with processing temperatures as low as 138 °C, most require upwards of 200 °C, which limits the materials that can be used in the assembly or means that the heat needs to be very locally delivered (e.g. with a hot-tip, laser, or focused hot-air).

Welded There are a number of welding methods that may be used to join parts but I will focus on two: resistance welding and ultrasonic welding. **Resistance welding** is potentially attractive for its simplicity. The part to be attached to the assembly is positioned in place, vertical pressure is applied to it, and then a current is run through the connector interface, locally melting the material and irreversibly joining the part to the assembly. Rather than interlocking slots, the parts may be designed with geometries that create current restrictions (like raised projections) to control where the weld energy is channeled [72]. The downside of this method is that it requires the parts to have conductive interfaces and possibly even requires the parts to be fully metallic depending on the locality of the melt zone and the degree of control in administering the current. **Ultrasonic welding** functions in a similar way but joins parts through melting generated by friction caused by ultrasonic vibrations applied to the interface between parts. While this technique is capable of working with both plastics and metals, it is not capable of working with both simultaneously and so restricts the joints to either plastic-plastic or metal-metal.

Chapter 3

Structure

3.1 Lattice Structures

Recent advances in digital fabrication such as additive manufacturing have spurred interest in the study of architected and micro-structured materials, especially sparse lightweight lattice structures. While trusses and space-frames are often used in large scale structures such as bridges and buildings, their incorporation into smaller-scale structures and assemblies has been enabled by the ability to more precisely and economically pattern material in arbitrary ways. In particular, recent work has shown the possibility of printing lattices to build ultralight and stiff structures at micro-scales [73] and a number of commercial offerings have recently appeared to enable the automatic generation of complex lattice structures within user-defined bounding volumes [74] [75] (Figure 3-1 A).

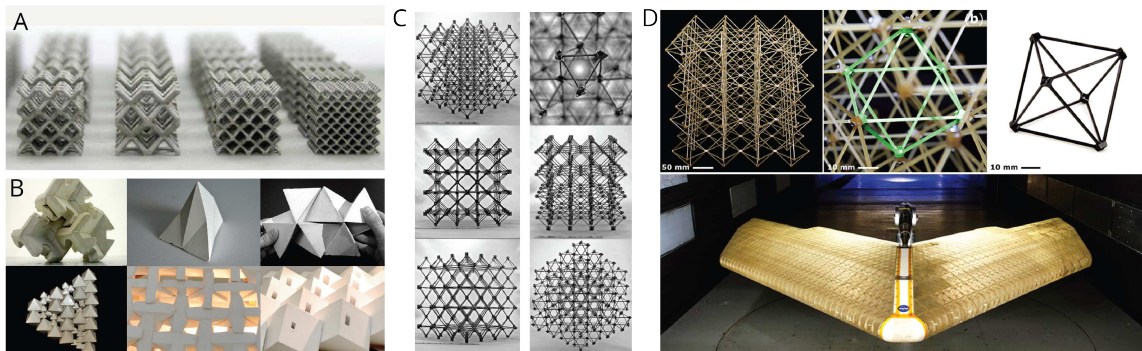


Figure 3-1: Recent research on lattice structures. Additive manufacturing has improved to enable the direct printing of complex lattices [76] (A). Topological interlocking materials use shape and frictional contacts to build tough materials from discrete parts [62] (B). Digital materials have set performance records for ultralight-but-stiff materials [20] (C) and have been used to assemble large scale structures like wings [77] (D).

While additive manufacturing focuses on building these structures monolithically and in a single process, it is possible to assemble architected materials from individual building blocks. Topologically interlocked materials (TIMs) is a field of study that looks at how structures can be assembled from shaped building blocks that interact through contact and friction interfaces. TIM structures often feature a boundary constraint and then generate all other constraints through the interlocking

shapes of the blocks. These structures have been shown to be highly damage tolerant and are able to absorb much more energy during impact than a monolithic structure of the same shape [78] [79] [62]. The design of these materials is often inspired by natural composite materials like nacre that exhibit incredible toughness, even with brittle constituent materials [80]. TIMs can sometimes be challenging to assemble, however, either requiring multiple degree-of-freedom motions or part stabilization until the global constraint is enforced.

The field of digital material systems represents another way to assemble highly performant structures that incorporate multiple materials or functionalities from individual building blocks. Digital material assemblies can be made using a wide variety of different part and lattice geometries. Digital materials designed for high-performance structural applications often take the form of sparse beam lattices such as cube-octahedra [20] [77] [65], Octet [20], or Kelvin [81] [82]. For functional electronic applications, the parts often take the form of tiles [23], dense interlocking assemblies [83] [84] [85], or sparser “Lego”-like assemblies [61].

3.2 Digital Materials

Digital materials have a number of desirable characteristics that make them well suited for the kind of high-density heterogeneous integration sought in this work.

- Digital material assemblies are capable of achieving high performance mechanical properties [20].
- They can incorporate heterogeneous materials or part types. For example, they can be used to assemble shape-morphing structures with the use of the rigid and flexural parts [21].
- Because the parts interlock with one another, there is a degree of error correction that happens during assembly. This means that the assemblies can be made more precise than the machine that assembles them [86].
- Furthermore, because digital material assemblies are often decomposable into simple two-dimensional parts, they can often be fabricated relatively easily at a range of different length scales, using a wide variety of processes, and made from a range of different materials.

Prior work has shown the ability to assemble electronic components from conductive, insulating, and resistive part types [22]. The parts used in these assemblies are referred to as “Lego-GIK” because they assemble in the same top-down fashion as Lego building blocks (Figure 3-2). The GIK acronym here refers to an earlier instantiation of these kinds of press-fit parts that was referred to as the “Great Invention Kit” [18]. These Lego-GIK parts feature four slots on the top of bottom of the part. The number of slots is the minimum number of slots to enable tiling in the X and Y axes.

In expanding upon these capabilities, an updated lattice geometry is beneficial for a few reasons. For one, while the multiple slots of Lego-GIK geometry serve the purpose of enabling a simple part to tile, they also make integrating functionality within the parts a challenge since there is very little extra area that can be used between each slot. Additionally, the redundant middle connections complicate the incorporation of mechanical functionality as they have no clear “input” and “output.”

Based on this, the middle slots are removed such that the building block only contains two slots on the top and bottom. This opens up the central portion of each building block for the

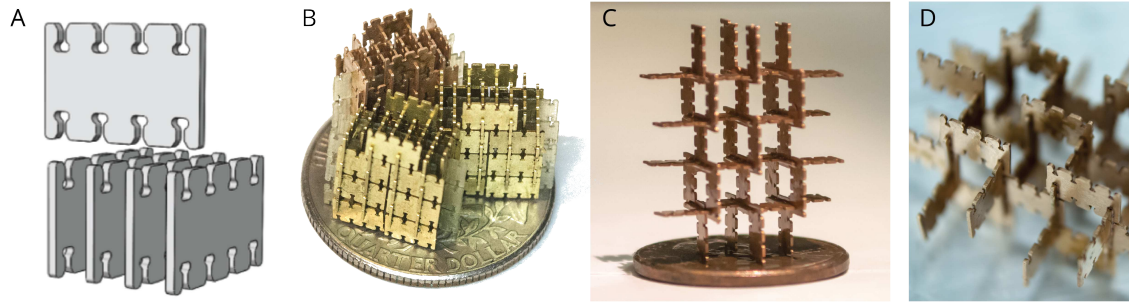


Figure 3-2: A series of structures built from “Lego-GIK” parts, which were used to explore the assembly of electronic digital materials.

development and incorporation of higher-level functions such as flexural hinges and actuation. This modified geometry has clear input, functional, and output regions within each building block.

This geometry still features a number of undesirable traits. For example, there is no way to tile these parts within a single plane. They rely on connections to parts above and below them and so require a minimum of four parts in the vertical direction in order to tile the plane. Furthermore, a number of the desired functions rely on the press-fit slots to impose an angular moment constraint. With only a single press-fit slot, repeated torques could cause unwanted wear and eventually result in degraded contact.

A further limitation can be observed by noting the minimum structural extension to the structure. That is to say, the minimum structural addition to the structure. In this case, that minimum structural extension is under-constrained, attaching to the structure through only a single press-fit connection. This under-constraint represents a challenge for automated assembly of the structure because it means assembly forces need to be controlled and directed in specific regions so as to not torque the part as it is being inserted.

3.3 A New Geometry

Based on these limitations, a further geometry was developed in order to better incorporate the mechanical and electrical functionality within the lattice. In my exploration of the design space of lattice-based discretely assembled structures, I restricted my search to regular rectangular lattices for their compatibility with press-fit construction methods and for their ease of laying out functionality in the cartesian axes (Figure 3-3).

Ultimately the new geometry relaxed the constraint of using a single part-type and introduced a secondary part-type, decomposing the lattice into edges and vertices, hereafter referred to as struts and nodes. In this decomposition, nodes are first assembled from four identical two-dimensional parts, connected through interlocking slots. Nodes are then connected to neighboring nodes through a pair of parallel struts (Figure 3-4).

This explicit decomposition into struts and nodes has a number of advantages. For one, it makes the parts more volumetric. Rather than two-dimensional panels, the parts are more cube-like, making them more amenable to automated assembly methods and allows them to be more easily manipulated. This volumetric nature also means that each slot is put under less torsional loading.

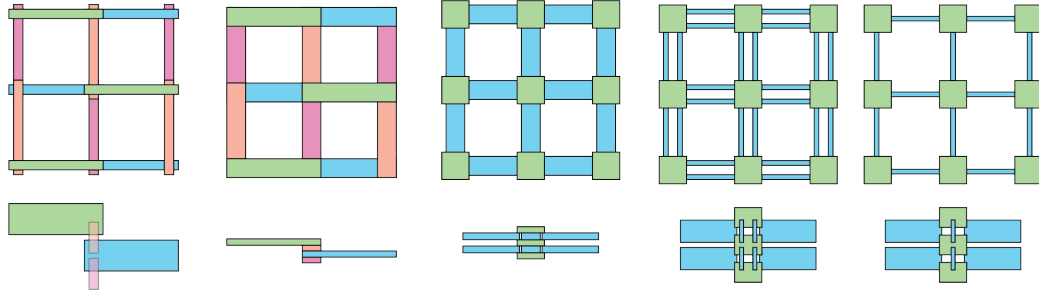


Figure 3-3: An exploration of the lattice design space. The leftmost design represents “Lego-GIK” construction while the second from the right represents the new geometry.

The rectangular nature of this lattice geometry allows these structures to tile the plane with a single layer and additional out-of-plane parts are not needed to give the layer its structure. The strut and node decomposition also provides a natural way to embed functionality in the lattice. As will be seen in the chapters to come, the struts often conveniently house functionality while the nodes provide connectivity.

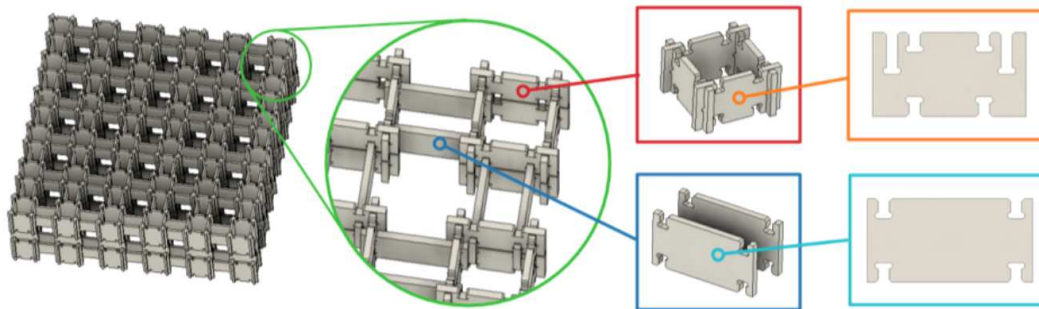


Figure 3-4: The rectangular lattice is composed to node and strut part types. Four node sub-parts are assembled to form a single node. Nodes are then connected to neighboring nodes through parallel struts.

With just these two part-types (node and strut), this assembly framework is 2.5D. This means that three-dimensional structures can be made through the stacking of individual planar layers. While this enables the assembly of a wide range of capabilities, it only enables functionality to be arranged within the horizontal plane. With two additional part types, these structural planes can be joined orthogonally. This capability enables the construction of orthotropic planes that are then assembled into three dimensional objects with functionality in any desired orthogonal plane. An example of this is discussed in Chapter 8.2.

3.4 Sizing

It is possible to make these parts and structures at a wide range of different scales. I’ve chosen to focus on the development of millimeter-scale parts for a few reasons.

- **Conventional millimeter-scale assembly is hard** [87]. The millimeter-scale is too large

to use photolithographic processes to produce integrated machines as is done in MEMS but too small to use any off-the-shelf components. Currently most machines made at this scale are produced in monolithic processes to avoid the assembly step. Automating assembly at this scale could help open up the fabrication of integrated machines with a more diverse range of functionality.

- **It is still amenable to rapid prototyping.** Laser micromachining, wire-EDM, and some machining processes are able to produce the required feature sizes at this scale to make interlocking parts in a direct-write way.

Given this, I sized parts based on the minimum feature sizes of the fabrication tools available to me. In this case, that meant standardizing around $254\ \mu\text{m}$ thick material and means the corresponding smallest feature size is also $254\ \mu\text{m}$. This enables relatively rapid production using the $150\ \mu\text{m}$ wire on the wire-EDM.

The parts are sized to balance two objectives: (1) minimizing the pitch-spacing of the lattice (to maximize resolution) and (2) maximizing the functional area available to each part. The design space can be pictured by looking at two extremes. In prioritizing objective (1) one may seek to shrink the parts entirely until they are the minimum possible size to allow for the interlocking joints to function. On the other hand, prioritizing objective (2) would mean stretching the parts until the joint-interfaces become infinitesimally small compared to the body of the part.

Similarly, there's a need to balance the size of the nodes and struts. Shrinking the nodes allows for the lengthening of struts (and therefore functional area) without affecting the pitch spacing of the lattice. However, doing this also necessarily shrinks the spacing between the pair of struts, reducing the overall strut volume. Ultimately the geometry that is used in this work strikes a balance between these but ensures that the struts are longer than they are wide, which is beneficial for a number of the functions that are developed and described in coming chapters.

3.5 Production

The parts that make this structure are two dimensional with relatively simple geometric features, allowing them to be easily fabricated using a range of different processes.

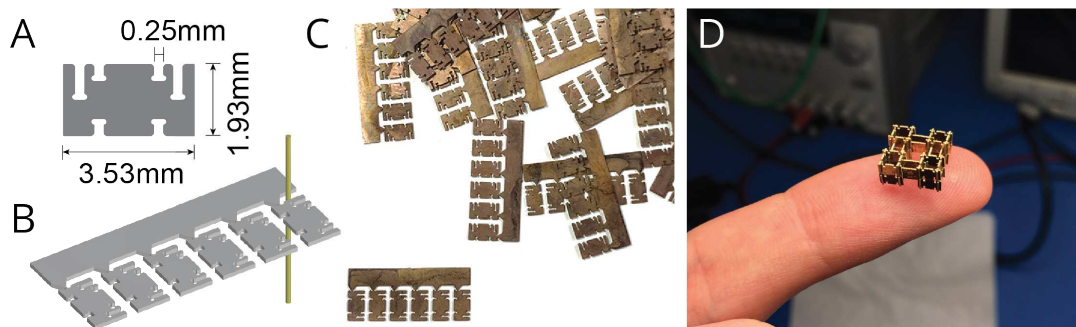


Figure 3-5: Node and strut parts are fabricated using wire-EDM, enabling the production of 108 parts in a single cut.

For prototyping, the basic structural (node and strut) parts are cut by wire-EDM (electrical

discharge machining) from 254 μm thick phosphor bronze. Arranging parts as a group (of six) and cutting a stack of (18) bronze sheets at the same time, enables the production of 108 parts with a single cut and takes just under one hour (Figure 3-5). These 108 parts are enough parts to assemble 27 nodes or 54 struts.

Nodes are assembled from four node parts manually using pliers. Automation of this assembly step is certainly possible and should be considered for scaling up the production rate of these parts.

Chapter 4

Mechanism

4.1 Compliant Mechanisms

In order to create machines, we need ways to constrain motion. Conventional machines at the macroscale often using bearings to constrain motion. Assembling bearings from individual discrete parts is hard to imagine unless the building block parts are significantly smaller than the bearing contact surfaces. In our case with millimeter-scale parts, this would entail building bearing surfaces from thousands or millions of parts.

Biology, however, demonstrates the potential for creating mechanisms and motion constraint without the use of bearings. While some biological bearings do exist [88], much of the movement that biology accomplishes is through the arrangement of rigid and compliant structures.

Compliant mechanisms is an emerging field of research that looks at recreating a wide variety of mechanisms and linkages using embedded flexural degrees of freedom rather than pins and bearings. These mechanisms offer advantages over conventional bearing-based degrees of freedom such as increased performance (high precision, low friction, low mass, reduced wear), lower cost (simplified fabrication, low part count), and ability to miniaturize [89].

Compliant mechanisms made using subtractive processes are normally limited to a single material and so their mechanism (force/displacement properties) is purely a function of geometry. Without the ability to spatially vary material properties such as stiffness and strength, these mechanisms often end up working only for a limited range of applications [89].

New methods in additive manufacturing have recently enabled the fabrication of compliant mechanisms directly from digital designs with spatially varying material properties. These methods are still limited, however, in the range of material properties that are available. Additionally, the resolution of this technique limits the utility of mechanisms made this way at millimeter scales.

Instead, rather than printing or shaping material, the assembly approach I use enables the integration of mechanism part types that exhibit a high degree of compliance about a certain axis while remaining stiff in other axes. These flexural parts can be produced using laminate based processes that enable the heterogeneous integration of materials giving the designer much more control over the resulting properties of the mechanism like stiffness and range of motion. Additionally, compared to multi-material additive technologies, the assembled mechanisms are able to take advantage of better material properties and much finer resolutions (e.g. thinner flexible regions) than are typical

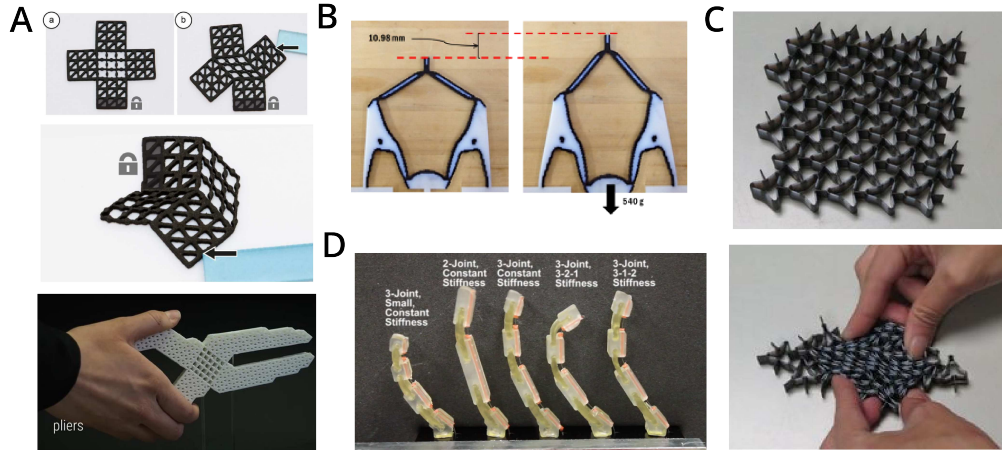


Figure 4-1: Recent research on compliant mechanisms. Compliant mechanisms can be designed as lattice metamaterials [25] and have been shown to be capable of being used as an amplifying and inverting mechanism [90], auxetic materials [91], and robot appendages [92].

for additive manufacturing approaches.

This laminate based approach to manufacturing compliant mechanisms has been explored increasingly in recent research [93][94][27]. The technique is often referred to as PC-MEMS (Printed Circuit Micro-Electromechanical Systems) [8]. Mechanisms made using this approach can be constructed to have a very high degree of compliance on-axis while remaining stiff off-axis [95].

4.2 Part Types

Two part types enable the assembly of a wide range of planar mechanisms (Figure 4-2): (1), a part with a single flexible degree of freedom and (2), a part with two flexible degrees of freedom. While it may not be possible to discretely assemble continuous rotary or linear constraints using discrete parts (at least at this scale and resolution), it is possible to assemble flexural mechanisms that approximate these motions, which exhibit a high degree of compliance within a certain axis or plane and high stiffness off-axis. Figure 4-2 shows common mechanism motifs that can be assembled from these two part types. In particular, two highlighted motifs are the simple rotary hinge and four bar linkage, which can be used to approximate linear motion.

4.3 Modeling

4.3.1 Kinematics

The discrete parts of this assembly framework provide a natural way of decomposing a complex linkage to evaluate its mobility. Parts assemble into a rectangular lattice framework in which pairs of nodes are connected by struts. This strut is what houses the mechanical degrees of freedom of the flexure hinges. Gruebler's equation can be used to characterize the mobility of some common

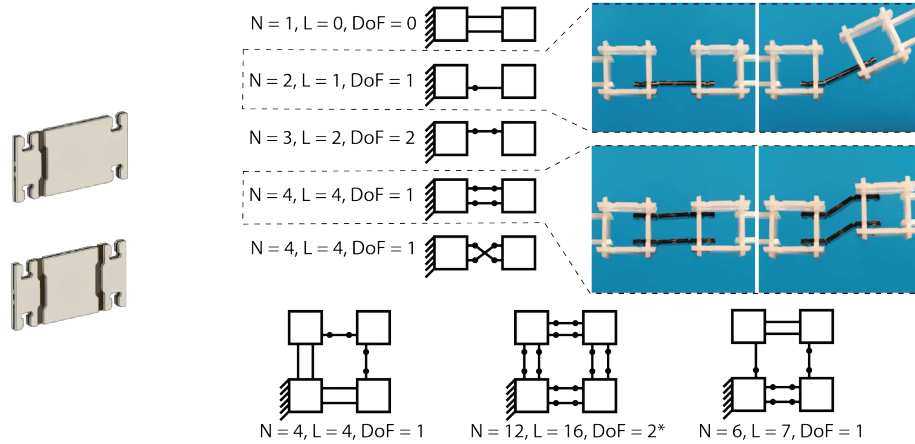


Figure 4-2: Two part types (left) are necessary to enable a wide variety of planar mechanisms. A series of strut motifs are characterized based on the Gruebler mobility criterion. Two motifs that are commonly used are highlighted: a revolute joint (top) and a parallelogram four-bar linkage mechanism that can be used for linear motion constraint (bottom).

strut arrangements (Figure 4-2). Gruebler’s equation is defined as:

$$\text{DoF} = 3(N - 1) - 2L - H$$

where N is the number of bodies or links (including the ground link), L is the number of lower order pairs (arresting two degrees of freedom), and H is the number of higher order pairs (arresting a single degree of freedom).

The constraint of linear motion rests on the ability of the parallelogram flexure to approximate linear motion over small displacements. The parallelogram mechanism is straightforward to model and simulate using simple rigid-body models. In this case, I find that the parasitic motion is related to two parameters: L (the distance between the flexure hinges) and d (the magnitude of linear displacement). The error motion is given simply by:

$$\text{Error} = e = L - \sqrt{L^2 - D^2}$$

True straight-line linear motion constraints can be assembled with a few more parts. For example, by stacking two of the simple parallelogram linkages on top of one another, perfect straight-line motion constraint can be achieved. The caveat with this design, though, is that it is only well constrained for small displacements. With large displacements (> 15 deg), it reverts from a single degree-of-freedom mechanism to a two-degree of freedom mechanism. Other researches have explored modifications and additions to these mechanisms that help constrain them over larger displacements [96] [97].

These two part types are able to assemble any planar mechanism (given unbounded size). Even within confined machines, they span a wide range of desirable mechanisms and transmissions. For example, Figure 4-3 demonstrates the assembly of a transmission that converts linear motion into the rotational motion of a gripper. It also shows the assembly of a transmission that converts rotary motion into straight line motion for use as a jumping leg. Finally it demonstrates the assembly of a

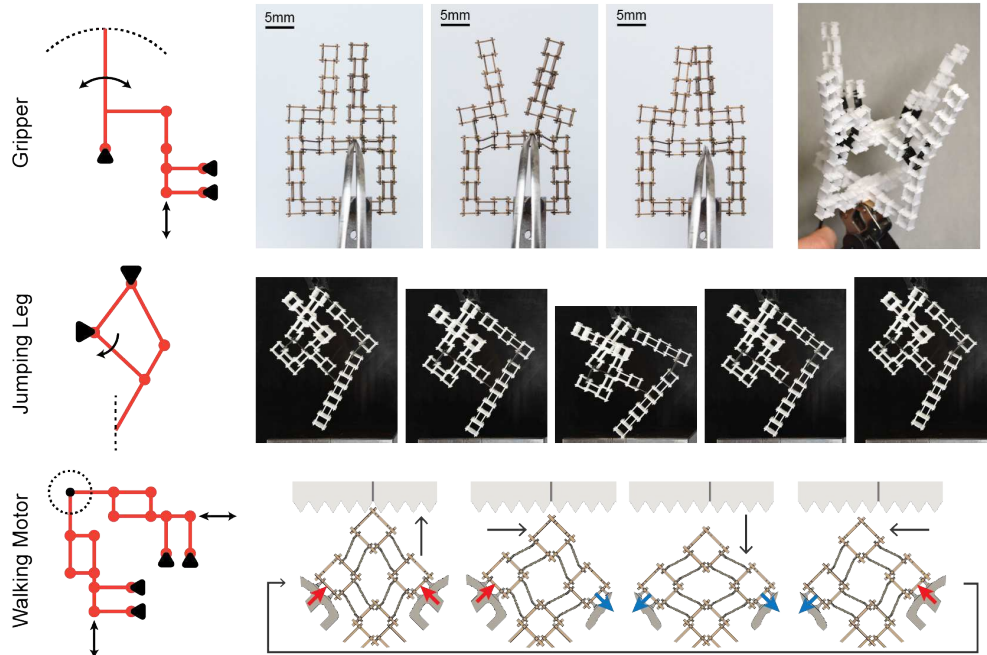


Figure 4-3: A variety of transmissions assembled from the two flexural part types. A gripper must convert linear motion into rotary motion. A jumping leg converts rotary motion into straight-line motion. And a walking motor decouples and distributes two independent degrees of freedom to a motor tip.

transmission that decouples and distributes two independent actuated degrees of freedom to a single drive tip in the case of a walking motor.

4.3.2 Quantization of a continuous range of transmission ratios

Given that these two part types enable the assembly of a wide range of mechanism, the question naturally arises: Can these two part types assembly any planar (pin-jointed) mechanism? To which, the answer is yes, but only if given an unbounded envelope. However, with volumetric constraints the answer is harder to define and a better question becomes: How closely can this discrete set of parts approximate a continuous range of transmission ratios?

A simple lever-based linear to linear transmission serves as a good representative test case for this analysis. With unlimited space constraints, pin-joints placed on a lattice can approximate any transmission ratio with arbitrary precision. To achieve ratios very close to certain desired ones, however, will require a very large number of parts. To achieve the exact ratio of 2.45, for example, would require $49 + 20 = 69$ parts (since the ratio is $49/20$).

This is improved by introducing a sidedness to each hinge such that it is located on a lattice but is either shifted to the left or right by an amount, D . In these assemblies, in which a pair of strut-parts makes up a single strut, this is equivalent to picking which of the strut-parts has the hinge. This simple additional parameter drastically reduces the number of parts required to achieve a certain level of precision.

To demonstrate this, I run a series of optimizations that adjust parameters to achieve a desired

transmission ratio. The objective function is:

$$\min((desired - discrete)^2 + \alpha * (b + a))$$

where α is a weighting factor ($\alpha = 0.001$), b and a are the unit lengths of the lever arms, and $discrete = b/a$. The optimization is subject to constraints such that a and b are integers and are perturbed by $\pm D$ based on the binary values $p1, p2, p3$, representing the sidedness of each of the three flexures.

The result of a sweep between ratios of 1 to 6 with steps of 0.0625 is pictured in Figure 4-4. The first plot shows the desired ratio against the actual ratio and the second plot shows the absolute percent error between desired and actual. The third plot shows the overall size ($a+b$) of the required linkage.

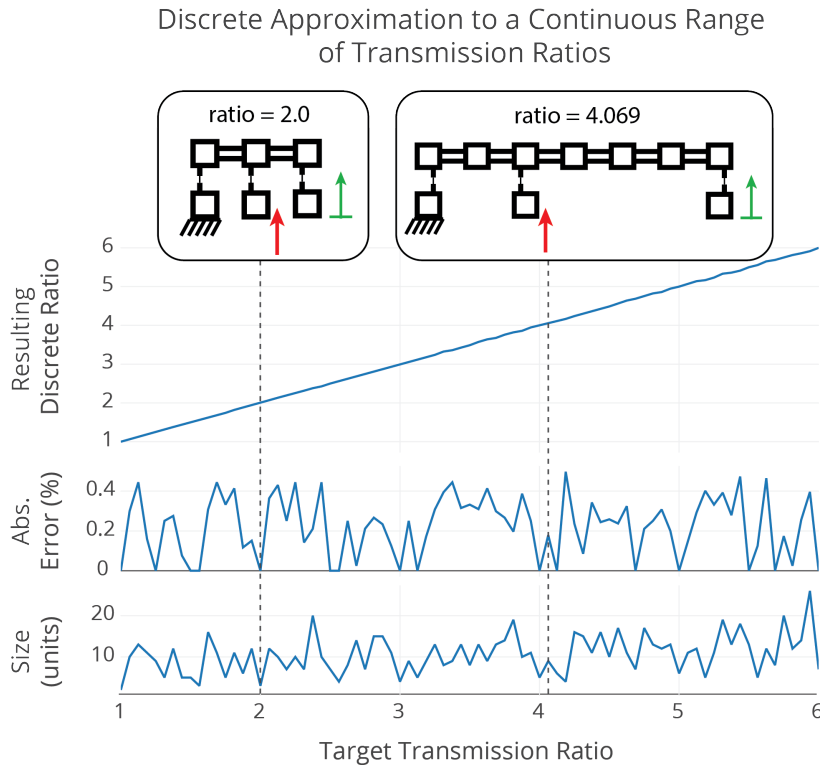


Figure 4-4: A plot showing that discrete parts on a lattice can representing a continuous range of transmission ratios. Ratios between 1:1 and 1:6 are sought at increments of 0.0625. By toggling which strut is made flexible, the continuous range can be represented in a finite area with less than 0.5% error.

What this shows is that these discrete mechanisms are able to represent a continuous range of transmission ratios with a small degree of error and in a finite length. Looking at a particular example is helpful to understand this. Take the desired transmission ratio to be 4.0625. With only discrete steps on the lattice in this straight lever-arm example, the smallest linkage that gets within 0.5% of the target ratio is 66 units long with a ratio of 4.077 ($b = 53, a = 13$). With a 5 mm lattice pitch, this entails a 0.33 m long lever arm, which is clearly not ideal. With the introduction

of the hinge-sidedness, the required size to achieve an error less than 0.5% is reduced by an order of magnitude to 7 units long with a ratio of 4.069 and entails only a 35 mm long lever arm.

Clearly this case of a straight lever-arm is constructed to illustrate this principle and real mechanisms can often take advantage of more than one dimension. For example, another way of achieving that 4.0625 transmission ratio is to construct a planar lever-arm whose hypotenuse approaches the target ratio. For example, without factoring in sidedness, a lever arm with $a = 2$ and $b = \sqrt{2^2 + 8^2}$ achieves a ratio of 4.062 within a 4 x 8 unit envelope.

4.3.3 Dynamics

Because these mechanisms must be capable of being displaced by actuators built into the lattice, it is important to understand their dynamic properties. By treating the flexural hinge as a beam, it is possible to model its stiffness using beam bending equations. The on-axis torsional stiffness is described by:

$$k_t = \frac{Ebh^3}{12L_{eff}}$$

Where E is the modulus of elasticity (≈ 2.5 GPa), b is the width of the hinge (2 mm), h is the thickness of the flexible layer (0.25 mm), and L_{eff} is the effective length of the hinge (0.216 mm). Since a castellated hinge geometry is used, the length of the flexing hinge is not well determined but can be approximated by taking the average of the minimum flexing gap and the maximum flexing gap. Given the geometry of our flexure hinges, the predicted torsional stiffness is 28.9 mN*mm/rad.

The on-axis stiffness of assembled mechanisms can be predicted for small displacements using conservation of energy:

$$\frac{1}{2}k_x\Delta x^2 = \sum \frac{1}{2}k_t\Delta\theta^2 = \frac{N}{2}k_t\left(\frac{\Delta x}{L}\right)^2 \implies k_x = \frac{NK_t}{L^2}$$

where N ($N = 4$) is the number of flexure hinges undergoing an equal deformation of $\Delta\theta$, which I approximate for small displacements as $\frac{\Delta x}{L}$, where L is the spacing between hinges ($L = 2$ mm). Given this, the expression to predict k_x from k_t is simply $k_x = k_t$.

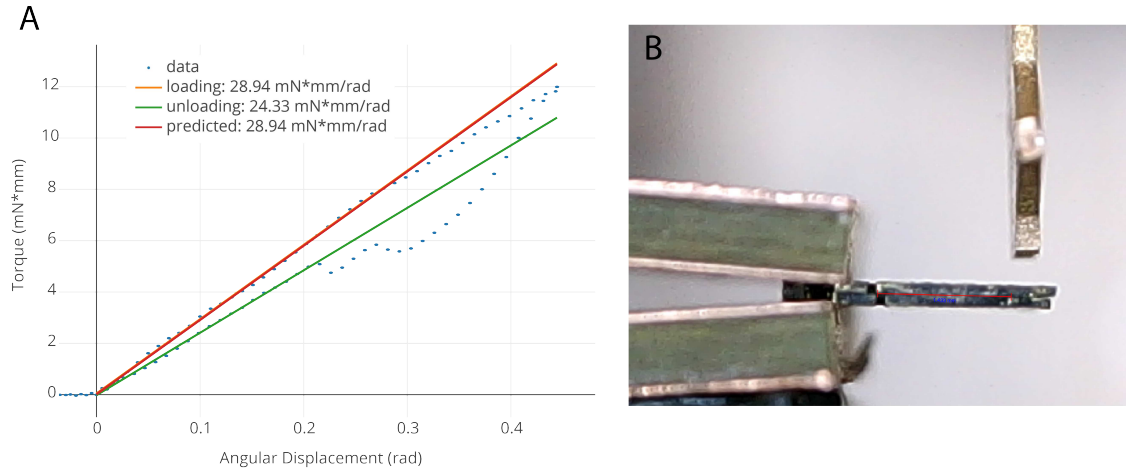


Figure 4-5: Stiffness measurement of a single flexure hinge. The flexure hinge exhibits some hysteresis such that the loading direction is stiffer than the unloading direction.

I validated this estimation with measurements of the on- and off-axis stiffness of a single flexure hinge as well as an assembled parallelogram linkage (Figure 4-5). Measuring the torsional stiffness of the single hinge, I found the behavior to be slightly hysteretic such that the stiffness in the loading direction (28.9 mN*mm/rad) is almost 20% more than the stiffness it exhibits as it is unloaded (24.3 mN*mm/rad). Even with this hysteresis, these values closely match the analytical prediction for on-axis stiffness. The same flexure measures 9.7 N*mm/rad off-axis, which represents a two orders of magnitude difference in stiffness between on- and off-axis directions.

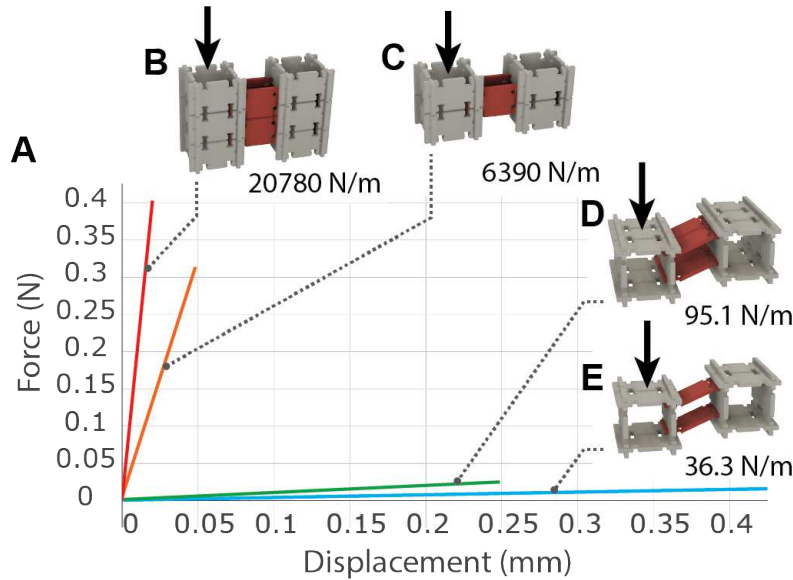


Figure 4-6: The flexures are measured with loads applied both on-axis (in the direction of motion) and off-axis. The flexures are much stiffer off-axis than on-axis and additional layers can be added to increase the anisotropy.

I performed the same test on an assembled parallelogram mechanism composed of two nodes connected by two double-hinged struts. I found the stiffness on-axis to be 36.3 N/m and off-axis to be 6390 N/m. By adding more layers to the parallelogram assembly, this off-axis stiffness can be increased even further. A two-layer parallelogram mechanism measures 95.1 N/m on-axis and 20780 N/m off-axis. These results are illustrated in Figure 4-6.

These results match the analytical predictions well. The measured stiffness of the single-layer parallelogram is approximately 20% more than that of our prediction. This difference is most likely explained by small geometrical differences and misalignment in the parts leading to over-constraint. When loading the assembled structure off axis, the stiffness of the fixturing becomes relatively significant. In order to remove this from the measurement, I measure the stiffness of the fixturing and then subtract out its contribution based on series springs.

4.4 Production Methods

The flexural parts are built using a laminate process that is often referred to as printed-circuit MEMS (PC-MEMS) or smart composite materials (SCM) [8]. This process is similar to how printed

circuit boards are constructed but rather than etching pre-laminated materials, this process involves the lamination of pre-machined layers of material using a thermoset adhesive.

In this case two rigid outer layers sandwich an inner flexible membrane. The outer layers feature cutouts to allow the inner flexible membrane to bend within these defined regions (but not elsewhere).

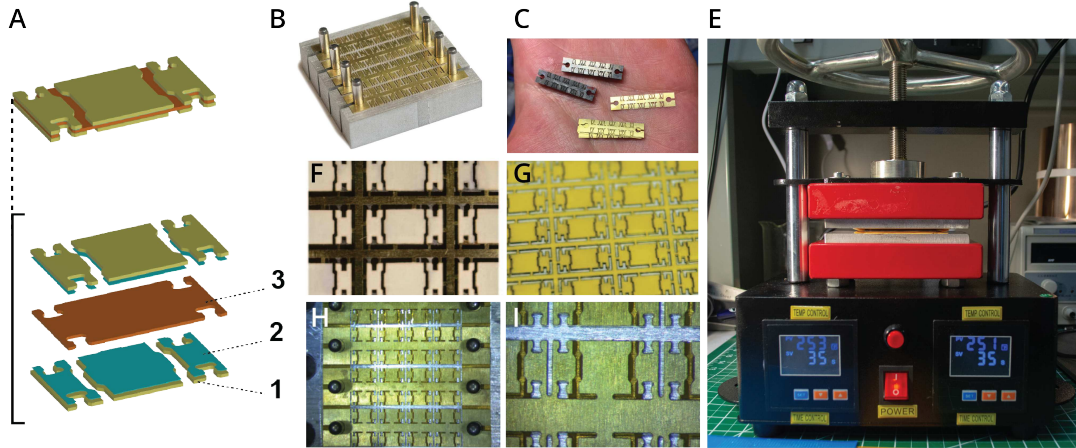


Figure 4-7: Part production methods for flexible parts. The flexible parts are made through a laminate process in which rigid metal layers (C) sandwich a flexible membrane (E) and are bonded together with the use of a thermoset adhesive (D). Alignment is accomplished using a jig with dowel pins (B) and results in an array of parts that are subsequently released.

Rigid layer machining The rigid layers are most efficiently machined using wire-EDM. I wire-cut the rigid outer layers from stacked sheets of 100 μm thick brass. I combine multiple parts onto a single central runner to enable the production of many parts with a single cut. In particular, I combine six parts into a single cutout and stack eight sheets of 100 μm brass, enabling the production of rigid layers for 24 parts with a single cut (Figure 4-7 C).

These rigid layers may also be cut using a micromachining laser (e.g. Oxford 532nm DPSS). This is sometimes attractive for small batches and test runs where time to go from the design to the first test article is more important than the production time per part.

Flexible and adhesive layer machining The flexible layer is laser micromachined (Oxford Systems) from 25.4 μm thick polyimide (Kapton) (Figure 4-7 G). After machining the rigid and flexible layers, they are subsequently bonded through the use of a 12.7 μm thick B-staged thermoset adhesive (Pyrulux 1500). The adhesive is skim cut using the laser micromachining system (Oxford) such that it is cut through the adhesive but not the backing. Alignment holes are then cut through both the backing and the adhesive. The adhesive is weeded using tweezers to eliminate unwanted adhesive regions. This weeding process can be slightly arduous and is the likely the most labor intensive and least parallelizable part of the production process.

Lamination A number of different methods can be used to generate the heat and pressure required for lamination. A toaster oven with Kant-twist clamps is perhaps the simplest but lacks precision both in the temperature of the laminate and the pressure applied. A benchtop heatpress can control the temperature much more precisely but it can be easy to apply too much pressure (Figure 4-7

E). Replacing the crank and leadscrew of the upper press-plate with a simple weight is the simplest method to achieve more precise control over the pressure. This has another advantage which is that it allows for thermal expansion of the laminate materials while maintaining consistent pressure.

The adhesive is first tacked to the rigid brass layers using less heat and pressure than necessary for a full cure (120 °C for 15 mins). Alignment is achieved with the use of a wire-cut two-sided fixture that features matching dowel pin holes to those of the pre-machined layers (Figure 4-7 B). Once the adhesive is tacked to the brass layers, the backing can be removed and the laminate can go back in the heat press with the inner flexible layer inserted for the full cure (200 °C for 1 hour).

Singulation After lamination, the parts need to be released from the sheet. I used a micromachining laser to cut the parts from the rest of the sheet. Dowel pin registration holes are first cut in a piece of sacrificial material (such as brass). This provides a simple method of re-aligning the laminated sheet with respect to the laser machine’s coordinate system. Subsequent production runs can be re-aligned to these drilled holes with the aid of registration crosses that are cut into the sacrificial substrate. A cutout toolpath is then generated and run, which trims the tabs connecting the parts to the scaffolding. The parts are then easily picked up and removed with tweezers. A quick (10 minute) immersion in an ultrasonic bath (with water) can be helpful to remove any debris generated by the laser cutting process.

This kind of lamination process is particularly attractive because the two-dimensionality makes it scalable. The process can be employed with small batch sizes of only a handful of parts for prototyping or can be scaled to much larger batch sizes for higher throughput production. Furthermore, the process is potentially amenable for implementation as a roll-to-roll process. In such a workflow webs of raw material may be continuously fed in, machined or stamped into shape, bonded, and exit as a roll of finished parts.

4.5 Discussion

While mechanisms made through the assembly of these laminated flexure parts can be highly performant, there are some aspects that need to be considered relative to more conventional mechanisms.

The thin flexure membranes can be prone to buckling if they are loaded in compression above their critical buckling load. This threshold can be calculated using the following equation:

$$F_{critical} = \frac{n\pi^2 EI}{L^2}$$

where n is a factor based on the bounding constraints ($n = 4$ for fixed-fixed), the Young’s modulus, E , for polyimide is approximately 2.5 GPa, and I , the moment area of inertia is $I = \frac{bh^3}{12}$. Since the rigid layers are castellated around the flexure hinge, there is not a clearly defined length but we can approximate it by taking the average of the maximum and minimum length between rigid boundaries. In this case, $L_{eff} \approx \frac{L_{max} + L_{min}}{2} = 0.216$ mm, $b=1.92$ mm, $h=25$ μm, and so $F_{critical} = 5.3$ N.

In order to avoid this buckling, a castellated hinge geometry can be used, which reduces the length of the unsupported flexible layer while still allowing a large range of motion [98]. This strategy, however, does contribute to reduced lifetime of the flexure hinge, which has been shown to

be a strong factor of the flexure hinge length [98]. In my testing, the earliest I have seen a flexural hinge fail is after 16 hours of testing at 20 Hz, or 1.16 million cycles (Chapter 8.1).

Another strategy to avoid buckling flexures is to use the principle of inversion. Flexures that are identified as having a predominately compressive load can be replaced with an inverted flexure part that converts that compressive load to a tensile load [99].

While these mechanisms can be stacked vertically to increase the off-axis stiffness, the scaling of off-axis stiffness with the total height of the flexure is less performant than with a monolithic construction. To measure this, I compared a finite element analysis of a series of monolithic flexures with the same conditions applied to a series of discrete flexures. I chose to study a the stack-up of a two-hinge flexure. Using the solid mechanics module of COMSOL Multiphysics, I applied a fixed constraint to one boundary and unit boundary load (1 N) to the opposite boundary. The distance between each layer is 1 mm and, in the discrete model, each layer is sized to be just less than this pitch (0.99 mm). The simulation is run at 20 intervals for a total flexure height ranging from 1 mm up to 20 mm. The results (Figure 4-8) show that the stiffness of the monolithic construction method increases more rapidly with each additional layer of material (slope = $0.134 \text{ N}/\mu\text{m}/\text{mm}$) than the discrete construction method (slope = $0.020 \text{ N}/\mu\text{m}/\text{mm}$).

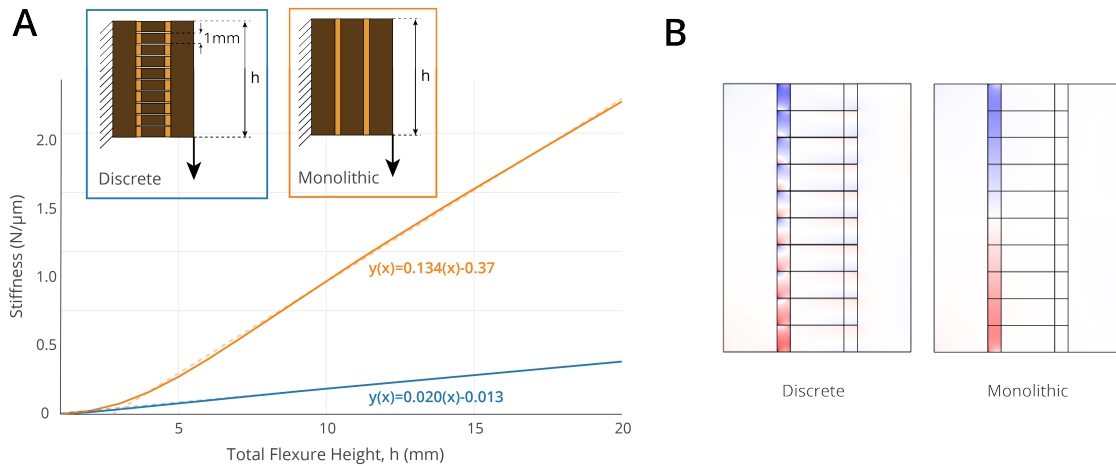


Figure 4-8: Simulation results comparing the off-axis stiffness scaling of monolithic and discretely assembled flexures. (A) Discretely assembled mechanisms have lower off-axis stiffness for an equivalent size compared with monolithic flexures and the different increases for increasing levels of discretization. (B) The strain distribution in the monolithic flexure is even and continuous while the discrete flexure is unable to evenly distribute forces evenly.

This difference in the scaling of off-axis stiffness can be explained by the fact that the discrete construction method is only able to transfer forces between layers at the bounds of the two-hinge flexure. Because the monolithic flexure is able to transfer forces through the entire region of material, strain is less concentrated in the flexure. This can be evidenced by comparing the volumetric strain distribution between these two simulations (Figure 4-8). The discrete construction method results in the top and bottom flexures being put in essentially pure tension and compression, respectively. Compressive forces within these flexural regions can be cause for concern as they can buckle the flexible membrane if they exceed the critical buckling threshold.

To perform better in this regard, future assembly systems could look at methods to join at

more regular intervals. It is likely challenging to connect the flexible region of one discrete flexure to another but entirely feasible to connect adjacent rigid regions on neighboring discrete flexures. Doing so would improve the scaling of off-axis stiffness significantly, at least in cases like this where the rigid region of the flexural part makes up a large proportion of overall part area. Another alternative would be to enable the assembly of parametrically sized parts. For example, if a particularly stiff flexure was needed to resist large off-axis loads, a tall flexure could be produced and assembled in place of many discrete ones.

Chapter 5

Actuation

5.1 Actuation at the millimeter scale

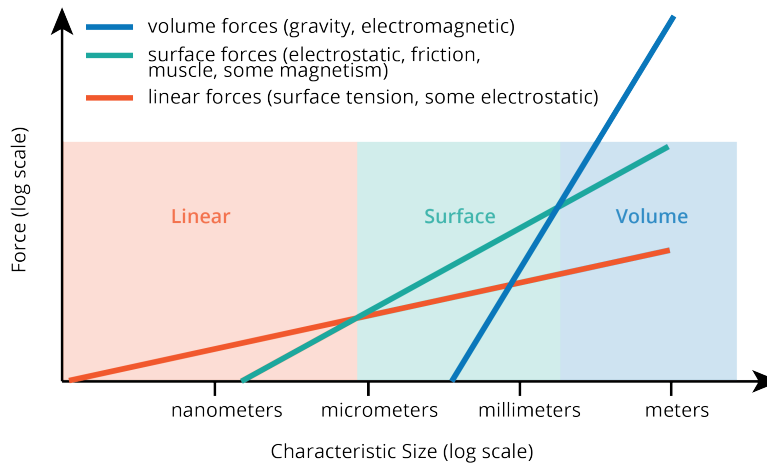


Figure 5-1: Derived from [87]. An overview of how forces scale across length-scales. At the millimeter scale the effects of volume forces, which dominate macro-scales, become less pronounced as surface and linear forces start to play a bigger role.

At the millimeter scale, a number of actuation techniques can be used to drive these mechanisms, including piezoelectric bending actuators [100], dielectric elastomer actuators [101], shape-memory alloy actuators [102], and electromagnetic actuators [103]. I performed analysis of a number of different actuation techniques in order to help down-select an appropriate actuator for integration in the millimeter scale assemblies. I will briefly review the high level analysis of these actuation techniques before exploring the detailed design of the electromagnetic Lorentz force actuators that I chose. In this analysis I assume that the actuator must be manufacturable using available direct write methods. Therefore the minimum feature size should be $20 \mu\text{m}$ if it's to be made on the Oxford Laser and should be greater than $180 \mu\text{m}$ if it's to be made by wire-EDM.

Electrostatic I looked both at electrostatic gap closing and lateral force actuators. Gap closing actuators are limited in displacement to 1/3 of the gap width due to the pull-in instability [104]. Due to this instability and the breakdown field strength of air, I found that this actuator would require on the order of 150 V to produce 5 mN of force with a maximum possible stroke of 20 μm . I deemed this force and stroke too limited to produce useful motion at the millimeter and centimeter scale. The lateral force electrostatic actuator was able to provide larger strokes but still provided insufficient force (Figure 5-2 B). For comparison, a Lorentz force actuator produced at the same scale is able to provide $O(100)\times$ the force and $O(100)\times$ the stroke of this kind of actuator.

Piezoelectric I also studied piezoelectric actuators, looking at unimorph and bimorph bending actuators as well as amplified stack actuators. A piezoelectric bimorph actuator at this scale is far more feasible than an electrostatic actuator and is able to provide forces in the neighborhood of 300 mN along with displacements of approximately 200 μm (Figure 5-2 C). A flexurally amplified piezoelectric stack actuator is able to provide even more force (≈ 1 N) but with much more limited displacement (30 μm) (Figure 5-2 A).

Electromagnetic Of electromagnetic actuators I looked at a number of different configurations including Lorentz force actuation, two-phase linear stepper motors, as well as a more conventional iron-based linear motor. I ultimately chose the Lorentz force actuation for its manufacturing simplicity, its ability to achieve constant forces over long strokes, and the lack of any force between the forcer and mover other than the Lorentz force.

The two-phase linear stepper motor is composed of three part types: a magnet tile that is placed on the top surface of an assembly and two coil parts, each of which is geometrically shifted by a half phase with respect to the other (Figure 5-2 E). My analysis showed that this kind of actuator could produce force peaks of approximately 65 mN and could do so over an arbitrarily long stroke defined by the constraining linkage. However, a number of practical concerns arose with this design. The magnet tiles would not want to be positioned the way they need to be. This means that the assembly of the magnetic tiles would be complicated by forces trying to prevent that assembly from happening. Even once the tiles were in place, it would exert potentially non-trivial forces on the structure. The minimum useful constrained actuator built with this technique would require a large number of parts and so would limit the number of systems that I could prototype and test.

A linear motor using an iron core to shape the flux loop was also considered. This design is able to produce 200 mN of force with a 1 mm stroke. The stroke, in this case, is actually limited by the four bar linkage's approximation of a linear motion constraint. Unlike the Lorentz force actuator, the force this actuator produces is highly nonlinear over the stroke and means that it is likely only able to operate in a "bang-bang" modality, moving quickly from one side to the other. While the actual force producing components take up roughly the same volume as the Lorentz force actuator, the flexure required to constrain the motion is much larger because it must kept in tension to account for the attractive force between the forcer and mover.

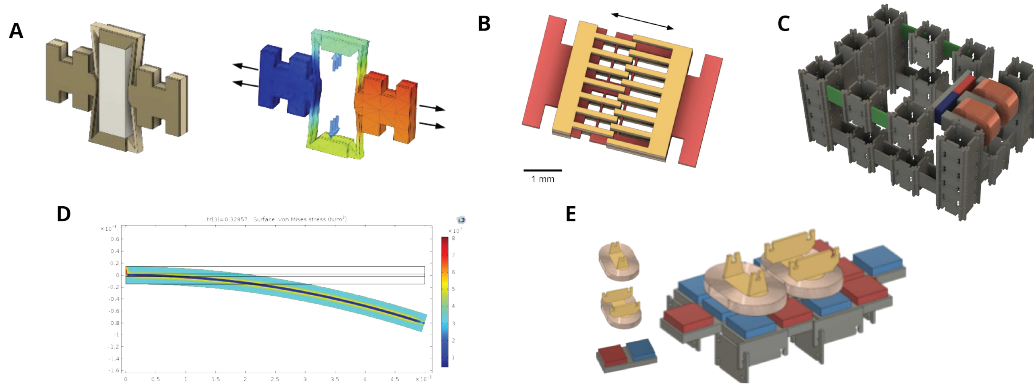


Figure 5-2: A number of actuation techniques were surveyed before Lorentz force actuation was chosen. (A) Piezoelectric stack actuator amplified by a flexural mechanism. (B) Lateral displacement electrostatic actuator. (C) Iron core electromagnetic actuator. (D) Modeling of a piezoelectric bending actuator. (E) An electromagnetic bipolar stepper motor concept.

5.2 Electromagnetic Lorentz Force Actuators

I ultimately decided to use Lorentz force actuators for these millimeter scale assemblies. The benefit of Lorentz force actuators over other electromagnetic actuators is that they can generate constant forces over large strokes and are capable of high-bandwidth operation. Lorentz force actuators are also appealing because there are no attractive forces between the forcer and the mover. This means that there is no cogging forces and output force is exactly proportional to input current.

The actuator components span two cells of the lattice geometry (Figure 5-3). This reduces the volumetric overhead associated with the integration of the coil and the magnetic core and means the force producing components can take up a larger portion of the overall volume. I designed the actuators to maximize their force over a 2 mm stroke. Like all other parts in this assembly system, the actuator components are designed to be vertically assemble-able and interface with the lattice using the same press-fit connections.

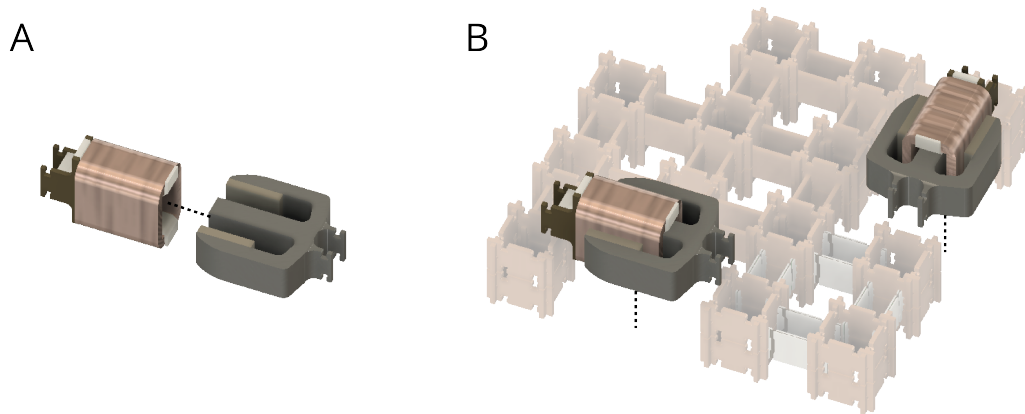


Figure 5-3: Diagram showing how the Lorentz force actuator fits into the assembled lattice. The actuator is composed of a coil part and a magnet part (A). It is assembled using the same press-fit connectors and takes up two cells of the lattice (B).

The actuator itself is composed of two parts: a coil part and a magnet part (Figure 5-3). The coil part consists of a frame around which a coil is wound. Two variants of the actuator have been developed. An earlier version with 80 turns of 34-AWG wire and, after refining the winding process, a later version with 320 turns of 40-AWG wire. The magnet part is composed of two neodymium magnets and a permeable core with the magnets oriented such that two opposing flux regions are created between the magnets and the central core. The coil is free to slide within the magnet part such that current flowing through the coil interacts with the magnetic flux in these gaps and produces a transverse force that is orthogonal to both the current and the flux. The detailed design and dimensioning of the actuator was based off of the modeling and experiments discussed in the next section.

In this section I will detail the modeling used to understand and predict the performance of this actuator, the experimental validation and characterization of the actuator, the production methods used to fabricate the actuator in small batches, and contextualize the performance of the actuator amongst other millimeter scale actuators in recently reported research.

5.2.1 Modeling

Magnetic Circuit Model

Voice coil actuators provide relatively high energy densities and produce constant forces over large strokes. In comparison with more traditional iron-core linear motors, voice coil actuators are less energy dense because of the necessarily large air gaps inherent in their design. They benefit, however, from having no inherent attraction between the forcer and mover and, as a result, have no cogging in their motion. This means that their force can be constant over a large stroke and their force varies linearly with the applied current. They are also more efficient, especially at high frequencies, because the iron is not cycled through its hysteresis loop. We can calculate their force from the standard Lorentz force equation for a current carrying wire in a magnetic field:

$$F = NIBL$$

where N is the number of turns of the coil, I is the current in the coil, B is the flux density in the air-gap, and L is the length (out-of-plane) of each coil turn that interacts with the magnetic field.

To calculate the flux density in the air gap we can use magnetic circuit analysis to get a first-order estimate and help establish intuition for the design space. We start with the assumption that there are no currents within the iron core so magnetomotive force sums to zero:

$$H_m t_m + H_g t_g = 0$$

and also assume an isotropic linear magnetic medium in the gap:

$$H_g = B_g / \mu_0$$

rearranging, we get,

$$H_m = -B_g t_g / (\mu_0 t_m)$$

Then, assuming straight-line magnetization,

$$B_m = B_r + \mu_0 H_m$$

and flux in equals flux out,

$$A_m B_m - A_g B_g = 0$$

we get the flux in the gap to be (with an added loss coefficient η):

$$B_g = \frac{B_r \eta}{\frac{t_g}{t_m} + \frac{A_g}{A_m}}$$

where B_r is the residual flux density of the magnet, η is a loss coefficient which accounts for leakage flux, t_g is the gap thickness, t_m is the magnet thickness, A_g is the area of the gap and A_m is the area of the magnet. For these kinds of voice coil actuators in which the air gap is significant, the loss coefficient may be as high as 20-30%. Based on this analysis, estimations of the force can be made by plugging in the flux density of the air gap into the Lorentz force equation above. This is summarized in Table 5.1.

Table 5.1: A summary of the geometrical parameters and analytical force estimates for the 80-turn Lorentz force actuator.

Parameter	Value
t_g/t_m	1.872
A_g/A_m	1
B_r	1.4
NI	$80 \times 0.6 = 48$
L	2 mm
$F, \eta = 1.0$	46.8 mN
$F, \eta = 0.75$	35.1 mN

Numerical Model

This model, however, over-predicts the force produced by the actuator since it neglects a number of losses inherent in the system. It assumes that all of the flux that leaves the magnet neatly re-enters the magnetic core without straying or folding back on itself. The model also neglects saturation of the iron. If the arms of the magnetic core are made insufficiently thick, the iron reaches the saturation region of the material's BH curve and limits flux density in the gap. This model also neglects eddy current losses in the iron, which become significant at high frequencies.

For a better estimation of the performance of this kind of actuator, I use a multiphysics modeling software like COMSOL. In COMSOL, I specify nonlinear magnetic materials to account for saturation, assign remnant flux densities to permanent magnets and calculate the force based on current flowing in regions of magnetic field (Figure 5-4).

I model only half of the voice coil actuator and use a magnetic insulation boundary condition to add a symmetric constraint. This forces all flux to be parallel at the mid-plane of the actuator and all currents to be perpendicular. While this assumption is not perfectly accurate, it is reasonable given the symmetry of this design.

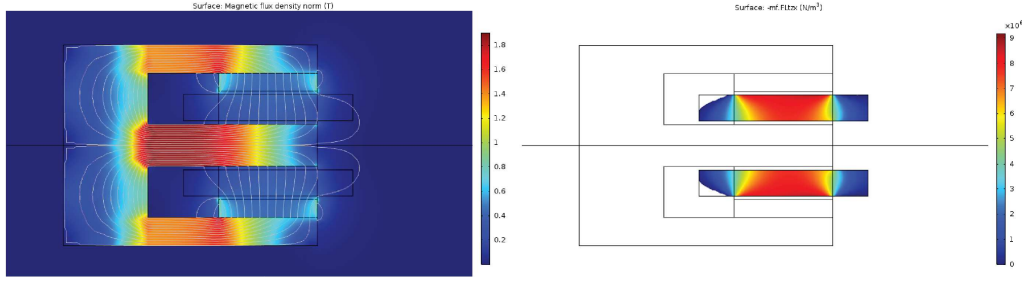


Figure 5-4: Magnetic field modeling of the magnet core and coil. (Left) Shows the flux density within the magnet core. (Right) Shows the force contribution within the coil cross-section.

There are many parameters that can be adjusted in both of these models that effect the resulting force prediction. Ultimately, however, we care about how well that simulation matches the physical hardware. Figure 5-5 shows the results of static testing. It's clear that the testing is in line with the experimental results. As expected, the analytical model over predicts the performance of the actuator and the numerical model comes closer to matching the experimental results.

Dynamic Modeling

Understanding about how the actuator performs dynamically can be gained by looking at the impedance of the actuator coil. I model the electrical dynamics of the voice coil actuator as an LR circuit and perform analysis using an electrical simulation tool (Spice [105]). The time constant of this circuit gives us an indication of how quickly the voltage and current within the coil will respond to changing stimuli. For the PWM drive to be efficient, the frequency should be high enough that the drop in voltage and current in the coil during the off-periods is relatively small compared with the average value.

I estimate the inductance and resistance of the actuator based on its multiphysics model. COM-SOL estimates the inductance of the 80 turn (34 AWG) coil to be nominally 15 μH with the magnetic core at its intermediate rest position. The resistance of the coil is estimated to be 1.4 Ω .

$$\tau = L/R = 15 \mu\text{H}/1.4 \Omega = 10.7 \mu\text{s}$$

$$1/(10.7 \mu\text{s}) = 93 \text{ kHz}$$

What this shows is that to keep the voltage drop during of the off-cycle of the PWM pulse below 63% of the source voltage, the off-period of the PWM needs to be less than 10.7 μs . For a 50% duty cycle, this corresponds to 93 kHz.

This ripple current negatively contributes to coil heating, which ultimately limits the performance of the actuator. Motor heating is proportional to the square of the root mean squared current (I_{RMS}). This current can be calculated with the equation:

$$I_{RMS} = I_{avg} + \frac{I_{pk-pk,ripple}}{2\sqrt{3}}$$

I evaluate the RMS current and resulting temperature rise for three different PWM scenarios:

- At 31.25kHz and a 50% duty cycle, I see an average current of approximately 700mA with a

peak to peak ripple of 400mA. This equates to an RMS current of $700\text{mA} + 115\text{mA} = 815\text{mA}$. This 115mA represents an extra 16% increase over the average current and becomes a 36% increase in power dissipated in the coil.

- At 1kHz and 50% duty cycle, I see an output current ripple that spans the full range of 1.4A. This equates to an RMS current of $700\text{mA} + 400\text{mA} = 1.1\text{A}$. This extra 400mA represents an extra 57% increase in current and results in a 147% increase in dissipated power.
- At 250 kHz with a 50% duty cycle, we see an output current which spans between 740mA and 690mA (averaging 715mA with 50mA pk-pk ripple). The RMS current is then $715\text{mA} + 15\text{mA} = 730\text{mA}$. This represents an increase in current of 2% and an increase in dissipated power of 4%.

Clearly it is beneficial in terms of power dissipation to drive these actuators with higher PWM frequencies and frequencies of at least 250 kHz appear to be suitable for these low inductance actuators. This testing was performed on the 80-turn coils but applies just as readily to the actuators made with 320-turn coils. Because the 320-turn coils have higher inductance, they are slightly less susceptible to losses derived from ripple current but still see benefits from being driven with high frequency PWM.

5.2.2 Experimental Characterization

Static Characterization

During static testing, I varied the current through the actuator coils from 0 to 900 mA and measured the resulting output force. The results, pictured in Fig. 5-5, show that the force of the actuator is linear with current and closely matches both analytical and numerical simulations. Because the models do not account for static friction or irregularities in the winding of the coil, they tend to over-predict the performance of the actuator. The analytical model also neglects leakage flux, which is unrealistic given the size of the air gap in the actuator.

As the currents exceed 0.75 A, the results and the prediction diverge slightly. This is likely a result of high temperatures in the coil affecting the effective flux density supplied by the magnets. Given this, I take 600 mA as the actuator's maximum steady state operating current, at which it reaches a temperature of 67 °C and produces an output force of 42 mN. This output force is enough to lift 28 nodes of the lattice or 7 other actuator components, which is sufficient to produce useful motions and forces in discretely assembled machines with multiple degrees of freedom.

Thermal Concerns

The Lorentz force actuator is limited by its ability to dissipate heat that is built up in the coil. At a certain point the power dissipated by the coil causes a temperature increase in the windings that's high enough to damage the insulation of the magnet wire, causing the coil to short circuit, and the actuator to fail. For the polyamide bondable magnet wire that I use, this temperature is in the region of 200 °C.

Before this temperature there are other thermal concerns that should be evaluated. Permanent magnets are sensitive to high temperatures and can become permanently demagnetized when

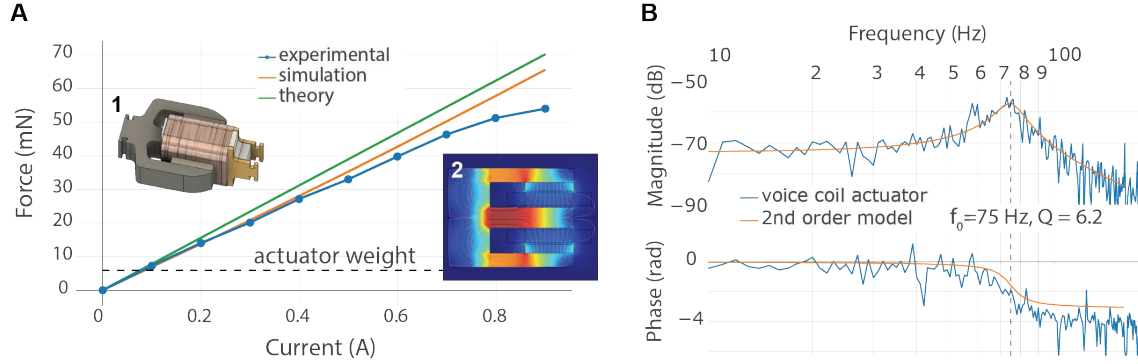


Figure 5-5: Actuator characterization. (A) Shows the results of static testing and comparisons with theoretical and numerical modeling. Current was progressively applied to the coils of the actuator component and the resulting force was measured by a milligram loadcell. (B) Shows the results of dynamic testing. A pseudo-random noise was used as the input to the actuator and the displacement was measured with a high-speed camera. Dividing the output response from the input signal resulted in the bode plot which shows the frequency response of the actuator and indicates it has a natural frequency of 75 Hz when constrained by an assembled parallelogram linkage.

operated improperly above their maximum temperature rating. This maximum temperature is dependent upon the geometry of the magnet and the surrounding flux guides, which can be represented by a permeance coefficient. In the case of this Lorentz force actuator, the permeance coefficient is defined with the following equation:

$$P_c = \frac{t_m}{t_g C_\phi}$$

where t_m and t_g are the thickness of the magnet and gap respectively and $C_\phi = A_{mag}/A_g$ which, in this case, is just 1. From Table 5.1, $t_g/t_m = 1.872$ so $P_c = 0.53$.

This permeance coefficient can also be described as the ratio of the flux density to the magnetic field at a given operating point. Using COMSOL, I looked at the average field and flux density in the permanent magnet. This method estimates a permeance coefficient closer to 0.81 which reflects a slightly more temperature resilient actuator.

Then, using the demagnetization curve, a load line can be overlaid starting at the origin with slope equal to the permeance coefficient (Figure 5-6). It's clear that above approximately 70 °C, the load line will be hitting the “knee” in the demagnetization curve and risk irreversibly reducing the residual flux density of the magnet.

To ensure that the actuators do not exceed this temperature, I use a thermal camera to measure approximate temperatures of the coil with various current levels. At 600 mA, the 34-AWG, 80 turn coil reaches 67 °C at steady state. At 800 mA, the temperature exceeds 96 °C when the current is applied for more than 30 seconds. So, this current is maintainable for short-bursts but not steady state.

While this design is acceptable for my application where I am operating in room temperature environments, it appears to be susceptible to demagnetization at high current operating points or in elevated temperature environments. A better design (in this respect) should have a thicker magnet per gap width. In brushless motors, permeance coefficients are often greater than 4 [107].

Even with this permeance coefficient, the current density that this actuator is capable of exceeds many macroscopic electromagnetic actuators. Dividing the drive current by the cross sectional area

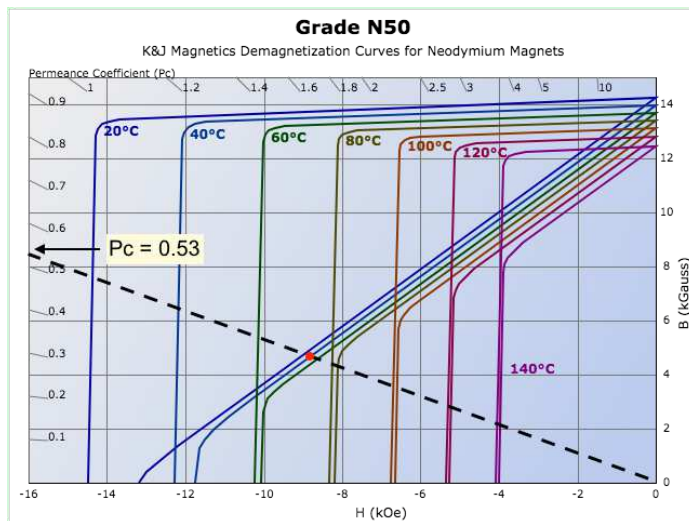


Figure 5-6: The demagnetization curve for N50 magnet from [106] with overlaid load line. Beyond 70 °C we risk hitting the knee of the curve and irreversibly reducing the residual flux density of the magnet.

of a single turn of the wire gives a measure of the current density. In this case the 600 mA operating current represents a current density of 24.2 A/mm², which is more than two times greater than the recommended maximum current density for macroscopic electromagnetic actuators [107]; this is possible because of the relative scaling of surface area and volume, which allows better heat transfer out of the coil [108].

Table 5.2: Measured Characteristics of the Actuator Component

Coil Turns	80
Max. Continuous Current	0.6 A
Max. Continuous Current Density	24.2 A/mm ²
Force (blocked mid-stroke)	42 mN
Stroke (no load)	2.1 mm
Resonance (incl. parallelogram linkage)	75 Hz
Overall Mass	511 mg
Energy Density	89 mJ/kg

Dynamic Characterization

To measure the dynamic performance of the actuator, I supply a pseudo-random voltage across the actuator and use a high-speed camera to measure its response. The coil component of the actuator is rigidly fixed while the magnetic component is constrained by an assembled parallelogram flexure linkage, which approximates linear motion for small displacements. Dividing the frequency response of the output displacement by that of the input voltage, results in the transfer function that describes how the output relates to the input over a range of frequencies. This data, presented in Figure 5-5B, is described well by a second-order spring mass damper model with a 75 Hz natural frequency and a quality factor of 6.2. This model is useful in predicting the performance of the actuated system

over a range of frequencies and gives an estimation of the bandwidth of the actuator. The static and dynamic performance of the actuator component is summarized in Table 5.2.

I use an A-Star microcontroller (Pololu) to generate the actuation signals. A 16-bit LFSR is used to generate white noise which is output as PWM and amplified by an H-bridge (DRV8838). To measure the displacement I use the high-speed camera (Chronos), processing the data with motion tracking software (Tracker), and synchronize the data collection with the actuation signals.

Replacing the parallelogram linkage with a rigid strut and performing this same analysis gives an upper bound for the maximum bandwidth that this assembly framework is capable of supporting. The displacements of this rigid structure are two orders of magnitude smaller than that of the actuated mechanism and so a laser displacement sensor (MicroEpsilon) is used to measure the displacement over time. The actuator is controlled to perform a frequency sweep and the magnitude of the displacement at each frequency is recorded. The measurements, shown in Figure 5-7, show that the structure has a first resonant mode of 620 Hz. This is in close agreement to the simulation result of 692 Hz without any parameter tuning. This frequency is not a clearly defined upper bound, but instead represents a rule of thumb that structures assembled in this way should be usable up to near this frequency without worry about exciting unintended resonant modes.

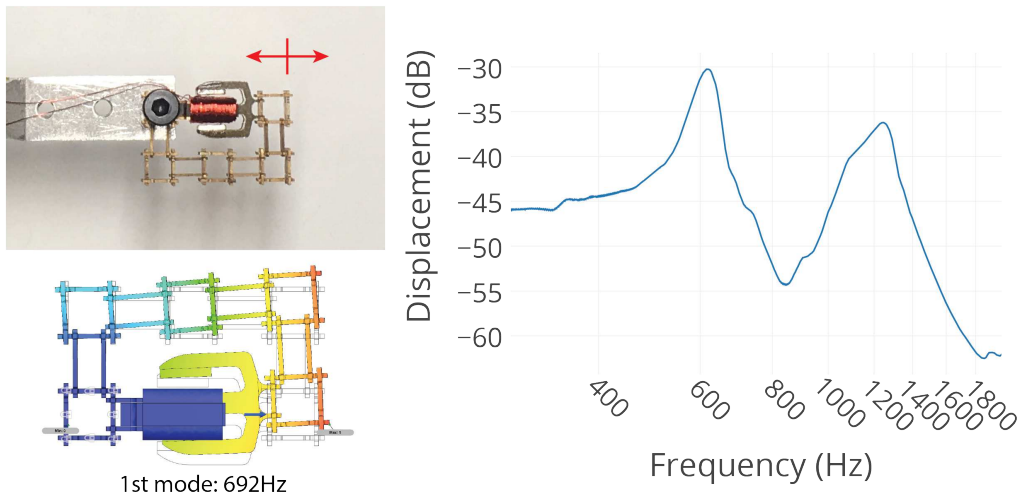


Figure 5-7: By using an actuator to excite a rigidly assembled structure it is possible to determine the resonant modes. The experimental results show a first resonant mode at 620 Hz, which closely follows the simulation result of 692 Hz.

5.2.3 Production

While the actuator components are more geometrically complex than the basic structural parts, they are still designed to be relatively easily mass produced and are made using a combination of direct-write processes including wire electrical discharge machining, laser micromachining, and CNC milling (Figure 5-8).

The actuator parts are composed of two part-types: the coil part and the magnetic part. The core of the mandrel that supports the coil is first machined on a Roland MDX-540 CNC milling machine. Conductive 254 μm thick phosphor-bronze layers are cut as a stack with the wire-EDM

and these are then bonded to the core using the same laminate process described above. I then wind the coil on the mandrel using a benchtop coil winding machine (Adams Maxwell). This process is surprisingly fast and I am able to wind a 320 turn coil in less than 60 seconds. Coils of this size are regularly produced in large quantities, relatively inexpensively using surface mount inductor coil production techniques [109].

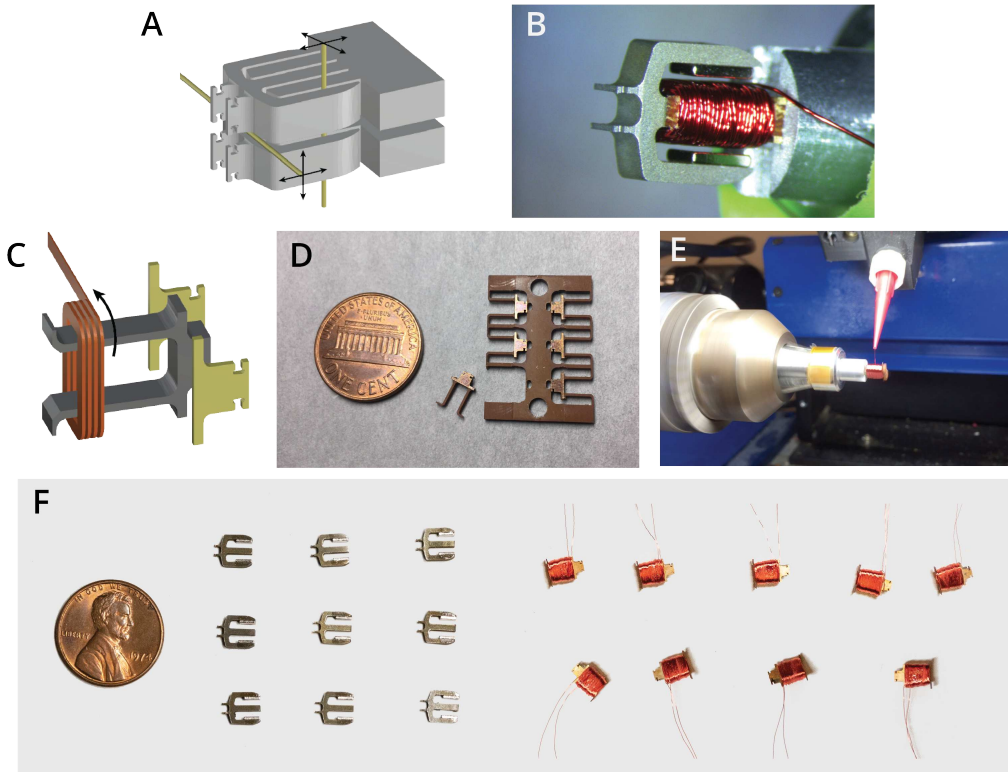


Figure 5-8: I developed a number of efficient methods to prototype these parts in small batches. The magnet part is cut in two orientations by wire-EDM (A,B). The coil part is produced in a two step process in which a mandrel is first made by laminating connectors onto a composite core and then wound in a coil winding machine (C,D,E). Using these techniques I produce 9 actuators in an afternoon (with the potential for many more).

The magnetic core is cut in batches from bar stock in the wire-EDM. Since the core features intricate geometry on multiple sides, I cut one profile, rotate the stock 90 degrees, cut another profile, and then cutoff all of the parts at once. Using this process enables the production of an array of nine magnetic cores in a little over an hour. Rare-earth permanent magnets (N50) are then fixed to the inside of the magnetic core arms with cyanoacrylate adhesive (Loctite 401). These production processes are illustrated in Figure 5-8.

5.2.4 Discussion

The bandwidth measured in this chapter is largely a result of the compliance of the mechanism elements. This bandwidth should be viewed as a design parameter that can be increased based on the requirements of task (up to the 620 Hz mode of the structure). This can be done, for example, by

simply stiffening the flexures using a thicker flexible membrane, shorter flexure length, or additional flexing elements.

The actuator component developed here compares well against other millimeter-scale actuators that have been recently reported in research. I compiled data regarding actuator force, mass, stroke, and bandwidth and plot the normalized actuator force (per weight) against maximum stroke (Fig. 5-9) for a number of piezoelectric, electrostatic, and miniature electromagnetic actuators. Wherever possible I include the mass of the whole actuator (stator and mover) as well as the mass of the motion constraint. I did not include shape memory alloy based actuators in this comparison because while they are capable of extremely high force densities, they were deemed to be too inefficient, too low speed, and too susceptible to ambient temperatures for the applications targeted in this work.

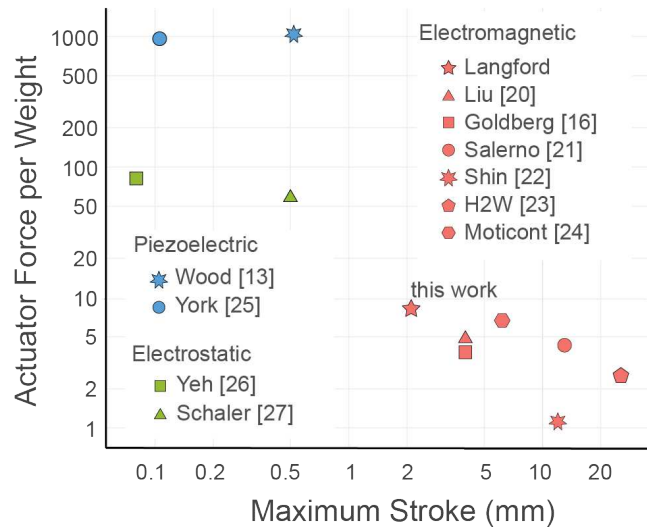


Figure 5-9: Comparison of normalized force versus stroke with other research and commercial millimeter-scale actuators. This actuator interpolates between existing small scale electromagnetic actuators and the force-dense but stroke-limited electrostatic and piezoelectric actuators.

The actuator component developed in this work has the highest normalized force (blocked force per weight) of any of the comparably sized electromagnetic actuators presented here [110] [103] [111] [112] [113] [114]. Piezoelectric [100] [115] and electrostatic [104] [116] actuators produce more force per mass but are more limited in their available stroke.

Even so, this actuator pails in comparison to biological muscles in terms of force density. Biological muscles have a specific actuation stress (pressure per mass) that is 25 times the maximum limit for an electromagnetic actuator [117]. On the other hand, biological muscles are relatively slow compared to these kinds of electromagnetic actuators with most working at a rate of up to approximately 7 Hz (with some exceptions such as small flying insects [118] [119]). Developing topologies and mechanisms that trade bandwidth for force density could be worth exploring in more depth. In chapter 6, an embodiment of this concept is developed as a walking motor. Section 11.2 does a more thorough analysis of this force density comparison.

Chapter 6

Walking Motor

Given the structure, mechanism, and actuation capabilities developed and covered in previous chapters, it is possible to start assembling machines that integrate these functionalities to perform useful behaviors.

I built a Discretely Assembled Walking Motor (DAWM) to demonstrate the integration of structure, mechanism, and actuation. The DAWM system takes small cyclical steps to produce long range motion of a sliding or rotating element. This principle of locomotion is most commonly used with piezoelectric actuators [120] for applications such as nanometer-precision stages [121] and focusing motors in DSLR cameras [122]. Here, I use the voice coil actuator components developed for the assembled structures to enable the same kinds of motion with larger displacements and lower voltages.

6.1 Design

The walking motor is composed of five part types: structural nodes, rigid and dual-hinged struts, and magnetic and coil part types (Figure 6-1). The two actuator components are oriented perpendicularly to one another and the output of the actuators is coupled to a motor tip through multiple four-bar parallelogram linkages, which distribute the two degrees of freedom at the tip into a single degree of freedom at each actuator. As the motor tip is driven cyclically, it engages with a grooved sliding or rotating element. In this design, the motor tip consists of a 0.5 mm cylinder, which provides quasi-kinematic mating with the triangular grooves of the rotor. The triangular grooves are spaced 0.75 mm apart and correspond to a segment of the approximately circular trajectory of the motor tip. This geometry is designed to allow for the correction of motor-tip positioning errors within ± 0.15 mm. The motor works with a variety of different surfaces including ones that are smooth; however, the grooved surface employed here provides the highest repeatability.

6.2 Characterization

To drive the actuator components within the walking motor, I use a custom control board which features an ATmega32u4 microcontroller and four DRV8838 H-bridges. A supply voltage of 1.4 V is provided to the board, which then modulates the current in the voice coil actuators with PWM. The

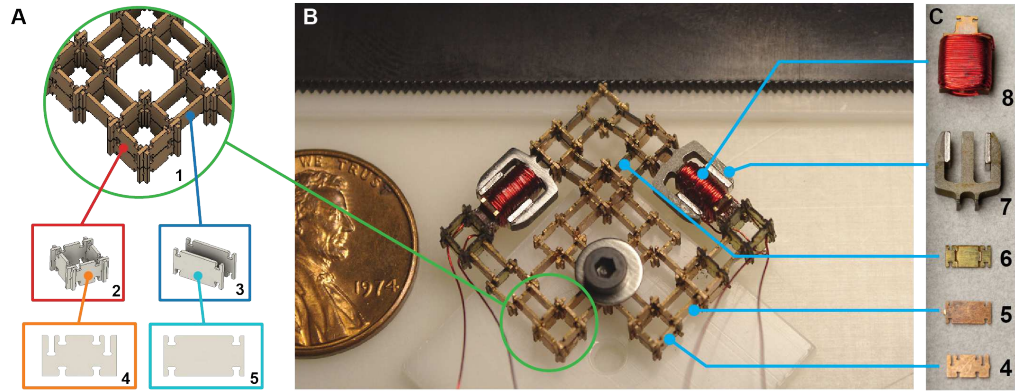


Figure 6-1: The walking motor is assembled from five part-types: rigid nodes and struts, flexible struts, magnet parts, and coil parts. Here, a single layer walking motor engages a linear slider.

current through the voice coils is monitored by a 0.1Ω sense resistor and a benchtop oscilloscope (Tektronix MDO3024).

For the rotary motor application, the walking motor is attached to a 3D printed fixture (Sindoh) which enables the distance between the motor and the rotor to be controlled precisely using a fine-adjustment screw (Thorlabs). The grooved rotor is laser cut or wire-EDM cut and press-fit on a 608 skate bearing, which provides a low friction rotational degree-of-freedom. This experimental setup is pictured in Figure 6-2.

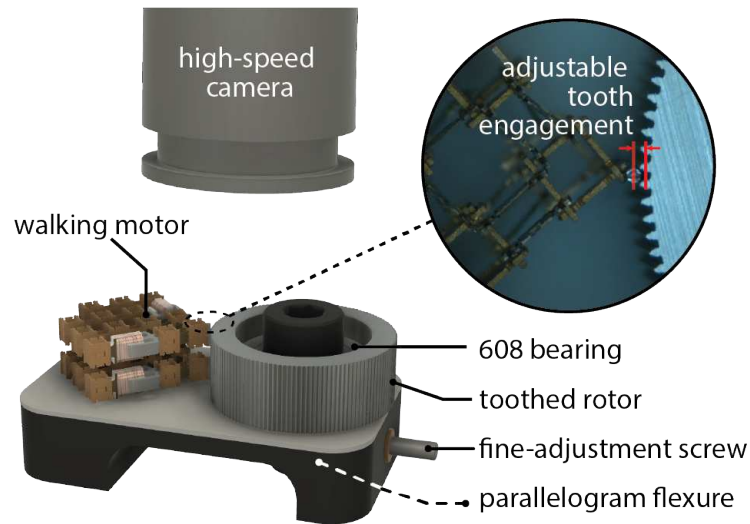


Figure 6-2: The experimental setup used to characterize the walking motor. A fine adjustment screw deflects a flexure to adjust the spacing between the motor and the toothed rotor.

6.2.1 Speed and Repeatability

Each actuator of the walking motor is driven with 90-degree phase-shifted sinusoidal or trapezoidal waveforms, corresponding to a roughly circular trajectory of the motor tip. I characterize the

repeatability of the walking motor across a range of stepping frequencies, by taking 10 steps at each frequency and computing the average velocity at each. The frequency is swept up and down, increasing and decreasing the step rate a number of times, to get a sample size of six at each tested frequency.

To measure the speed of the rotor, a standard video camera is used to track a feature on the rotor to extract the position over time and measure the effective velocity. I use a high-speed camera (Chronos) to inspect tooth engagement with the rotor at high step-frequencies.

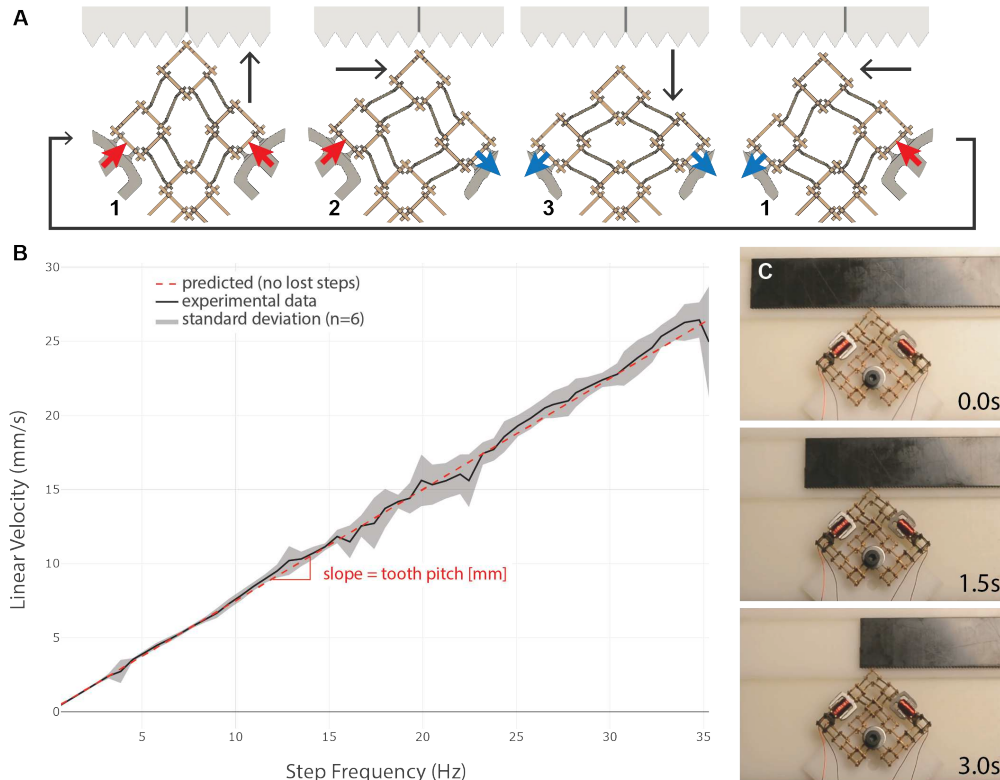


Figure 6-3: Speed and reliability testing done on a single-layer walking motor illustrates the series of steps during one actuation cycle (A) as well as the progression of a slider over three seconds (C) and the resulting velocity of the mover/rotor (B). The results show good agreement to the idealized relationship between frequency and velocity.

The results (Figure 6-3) show good agreement to the predicted performance. Below 12 Hz, the difference between measured and predicted velocities is negligible. Between 12 Hz and 34 Hz, there is more variability in the relationship between step frequency and velocity with the largest standard deviation being 25% of the mean. However, the overall slope remains consistent with our predictions. This indicates that at the higher step-rates the motor is just as likely to take a double-step as it is to miss a step. I hypothesize that step variability occurs because the motion amplitude increases as the step-rate approaches the resonant frequency of the walking motor and causes the motor to occasionally skip a tooth. Beyond 35 Hz the velocity drops dramatically as the steps become very erratic and intermittent, indicating a maximum open loop speed of approximately 25 mm/s.

This 25 mm/s maximum exceeds many commercially available piezo walking motors [121]. The corresponding 35 Hz maximum frequency is limited, in part, by the electronic drive circuitry. The

actuator uses 34-AWG wire, resulting in a low inductance coil ($15 \mu\text{H}$) that experiences current ripple losses when driven directly by an H-bridge with insufficiently high frequency PWM (1kHz, in this case). Decreasing the wire diameter to 40-AWG and increasing the PWM frequency to 31.25 kHz would reduce the current ripple by 88% and the resulting dissipation by 70%, potentially enabling actuation rates up to the 75 Hz bandwidth of the actuator-flexure combination.

The actuation rate could be further increased by stiffening the flexure degrees-of-freedom. These flexures were designed to be highly compliant to enable long strokes to suit a wide variety of applications. Given the electrical time constant of the actuator coils ($\tau = L/R = 100\mu\text{s}$), actuation rates of several hundred cycles per second (up to the bandwidth of the structure) should be possible at the expense of the actuator stroke. While the DAWM system has not been tested to fatigue, prior research has shown that the flexural hinges used here can be made to survive millions of cycles before failure [98].

6.2.2 Force Additivity

In the case of a single walking motor, it is impossible to generate continuous force since the motor tip needs to disengage from the rack in order to move to the next tooth. However, using multiple walking motors in a stacked configuration, as depicted in Figure 6-4, enables continuous force production. In order to ensure that one tooth is always engaged with the rack, it is advantageous to be able to modulate the duty cycle of the motor-tip trajectory; that is to say, I control the time the tooth is in the engaged position relative to the disengaged position. I do this with a parametrically defined trapezoidal waveform, which is described by two parameters: on-time (engaged in rack) and off-time (disengaged from rack). Within a given walking-motor layer, the phase offset is always set to 90-degrees to ensure the trajectory of the motor tip is roughly circular. The phase between layers can be adjusted to modulate the degree to which the multiple walking motors are engaged with the rack simultaneously. At one extreme, in which there is no phase offset between walking motors, I expect the stacked walking motor to have the same behavior as a single walking motor but with twice the amount of force with each tooth engagement. At the other extreme, in which the two motors are out of phase with a phase offset of 180-degrees, I expect to see overlapping engagement of the motor tips and expect a more continuous force output from the stacked motor.

To characterize the effects of phasing multiple walking motors, I measured the blocked force of a stacked two-layer walking motor while driving at a 1 Hz step rate to ensure sufficient resolution to resolve the full force profile (Figure 6-4). To measure the blocked force of the motor, I use a milligram loadcell with a 24-bit ADC and amplifier (TI-ADS1231). The blocked force varies depending on where the motor engages the tooth of the rotor, which, in turn, is affected by where the motor and rotor are positioned relative to the load cell. To ensure consistent results, I take data wherever the peak force is maximum for a given trial. I determine this position by plotting the force output in real-time and slowly adjusting a micrometer to move the motor and rotor assembly relative to the loadcell.

When the two motors are driven in phase, their peak force is approximately twice (70 mN) that of the single motor (30 mN). When the two motors are driven out of phase, they produce a more uniform force which varies between 20 mN and 50 mN. The magnitudes of these forces are on par with the maximum blocked force of the individual actuators themselves. In the single motor case, 79% of the maximum blocked force of a single actuator is translated to the rotor at its peak force.

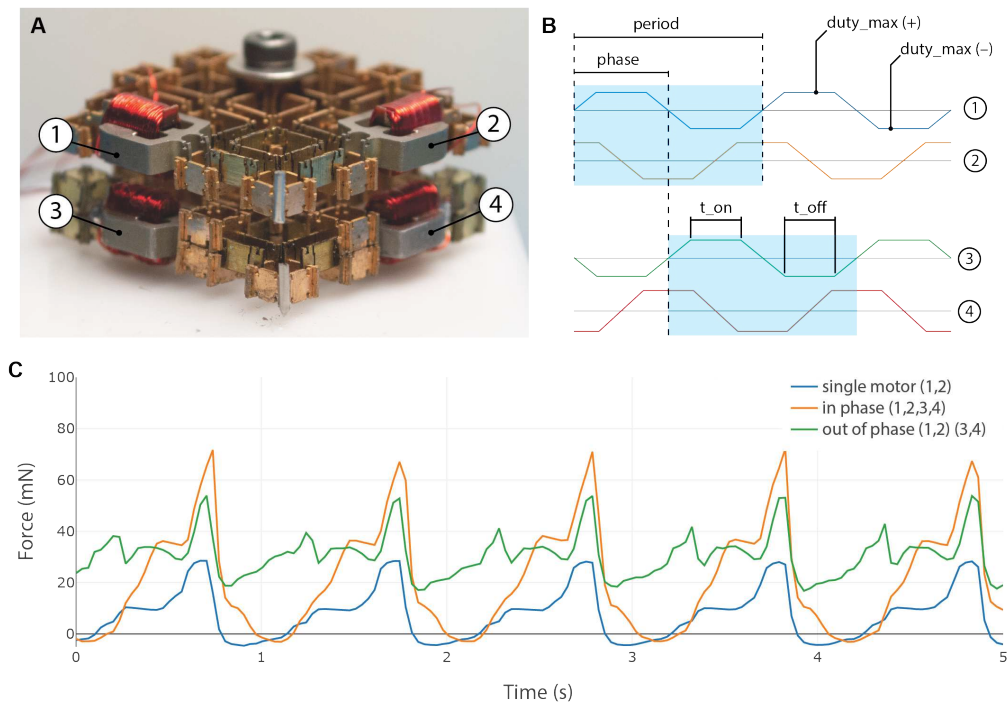


Figure 6-4: The force output of the walking motor (A) driven by a trapezoidal waveform (B) out-of-phase and in-phase (C). Continuous force production is possible when driving multiple walking motor layers out of phase with each other.

In the two-motor case, 92% of the maximum blocked force of two single-actuators is translated to the rotor at its peak force. This indicates that the assembled transmission is relatively lossless, at least in terms of static force transmission.

6.3 Discussion

This chapter has demonstrated the ability to assemble long range linear and rotary motion from individual discrete parts. Stacking two walking motors has been shown to both increase the force output and enable continuous force production. This could be extended with the use of even more walking motors to enable greater force production. A question remains about the possibility of using multiple walking motors to increase the speed of actuation. Doing so would likely require very low duty cycle strokes such that the motor tip is only engaged for a very short period of time. This is how biological muscles amplify the speed of relatively slow (≈ 5 Hz) individual molecular motors to the 1500 Hz effective stepping rate [123].

The efficiency of a walking or inchworm motor in most cases is not high. This can be evidenced by looking at the drive cycle and realizing that only a fraction of the time is the input energy converted directly into output work. (1) Current flows into locking actuator, producing electromagnetic force proportional to the current. This force balances with the reaction force of the flexural mechanism, and the motor tip displaces. (2) At some point the motor tip engages the rack of the moving element and the flexure displaces no further. (3) The drive coil now start producing force which goes into

displacing its own flexures and accelerating the moving mass. (4) Once it reaches its maximum stroke, the current in the locking actuator is reduced and eventually reversed to disengage from the rack. The drive coil is then also reversed and the cycle repeats. Of these four actuations only one (#3) goes into producing useful work.

Techniques exist to improve the efficiency of these actuators. First of all, these kinds of motors can operate much more efficiently if driven at resonance since the actuators are effectively used to pump energy into the dynamic system [122]. Rather than quasi-statically overcoming the flexure stiffness, the flexure stiffness is excited, keeping energy in the system. Other strategies such as using flexible drive elements have been shown to be capable of achieving 8% efficiency for electrostatic inchworm motors. However this strategy requires a shaped ratchet-pawl interface that restricts motion to a single, irreversible direction [124].

To constrain the long range motions, I use commercially available ball bearings and sliding surfaces for rotary and linear motion, respectively. The part set developed in this assembly framework is capable of making linear and rotary constraints, but would require custom part-types in order to interface with the motor-tip and so I leave that for future work.

Chapter 7

Walkers

Once I was able to assemble the walking motor. I wondered if I could make something that walks and locomotes. To do this required the addition of a foot that can attach and detach from a surface. Electropermanent actuators are ideally suited for this kind of latching actuation on ferrous surfaces.

7.1 Electropermanent Feet

Electropermanent actuators are made by biasing a hard magnet with a soft one (Figure 7-1). A coil is wrapped around both (or, alternatively just the soft magnet). A pulse of current through the coil is able to flip the polarity of the soft magnet. This either confines the flux to circulate only between the magnets (when the polarities are mismatched), or allows the flux to flow out through the poles of the actuator to create attractive force with the permeable surface.

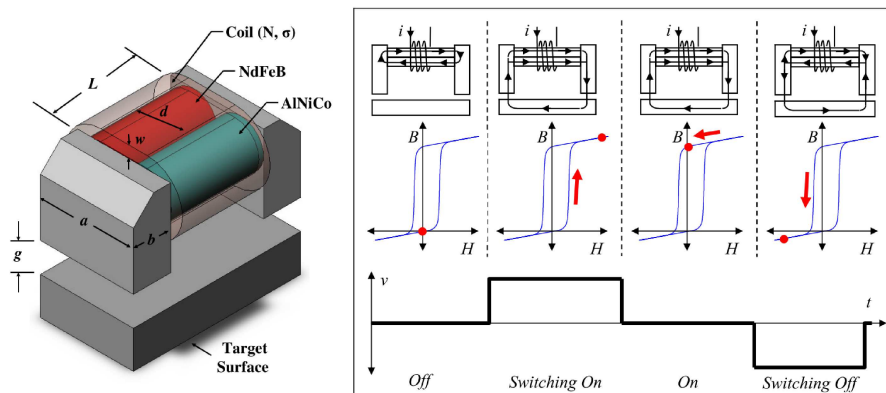


Figure 7-1: Reproduced from [58]. (Left) Construction of electropermanent magnet. (Right) Operation of the electropermanent magnet through the hysteresis loop of the BH curve.

Electropermanent actuators are better suited for this task than electromagnets for two primary reasons. The first is that below a frequency threshold electropermanent actuators are far more energy efficient. This is because they hold their state without any current. To attach to a surface a pulse of current is used to flip the soft magnet and then the actuator functions just like a permanent magnet would. The second reason is that the electropermanent magnet is a high reluctance magnetic

circuit by design. This is because the permeability of the hard and soft magnets is much closer to air than it is to iron and so their presence in the circuit is essentially a large air gap. This means that an air gap between the actuator and the surface contributes far less to a reduction in attractive force than it would in an equivalently sized electromagnet (Figure 7-2 A).

I had initially tested making a walker with electromagnets rather than electropermanent magnets and found that the attractive force was highly sensitive to very small air gaps between the foot and the surface. This manifested in the walking robot being very sensitive to the orientation of the wires that were providing power to the actuators. A walking robot using electropermanent feet does not suffer from this same sensitivity.

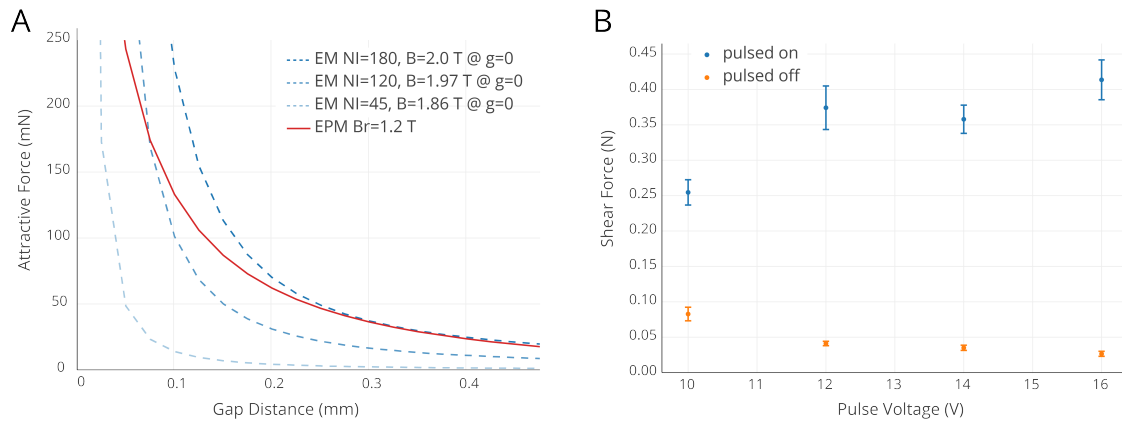


Figure 7-2: Electropermanent magnets are far less sensitive to large air-gaps and produce more attractive force than an equivalently sized electromagnet (A). The degree to which the electropermanent actuator is switched can be controlled (B). For this application, the 16 V actuation is beneficial for the biggest change in frictional force.

I tested the shear force exerted by the electropermanent actuator in its on and off state at a number of different voltage levels from 10 V to 16 V (Figure 7-2 B). The pulse duration was set to 300 μ s. I found little difference in performance by increasing this pulse duration any further. I used a custom tabletop materials testing machine with a milligram load sensor to perform these tests as I anticipated very small (<1 N) forces.

The actuator is placed on a ground steel surface and a post is used to couple the actuator to the load cell. The steel piece is attached to the moving table of the testing machine. During the test the steel is advanced towards the loadcell and the maximum force seen by the loadcell is recorded. This provides measure of the dynamic friction between the ground steel surface and the actuator.

Testing the electropermanent feet at multiple different pulse voltages shows how the magnitude of the current pulse effects the performance of the foot. It's clear that a greater difference between the on and off state is achieved for higher voltages. In particular, it's clear that 16 V (the maximum voltage permitted by the H-bridge I'm using) should be used for optimal performance.

It is also apparent that the actuator does not switch fully off since shear force does not drop fully to zero in the off state. This could be an error in the construction leading to the soft magnet not fully switching polarity. For example, the winding may not be evenly distributed or leave some portion of the magnet exposed. While it would be ideal that the force in the off state drops perfectly to zero, the almost 20x increase in shear force between the on state (0.425 N) and off state (0.025

N) is entirely sufficient to provide attachment and detachment for an assembled walker.

I also measured the normal force exerted by this actuator. On a ground steel surface the normal force measures $2.23 \text{ N} \pm 0.24 \text{ N}$ ($n=6$). This is enough force to support the weight of over 400 actuator components (511 mg).

7.2 MOTILE – Modular Tiny Locomotion Element

The walker, MOTILE, is assembled from six part types: rigid struts, rigid nodes, 2-DoF struts, a magnetic part, a coil part, and electropermanent feet. A central Lorentz force actuator provides the motive force and the relative order of when the electropermanent feet are switched determines the direction of motion.

I tested the MOTILE on a number of different ferromagnetic surfaces including ones with a thin layer of lower friction material (Kapton). I ultimately found the best performance had the electropermanent feet in direct contact with a ferrous surface with a thickness greater than or equal to 1.5 mm. This ensures that the foot provides the full attractive force that it is capable of. I also found that adding a small plastic spring helped accentuate the difference in friction of the on and off states of the feet and was beneficial for consistent locomotion. These two springs (one per electropermanent foot) have the effect of reducing the friction between the unlatched foot and the surface without significantly effecting the friction force of the latched foot and the surface.

In addition to testing a range of different surface materials, I also tested the robot in a number of different orientations. Because the potential shear force ($>0.4 \text{ N}$) and the normal force (2.2 N) of the feet are both much greater than the weight of the robot ($\approx 0.02 \text{ N}$), the robot is able to walk up vertical walls as well as upside down on inverted surfaces (Figure 7-3).

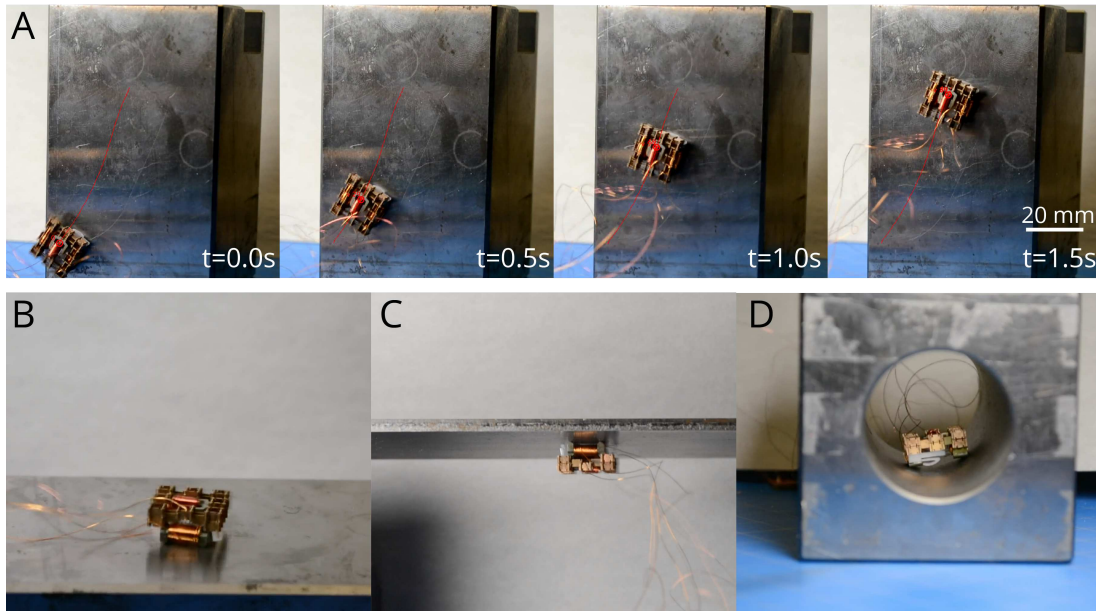


Figure 7-3: The walker is able to walk on surfaces of a variety of orientations including up vertical walls (A), on horizontal surfaces (B), upside down (C), and on non-flat surfaces (D).

I used motion tracking software (Tracker) to measure the speed of the MOTILE in a variety

of orientations. In analyzing the speed of the walker as it climbs a vertical ground steel block, the walker takes a trajectory that's roughly 60-degrees from horizontal. The MOTILE is driven at approximately 45 Hz. The speed is very consistent and measures approximately 36.2 mm/s going up and 44.2 mm/s going down. Doing the same on a flat surface, I measure an average speed of 37 mm/s over 5 trials.

It helps to translate these speeds to a “body-length per second” equivalent in order to compare this performance to other mobile climbing robots. Given its 15 mm body length, it climbs up the block at 2.4 BL/s and down at 2.95 BL/s. It moves on a flat surface at 2.46 BL/s. Comparing these values to others reported in recent literature reveals, surprisingly, that this little robot is among the fastest vertical climbing robots. That being said, there are certainly many caveats and limitations with this statement. For one, this walking "robot" is driven entirely off-board by external control electronics and as such carries less weight than robots that are untethered. Another severe limitation of this robot is the need for a ferromagnetic surface. However, this is certainly not the only robot to use magnetic forces for climbing and others have argued that many desirable applications for mobile climbing robots would be satisfied with the use of magnetic forces [125][126][127][128].

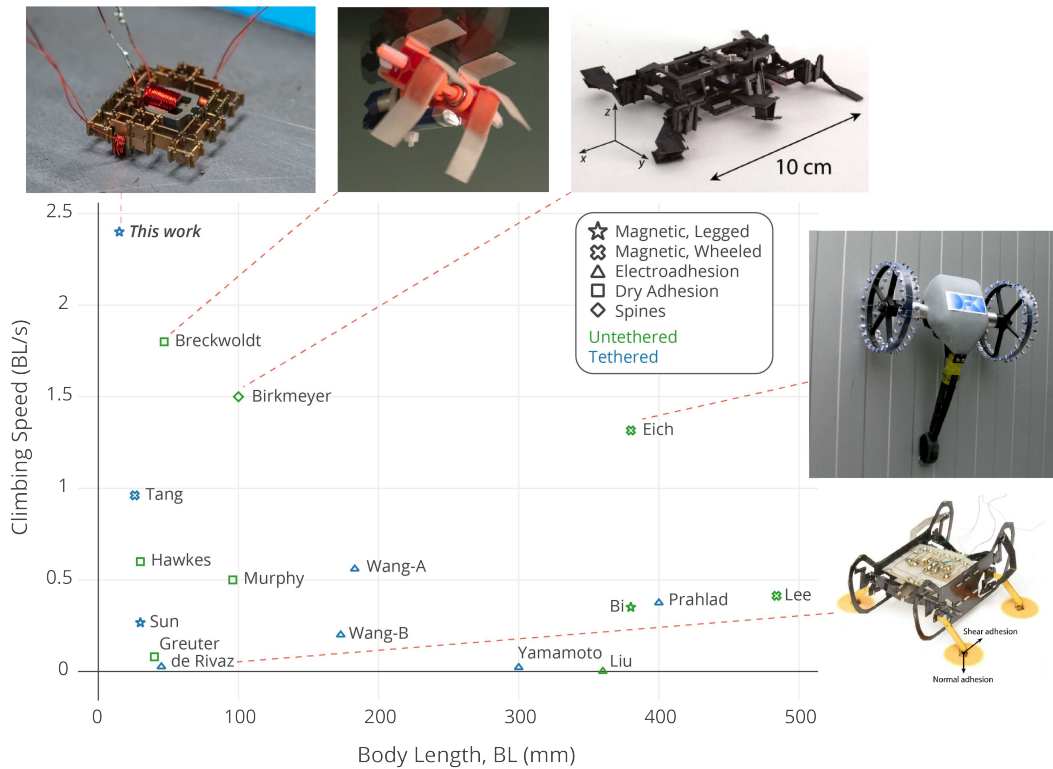


Figure 7-4: Comparing the climbing performance of the single degree-of-freedom MOTILE walker to other vertical climbing robots. This “robot” represents both the smallest and fastest (in body-lengths per second) of any robot in recently reported research but is not able to turn and doesn't contain onboard power or control.

7.3 Discussion

While I've demonstrated the assembly of a single degree-of-freedom walker, MOTILE, that can only move forward or backward, these modules can be composed to build positioning devices with the ability to move in multiple directions. Two MOTILE's placed side-by-side can be used to move forward and backward as well as turn left and right (Figure 7-5). Four MOTILE's arranged in a cross-shaped circular array can be used to translate in any direction as well as rotate about the plane.

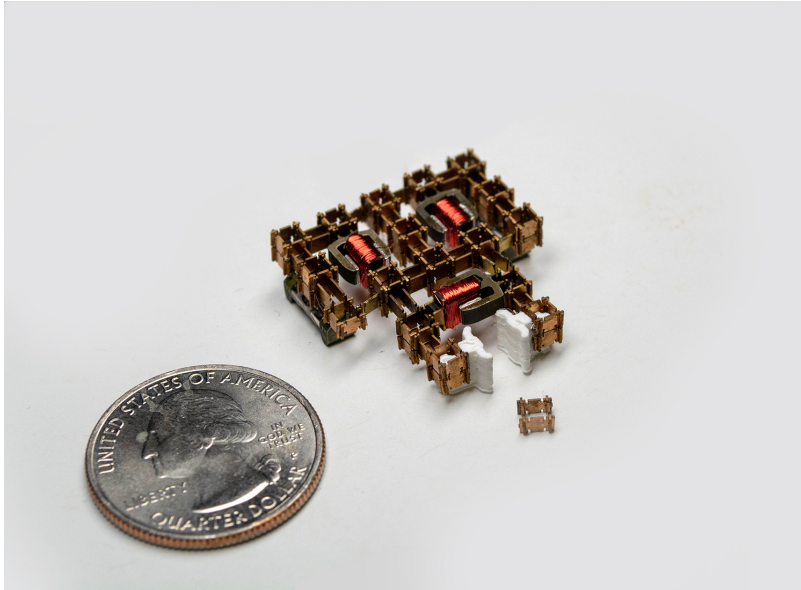


Figure 7-5: Two MOTILEs along with a gripper can be combined to form a mobile assembler that can pickup and place the same building block parts it is made of. This concept is developed further in Chapter 10.4

The motion of an individual MOTILE relies on a friction interface with the surface and so the exact size and direction of each step can vary from step to step. This results in motion that is sometimes not perfectly straight or that varies in speed (for example, climbing up versus down the steel block). It would be beneficial to eliminate these sources of uncertainty in order to build machines that can position precisely and repeatably without requiring an additional sensing mechanism. This could be accomplished with the use of a structured surface that attracts each step to a potential minimum. This structuring could be done with a physically grooved surface. I began testing versions of the feet and grooved surfaces that could be used in this way but encountered difficulties with the feet getting stuck in the grooves. While more complicated, one solution could be to include an additional actuator (or two) to raise and lower the feet with respect to one another. This would allow the disengaged foot to clear the top surface of the grooves before planting down in the next groove. Another potential way to structure the surface for repeatable open loop motion could be with a surface with spatially varied permeability. This strategy is what is used in linear stepper motor platens to give the motor its discrete steps. This could be fabricated relatively easily by incorporating permeable slats in a non-permeable surface and certainly seems worth exploring.

Beyond electropermanent feet, there are certainly other kinds of “feet” that could be used to

create locomotion. Directional friction pads, for example, would enable motion on arbitrary material flat surfaces. This strategy would only permit movement in a single direction (not bidirectionally). However, multiple walker modules could be combined to produce forward and turning motions.

Chapter 8

Positioning and Manipulation

Beyond the locomotion capabilities developed in Chapters 6 and 7, the ability to assemble systems that combine structure, mechanism, and actuation also enable the development of positioning and manipulation devices.

8.1 Positioning

Compliant flexures are often desirable in micro-positioning and scanning applications since they eliminate both backlash and friction, making open-loop positioning repeatable and reliable. These kind of systems are often powered by either electromagnetic and piezoelectric actuators. Positioning stages for precise high-speed tasks often use parallel configurations, where there is a closed kinematic chain, rather than serial configurations [129]. These tend to be higher-performance because the moving mass can be kept to a minimum [94].

A planar positioner amplifies the motion of two actuators to larger displacements of an end-effector tip. The positioner is designed such that the end-effector remains parallel to the base coordinate system through the whole range of motion. This is accomplished with the use of an extended four-bar linkage attached to one of the two arms. The linkage amplifies the motion of the individual actuators by 3.5 times, resulting in a peak to peak displacement of the end-effector of approximately 7 mm.

I conducted a frequency response measurement of the positioner system. Using a multi-functional oscilloscope (Digilent Analog Discovery 2), I measured the complex impedance of the the system from 1 Hz to 2 MHz. The results, pictured in Figure 8-1 B, clearly show a mechanical resonance around 10 Hz, representing the maximum bandwidth for controlled sub-resonant positioning. Near resonance, the displacement of the mechanism increases to 9 mm.

8.2 Manipulation

It is also possible to assemble mechanically actuated grippers and manipulators. I assembled a gripper that converts the linear displacement of two actuator components into a rotational motion of the gripper fingers (Figure 8-2). The ± 1 mm displacement of the actuators is converted into a 4.25 mm stroke of each finger, resulting in a total 9.5 mm displacement between maximum (ungripped)

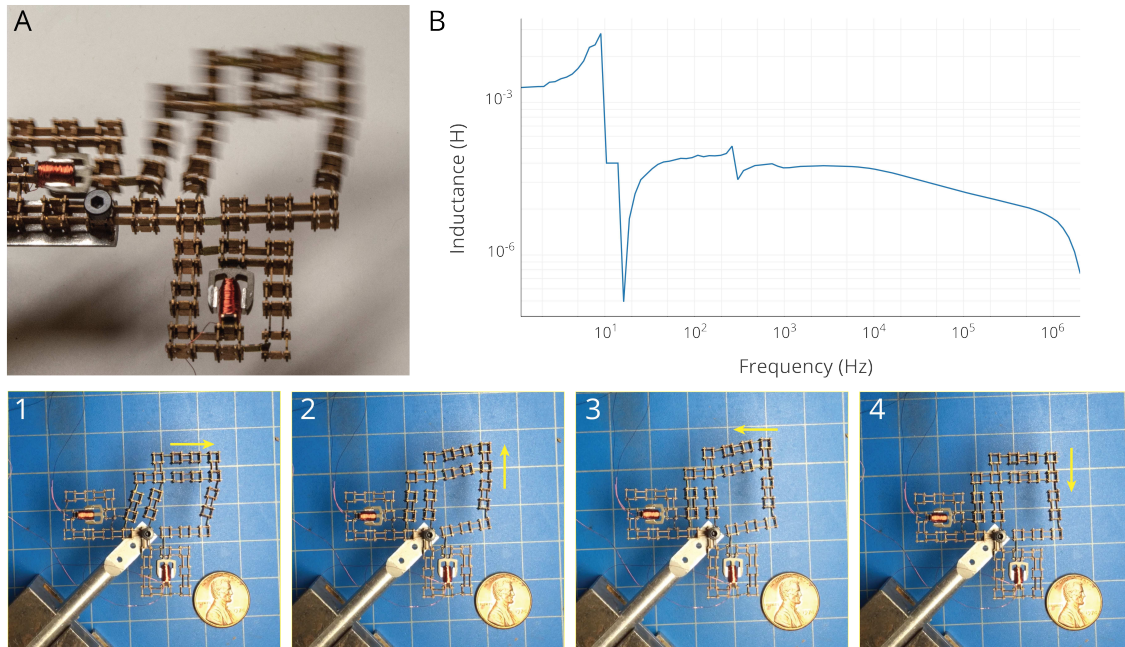


Figure 8-1: An assembled XY-positioning system (A) has a mechanical resonance around 10 Hz (B) and amplifies the motion of two actuators by 3.5 times (1-4).

and minimum (gripped) states. This enables the gripper to pick up, among other things, the parts that it is made of.

The two actuators can be coupled or decoupled. Coupling results in better open-loop coordination of the two gripper fingers. Decoupling could potentially allow for more advanced manipulations, enabling independent control of each finger.

With one extra geometric part-type, it's possible to extend this design from 2.5D to 3D. The additional part type serves to join pre-assembled orthogonal planes (Figure 8-2 C).

8.3 Discussion

Positioner The resonant frequency of the positioner is largely determined by the compliance of the flexure hinges and the moving mass of the end-effector. To increase the possible bandwidth of operation, the bronze parts could be replaced with lighter-weight parts made of fiberglass or carbon fiber, for example.

The positioner provides a good test case to evaluate the longevity of the flexure hinges since it represents a large off-axis load and requires large displacements. I excited the linkage at 20 Hz and let it run continuously for many hours. After 16 hours, an equivalent of 1.16 million cycles, one of the flexure hinges failed. This hinge was supporting a cantilever of 15 connected nodes, which represents a torsional load of approximately $0.223 \text{ N}\cdot\text{mm}$ divided amongst three hinges ($75 \text{ mN}\cdot\text{mm}$ per hinge). This performance could be improved by simply building up more layers to better support the off-axis load.

Another possible way to improve the performance would be to use flexure hinges which a thicker flexible membrane. The current hinge design uses a $25.4 \mu\text{m}$ thick polyimide layer and is designed to

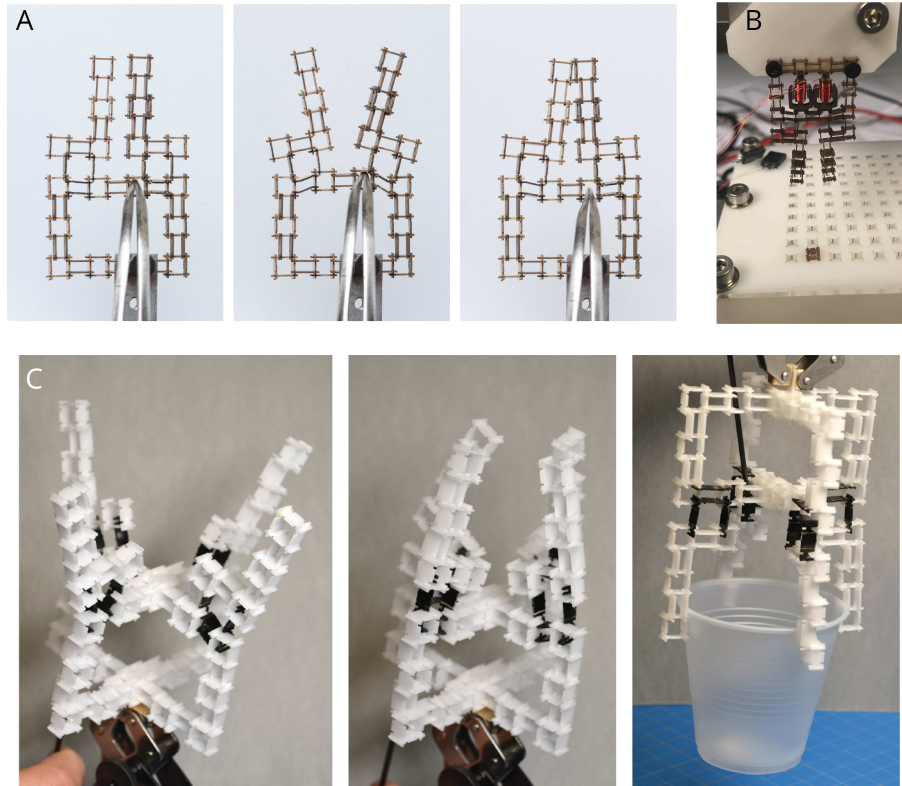
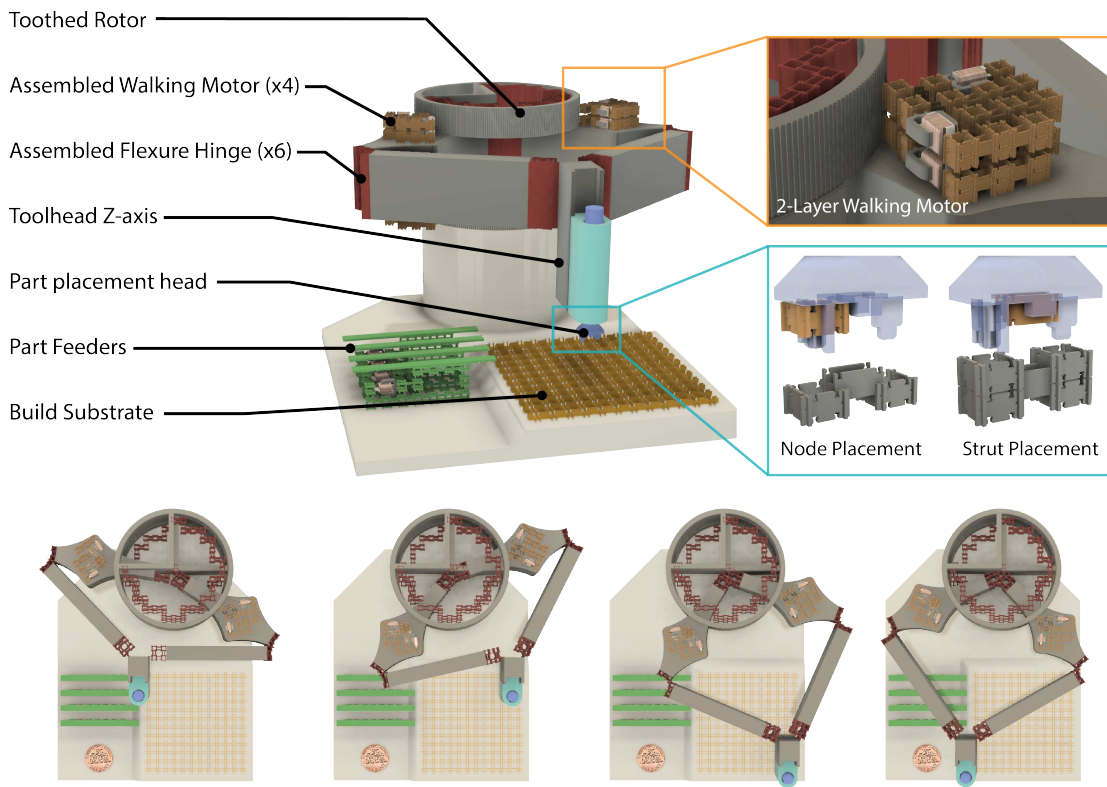


Figure 8-2: An assembled gripping mechanism (A) can be used to pickup and manipulate its own parts (B). The design can be extended to three-dimensions with an additional part-type (C).

be highly compliant. Substituting this layer with one that is $50.8 \mu\text{m}$, or even thicker, may reduce the stroke of the mechanism slightly but would greatly increase both bandwidth and longevity.

Gripper In contrast with other “micro”-grippers that use piezoelectric actuation (e.g. [130]), this kind of electromagnetic gripper does not require significant mechanical amplification to achieve large displacements. While the gripper demonstrated is quite rudimentary, the building block approach potentially enables more extensible designs that incorporate additional degrees of freedom. Custom end-effector interfaces, made using separate processes like 3D printing, could also be incorporated to aid in the manipulation of certain kinds of parts.

Manipulation Tools Based on these positioning and manipulation primitives it should be possible to assemble more advanced manipulation tools that can be used to precisely arrange small parts. Prior work has shown the dexterity that is possible with flexure based linkages for translating, rotating, and assembling small parts [131] [132]. A concept using walking motors to provide large displacement actuation is developed in Figure 8-3. This concept uses a parallel kinematic chain to position and place parts on a lattice. The important functional parts of the machine are predominately assembled using the building block parts developed in this thesis. Concepts for assembling assembly tools are developed further in Chapter 10.4.



12 x 12 x 8 (Lattice-Unit) Build Envelope

Figure 8-3: An assembler concept that uses walking motors to produce large displacements of a parallel kinematic chain to position and place parts in a lattice.

Chapter 9

Circuitry

Up until now all of these machines and systems developed in this thesis have been powered and controlled by off-board electronics. However, because this assembly framework is agnostic to the part production methods used to make parts, it is possible to incorporate parts made using printed circuit board methods to incorporate circuitry into these structures. In this chapter I'll describe how routing, logic, and control systems can be assembled from a small set of parts to enable the integration of electronic functionality within these assembled machines.

9.1 Background

Research as far back as that 1950's has looked at ways to modularize and automate the assembly of electronics. Before printed circuit boards and integrated circuits had established themselves as the standard in the production of electronic circuitry, the US National Bureau of Standards had developed Project Tinkertoy, which sought to mechanize the assembly of electronic components [133] [134]. Project Tinkertoy was based around a set of modular ceramic wafers, each containing a single electronic functionality (such as resistance, capacitance, or a connector for a vacuum tube). These ceramic wafers could be produced in large quantities and patterned with these functionalities relatively efficiently. Then, a machine called the module assembler was able to pick from a feedstock of tiles, stack them, and then solder a set of wires on each side of the module to connect the wafers to one another and give the module its structure. Each of these modules housed the same functionality as a handful of discrete parts and simplified the assembly electronic assemblies by providing this common interface.

More recently, research efforts in digital fabrication have looked at integrating electronic functionality into additive manufacturing processes. Researchers have recently developed conductive ink formulations that enable the controlled deposition of highly-conductive traces [135] [136]. Still, these formulations are one to two orders of magnitude less conductive than bulk metal and often require a post-bake processing step to evaporate the solvent, which limits the substrate material choice. With these conductive inks, researchers have started to show that it is possible to print functional electronics. Using specially formulated anode and cathode inks, researchers are able to print lithium ion [137] and zinc-air [138] batteries. In another study, the conductive inks were conformally printed on 3D substrates to fabricate efficient antennas [139]. Ink-jet printing has also been used in similar

ways to deposit highly conductive silver traces to create electromechanical functionalities like an electrostatic motor [140]. While these printing techniques have shown promise, their integration into useful devices, which combine both electronic and mechanical functionality, have been lagging the research.

An alternative method to automate the assembly of electronics has looked at building block based approaches, in which electronic functionality is abstracted into individual building blocks and then assembled. These building blocks can range in complexity from high-level modules for modular cubesats [141] to simple raw-material parts [85] [61]. Between these extremes are architectures that employ parts that contain limited functionality such as resistance, capacitance, diodes, connectivity, or insulation [23]. In this work, MacCurdy et al., assembled functional electronic circuits from individual component building blocks. The building blocks themselves were made from printed circuit boards and commercially available press-fit connectors were used to join the blocks to each other. A 3D printer was modified with a part placement head and automated assembly was demonstrated through the assembly of an infrared remote control composed of 17 blocks. This building block based approach has proven the feasibility of assembling advanced electronic functionality from a limited part set and is the approach pursued and developed upon in this work.

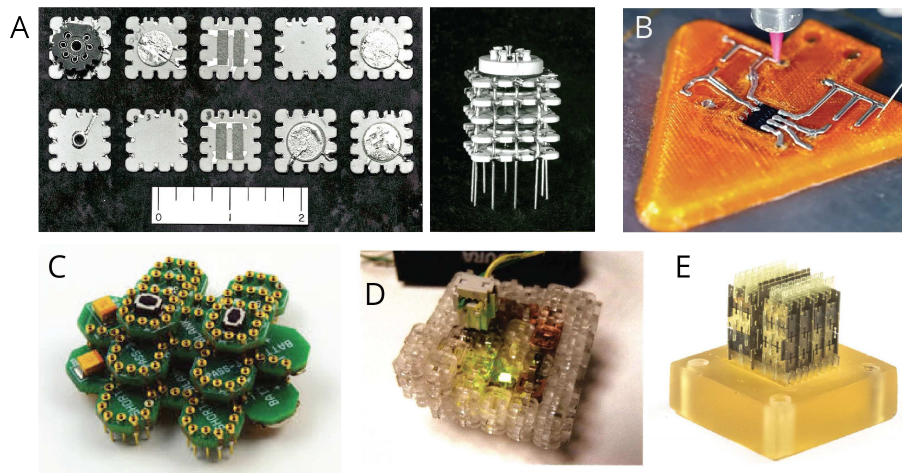


Figure 9-1: Prior work in automating the assembly and integration of electronics. In the 1950's Project Tinkertoy developed a standardized assembly framework for electronic building blocks (A) [133]. Recent work in digital fabrication and additive manufacturing have looked to integrate the printing of conductive traces (B) [142]. Building block approaches have shown the possibility of building advanced electronic functionalities from a small set of parts (C,D,E) [23] [85] [61].

9.2 Routing

The first capability that's necessary to integrate electronic functionality is the ability to route electrical traces. One way to do this within the assembly framework is with the introduction of seven part types to enable routing within the structural lattice. The seven part types include three kinds of node parts (conductive, insulating, and split-conductive) and four kinds of strut parts (conductive, insulating, split-conductive, and crossover) (Figure 9-2). These parts are likely not the minimal set of parts required to route, but have been found to enable the routing of most schematics in a

relatively space-efficient way.

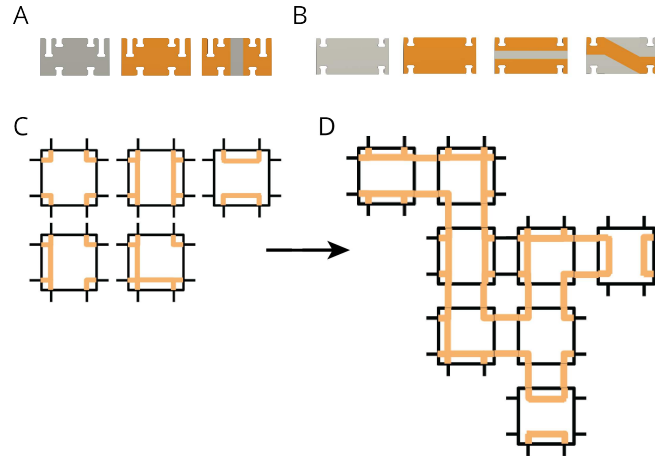


Figure 9-2: Circuit routing is accomplished with seven part types. Three node part-types (A) are assembled to form a variety of routing cells (C). These cells are then linked by variously conductive struts (B) to route traces within an assembled layer (D). The fourth strut type connects traces across layers of the assembly.

The three node parts enable the assembly of a variety of different “routing cells”. These routing cells can then be oriented, arranged, and connected by various kinds of struts to enable the routing of traces within an assembled layer. This routing scheme allows each layer of the assembled structure to be treated like a two-layer circuit board. The fourth strut part-type, a crossover strut, acts as a “via” in this analogy, transferring signals between the top and bottom layers.

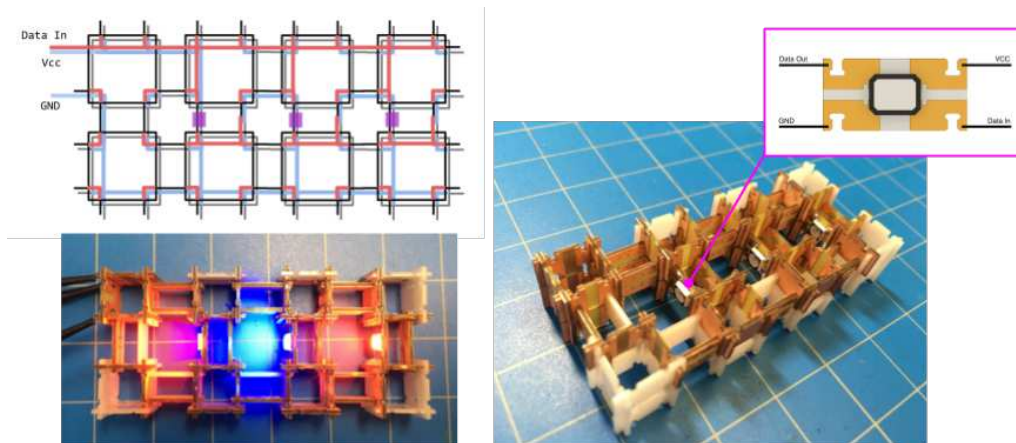


Figure 9-3: A series of serial-controlled RGB LED's (Neopixel) are routed and controlled within an assembled lattice. A serial data line snakes through the middle of the structure while a power and ground rail wraps around the outside.

Based on this routing methodology its possible to route various kinds of circuits within this assembly framework. As an example, I assembled a structure containing three Neopixel RGB LED's (Figure 9-3). These LED's take serial data input to control the output of the red, green, blue LED's. To control multiple LED's, their serial data inputs can be daisy-chained such that the serial data

output of one is connected to the input of the other. In the assembled structure, a serial data line is routed in a serpentine way through the assembly to connect all of the Neopixel LED's. The LED's also need power and ground connections and these are routed in a loop around the edge of the structure.

9.3 Logic

More complicated routing examples involve the creation of digital logic devices from logic gate building blocks.

Using various production methods, it's possible to embed an individual logic gate on an individual building block. Pictured in Figure 9-4, is a design of a logic block that embeds the smallest commercially packaged logic IC's (SOT1226) onto a strut, which can be assembled in the lattice architecture. Logic gates require a maximum of five input/output (I/O) pins: Vcc, GND, A, B, X (where A and B are two inputs and X is the logical output). In routing these building blocks, it's convenient if the Vcc and GND pins are symmetric and appear at both ends of the part. This number of input outputs (7) is compatible within the eight electrical connections available within a single strut-pair.

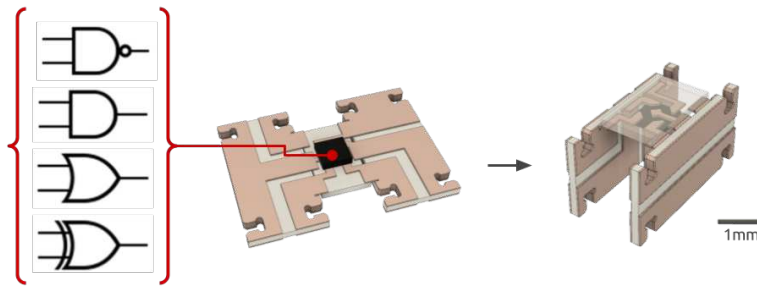


Figure 9-4: Building blocks can be made to incorporate the smallest commercially packaged logic gates.

With two NAND gate building blocks along with a few additional parts to route the required traces, it's possible to assemble an set-reset (SR) flip flop. A D-type flip flop augments an SR flip flop with two additional NAND gates such that the state can be latched and unlatched with a clock pulse. This is assembled with three additional layers to house the two extra NAND gates and an inverter. Furthermore, adding routing to connect Q-NOT to the D-input configures this flip flop to serve as a frequency divider with feedback.

The routing diagram to reproduce the desired circuit within the assembly framework is pictured in Figure 9-5. Power and ground are routed on inner loops of the structure such that they are accessible to all components in the system and so that the signal wires are accessible from the perimeter. Most of the routing is accomplished in a 2x2x3 grid of our lattice with the exception of the feedback loop connecting Q-NOT to D (required for serving as a frequency divider). With the D-type flip flop structures as building blocks, it's then possible to assemble higher-level assemblies like a ripple counter or frequency divider. This structure takes a clock pulse in and counts in binary on the Q outputs and provides an output square wave at one-sixteenth the frequency (Figure 9-5 D).

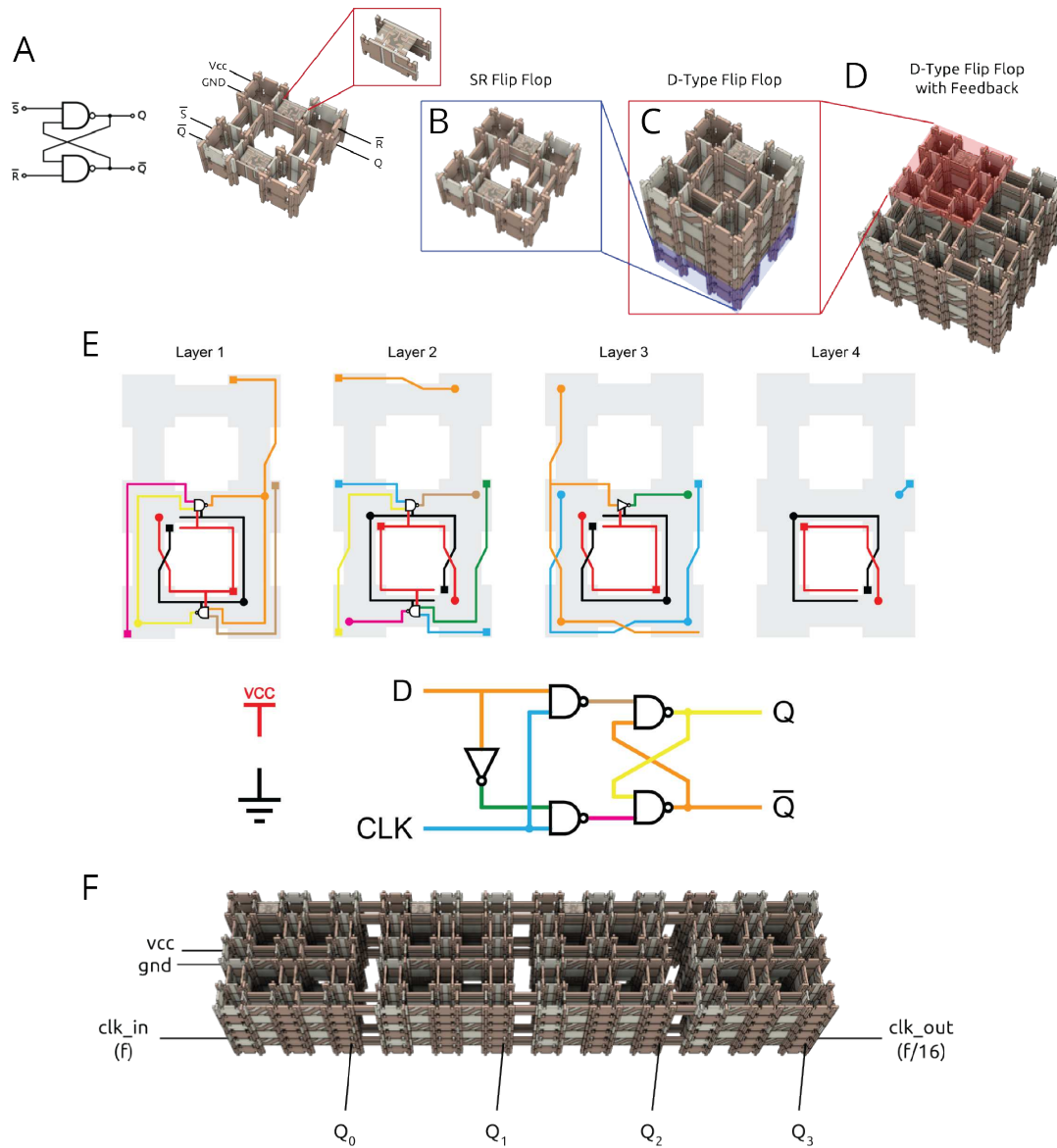


Figure 9-5: With logic gate building blocks a series of digital circuits can be assembled. An SR flip flop is assembled from two NAND gates (A,B) and then is composed to form a D-type flip flop (C). Feedback is added (D) and then used to construct a counter and clock divider (F). The routing for the D-type flip flop is shown (E).

9.4 Control

Beyond integrating logic gates on an individual building block, it's possible to embed even more functionality by taking advantage of the miniaturization of semiconductor products and incorporating whole processors and other devices (H-bridges, Op-Amps, FPGA's) directly on a building block part.

At the scale of the mechanical degrees of freedom in the assembly architecture it is possible to integrate more complex electrical behaviors. In particular, the smallest commercially available microcontrollers are able to fit within a single building block part within the same lattice. This both enables complex behaviors and control systems to be programmed into the parts as well as enables a high degree of flexibility, enabling serial communication, pulse width modulation (PWM), and analog to digital conversion, among other possibilities with a limited part set.

In adding these higher level parts to the assembly framework, higher density routing is sometimes necessary. The development of these higher level electronic part types went through a number of design revisions. I think it's instructive to enumerate them and provide explanations about what makes each attractive and why I ended up abandoning some directions in favor of others.

9.4.1 Control in struts

Embedding processors and amplifiers into individual struts enables the assembly of simple control systems for actuated degrees of freedom.

The first prototype of an assembled control system used an ATtiny10 microcontroller. This microcontroller has just four I/O pins, which is enough to demonstrate the feasibility of integrated a microcontroller into one of the parts of the assembly ecosystem. The details of how the part is fabricated is discussed in section 9.5.

The microcontroller is programmed to generate a triangle wave actuation signal. The building block is arranged in the structure such that the output of the microcontroller feeds into the input of an H-bridge building block. This component amplifies the actuation signals and passes them onto the actuator itself, producing motion. This enables the assembly of actuated degrees of freedom with only two external connections for power.

Beyond controlling a single degree of freedom with a single program, the I/O capabilities of this microcontroller and its integration in the lattice were ultimately found to be limiting. In particular, the bus-width in the lattice needed to be increased. The strut-pair model that works so well for mechanical degrees of freedom, is limiting when trying to assemble control systems that integrate and network multiple microcontroller and h-bridge building blocks.

9.4.2 Control between struts

In order to integrate networks of processors and components, I developed a design that enables higher density routing (Figure 9-7) while still leveraging the in-lattice electrical routing capabilities explored in Section 9.2. This meant positioning devices requiring more than eight I/O in locations spanning multiple lattice positions.

This next series of prototypes used ATtiny20 microcontrollers. This microcontroller is available in a wafer level chip scale package (WLCSP) that is approximately 1.5 mm x 1.5 mm and is the smallest off the shelf microcontroller at the time of this writing. It features 14 pins, which allows

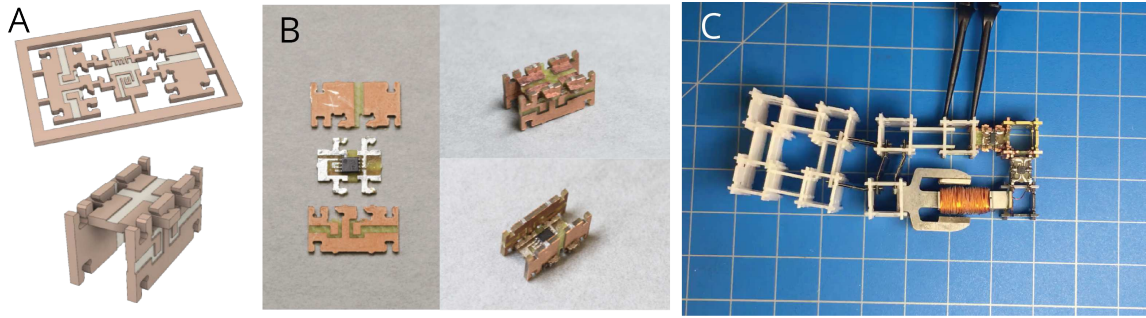


Figure 9-6: Embedding integrated circuit building blocks in struts enables the straightforward assembly of integrated controllers. A microcontroller within a building block (A,B) generates actuation signals that are amplified by an H-bridge building block to power an actuated degree of freedom (C).

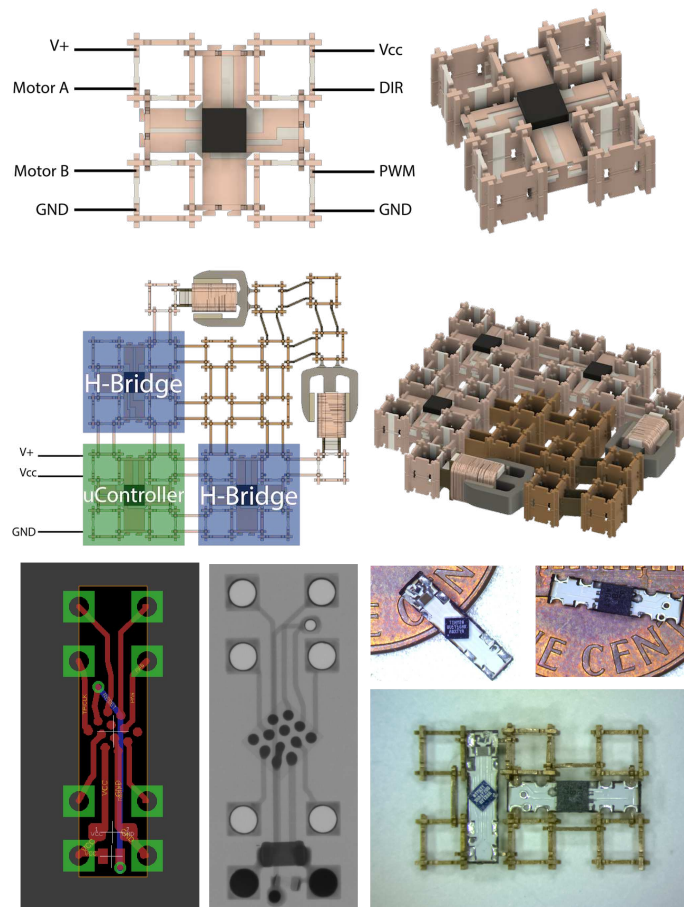


Figure 9-7: More advanced capabilities can be integrated by spanning multiple lattice sites. Wafer level chip scale package (WLCSP) microcontrollers and H-bridges are embedded on parts that interlock with the lattice.

for more connectivity between adjacent parts. However, given the pitch of the ball grid array, it is not possible to route more than eight I/O pins from the board without resorting to more advanced PCB construction methods (e.g. plugged vias), which I was looking to avoid. That being said, only six I/O pins are necessary to enable the control of two degrees of freedom based on some input.

In this design the integrated circuit building blocks fill the negative space of the lattice. This is beneficial in term of spatial density. This design can be implemented in a variety of ways. For example, Figure 9-7 depicts a design where each microcontroller and H-bridge span four lattice locations while other variants are stick-shaped and span just two cells. These stick-shaped parts are still able to incorporate and the same number of I/O as the cross-shaped parts because ultimately the bottleneck in this configuration is the escape routing through the nodes of the lattice. While there are ideally 16 output connections coming from the four nodes, only eight of those are uniquely addressable. For this reason, the stick-shaped parts, which span two cells and still have eight possible I/O, are preferred.

9.4.3 Redefining struts for greater routing density

Having developed this first iteration of computation parts, I looked to enable even greater routing density through the modification of the part geometry. To overcome the routing constraints of the nodes and struts, I developed a laminated strut design that allows up to eight signals to be passed within each strut. The design also instantiates a new “strut-node” part type that merges two nodes and a strut. This merging greatly simplifies the routing of the electronic connections out of a high-density component like a microcontroller and reduces the overhead of the electrical connectors in the assembly.

The routing of signals in this framework is done with the use of variously patterned node parts. These instantiate the basic “routing cell” motifs developed in section 9.2 with capabilities such as 2-way pass-through, 90-degree turn, 3-way connection, 4-way connection, and no connection.

This design incorporates routing at a higher density than the other designs but retains a sparse lattice. The sparsity of the lattice is a free design parameter.

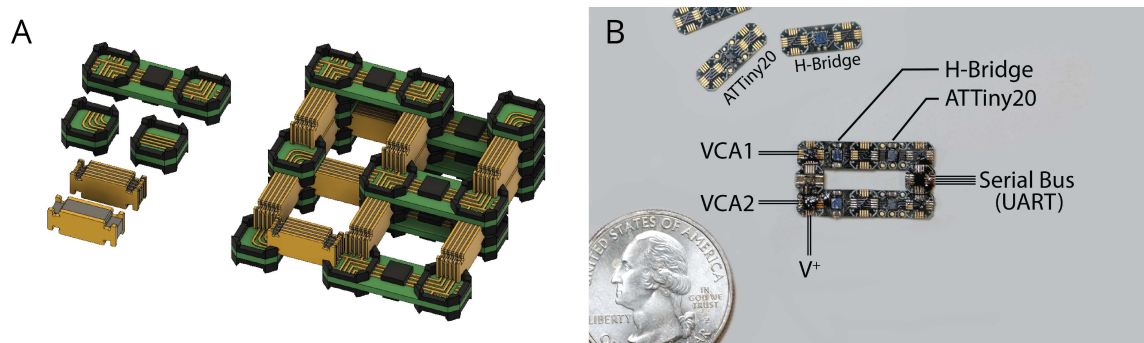


Figure 9-8: By adding higher density electrical connections between parts, more advanced functionality can be implemented (A). A two degree-of-freedom motion controller is assembled from individual microcontroller and H-bridge building blocks (B).

9.4.4 Tiles – Decoupling mechanical and electrical routing

A four-connected lattice is much better suited for routing electrical degrees of freedom. This meant moving the electronic functionality into the nodes rather than the struts. This design breaks from prior designs in decoupling the electrical routing requirements from the mechanical construction of the lattice.

The tile parts feature an upgraded microcontroller processor, an ATSAM10D14. This 32-bit ARM processor runs up to 48 MHz and has UART and PWM peripherals that can be mapped to pins in firmware. Four ports are defined, one for each side of the tile, each having two pins. The ports are configured either to function as a bidirectional UART or to output PWM on the two channels. As such, each tile has four electrical connections on each edge: Vcc, signal A, signal B, GND.

Using this assembly framework I assembled a two degree-of-freedom motion controller. A USB serial connection from a computer serves as the input. Commands are sent from a command-line terminal. The UART peripheral on the microcontroller interprets these commands and generates the specified actuation signals, which are sent to the H-bridge to be amplified and sent to the actuator.

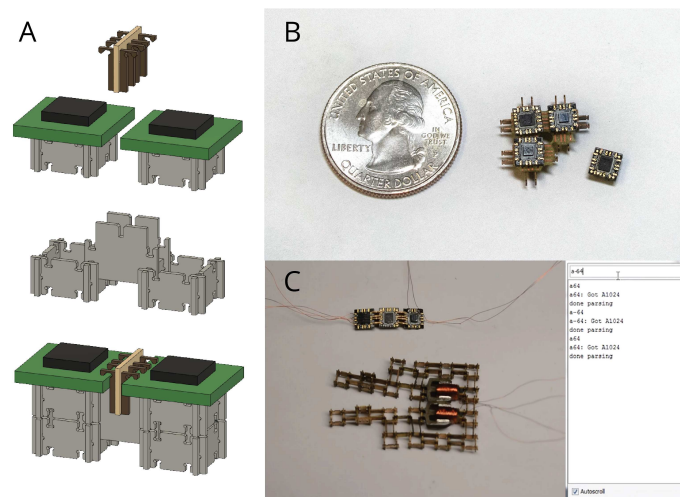


Figure 9-9: By decoupling the electrical connectivity from the mechanical lattice, higher density integration is possible with “tile” parts. These tiles are configured to accept commands from a computer terminal and control the actuated gripping mechanism (Bottom).

Routing of the electronic functionality with these tiles has different requirements than routing signals through the mechanical lattice. Instead, I find that two part-types enable planar routing with sufficient density. The two part types are:

- **Translator:** A translator connects the four edges of the tile in such a way that the polarity of the connections across the tile is not changed.
- **Rotator:** A rotator, in contrast, connects the four edges of the tile such that the polarity of the connections across the tile is reversed.

These two part-types are further configured by the presence or absence of an edge connector. For example, a rotator tile with edge connectors only on the North and East edge, acts as a 90-degree

connector, connecting the South neighbor to the West neighbor. The routing of a six degree of freedom controller is presented in Figure 9-10.

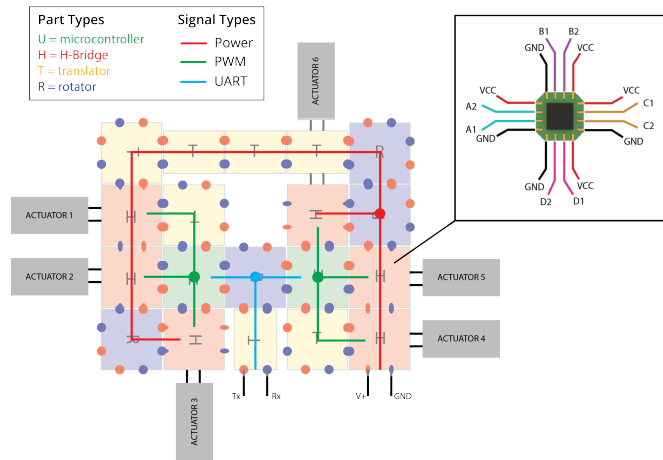


Figure 9-10: A six degree of freedom controller is routed using the tile parts. Red and blue circles on the edges represent the polarity of the signals.

9.5 Production Methods

The parts required to route circuitry and integrate computation in this assembly method can be produced using a number of different methods but printed circuit board processes tend to be well suited for most of these parts.

Routing Parts The seven part types required to route traces within the structure are just at the edge of commercially available PCB board-house capabilities (Figure 9-11 A). The parts are arrayed in a large panel. Fiducial markers and three holes are added to the frame for alignment of subsequent post-processing operations. The size and tolerance of the plated slots in the parts fall below what most manufacturers are capable of. However, a few manufacturers were able to meet the specifications with the use of laser-routing (Gold Phoenix and PCBUniverse). In addition, the printed circuit board manufacturers are unable to control the thickness of the boards within an acceptable tolerance for a press-fit connection. They can only hold ± 0.06 mm on the overall thickness. Clearly a 0.31 mm part is not going to fit in a 0.25 mm slot and a 0.19 mm part is going to fall right out of the same slot. The actual specification varies from panel to panel and from production run to production run and so for small prototyping runs it can be a reasonable strategy to just pick panels that fall within the desired tolerances from a much larger batch. In one particular representative case, I measured the thickness of the parts to be an average of 0.288 mm with a high of 0.3 mm and a low of 0.280 mm. Because these dimensions are all greater than the desired thickness, I can polish the parts down to size. In order to bring the thickness down, I polished with combination of 2500 grit sandpaper and 1200 grit polishing compound between flat acrylic sheets to bring the thickness between 0.251 mm and 0.271 mm. These parts are then able to interlock with parts made using the wire-EDM without deforming them.

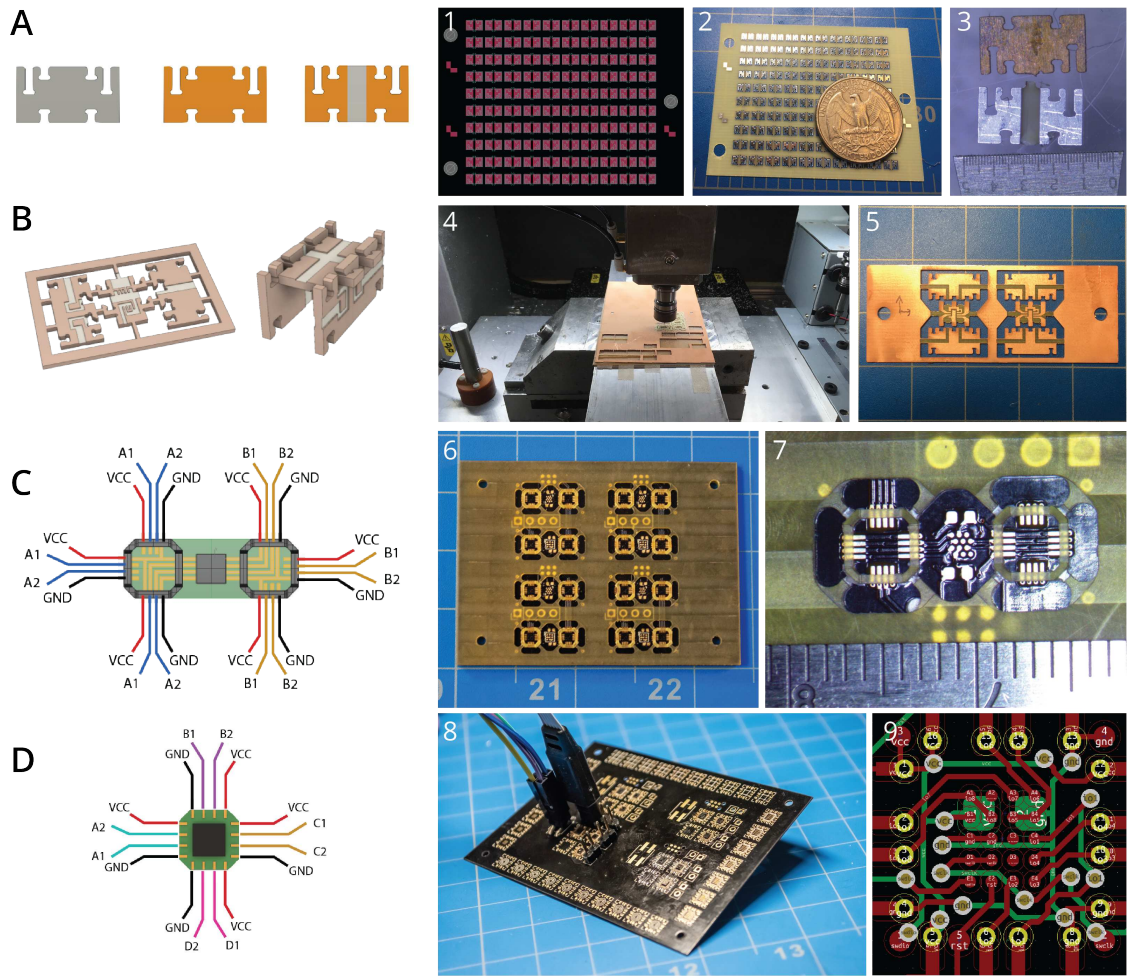


Figure 9-11: Circuit part production methods. (A) Production of routing parts is done using laser routed PCB processes. (B) Isolation routing of FR1 copper clad substrates enables the fabrication of three-dimensional struts with integrated circuits. (C) Strutnode parts are produced as a PCB and then laminated or overmolded with mechanical interlocking features. (D) Tile parts are also produced as a PCB and then affixed on top of a node part-type with epoxy.

Integrated Circuit Struts For the larger-scale parts, in-house PCB fabrication methods can be used (Figure 9-11 B). In particular, isolation routing (milling) of copper clad FR1 can be used to rapidly fabricate building block parts with integrated circuitry to incorporate microprocessors and other integrated circuits. Three-dimensional struts are produced through the assembly of two dimensional parts. The parts are milled together as a panel. The panel features traces on both sides so alignment features (dowel pin holes) are used to align the panel for double-sided machining. Once the panel is machined on both sides, the tabs can be cut with a sharp knife to release the individual parts. At this point, the microcontroller or H-bridge is soldered onto the part. The microcontroller is programmed by attaching clips to the required pins, which have been broken out. Finally, the three-dimensional strut is assembled manually with pliers.

Strutnode Parts For parts that integrate off-the-shelf integrated circuits, printed circuit boards processes can be used in a way that is a little more natural but then augmented with lamination or molded features (Figure 9-11 C). The microcontrollers selected for integration into the strutnode building blocks use a wafer level chip scale packages (WLCSP) with micro-ball grid arrays (μ BGA), which have a pitch between solder balls of 0.4 mm. It is possible to adequately route these parts on a two layer PCB using a 4-mil/4-mil trace/space routing design rule. Furthermore, via-in-pad (masked-plugged-vias) construction methods are not necessary in order to escape route the necessary functionality for these building block parts.

The boards are sourced from a commercial PCB fabricator (PCBWay). The thickness of the board is specified to be 0.6 mm. Gold plating is used on the contacts for improved definition, ease of soldering, and to enable wire-bonding, if required.

Once the boards have been fabricated, the components need to be soldered. A stencil makes the application of solder-paste relatively straightforward. Incorporating alignment features on both the circuit board and stencil can be helpful to establish the initial alignment. Once the paste is applied, the components are arranged on the board and the whole board is reflowed following the time and temperature protocol specified by the solder-paste. At this point, the functionality of the parts can be tested using the connectors neighboring the parts on the PCB panel.

At this point the boards are functional but have no way of mechanically interlocking with one another. To add the interlocking features I pursued two different strategies: lamination and molding.

The lamination process begins with the machining of top and bottom laminates that are to be bonded to each side of the PCB. Ultimately, I found that the lamination strategy was incompatible with the materials and geometries that were required given the required processing temperatures. Either the materials are too brittle to robustly support the feature sizes I require or their coefficient of thermal expansion ensures poor adhesion to the PCB substrate.

To mold the features on the PCB, I developed a vacuum-assisted molding workflow. The vacuum-assist is beneficial in ensuring that whole surface of the mold remains in tight contact with the PCB so that flashing is minimized and the PCB surfaces remain clean. A soft-tool (Oomoo 25) was cast from a machined laminate layer. Ports were added at both ends of the tool and this was then aligned to the PCB panel. A hard polymer resin was mixed and then pulled through a tube into the mold by a vacuum tube attached to the other port of the tool mold. This strategy was able to reliably produce the geometric features on top of the PCB surface. However, the soft tool deformed from the vacuum pressure and the resulting geometry differed significantly from the design intention.

Finally the parts are singulated from the panel by machining with a 1/32" endmill.

Tile Parts The tile parts, like the strutnode parts, are based around PCB fabrication processes. Fabrication of the tile parts proceeds in the same way as the strutnodes described above. However, instead of laminating or molding features on to the PCB surface, the tile parts are affixed on top of node parts. This is done as a final step once the tiles have been soldered and singulated from the panel. Individual tiles are arranged in an array of cutouts in a fixture. The fixture, with tiles firmly in place, is turned over, a drop of epoxy is dispensed on the bottom surface of each tile, and a node part is inserted into the alignment hole in the fixture to be attached to the tile.

Connectors for the tile parts are made from wire-cut bronze parts and laser micromachined fiberglass parts. These parts feature interlocking slots that are used to join four bronze connectors to a single fiberglass stabilizer. Press-fit forces are enough to rigidly affix this assembly without the need for any adhesive.

9.6 Discussion

Beyond the part types developed here, a number of other parts may be beneficial for the assembly of robotic systems and assemblers in particular. For one, power storage is an important capability that is still undeveloped. This could likely take the form of a battery or super capacitor part type. Zinc-air batteries have among the highest energy densities of battery technologies. These batteries are commonly used in hearing aids and are designed to provide energy for a low draw (a few milliamps) for a week or more. While they have great energy densities, zinc-air batteries are not rechargeable and expire with or without use in a few weeks time (after the tab is removed and air is let in). A size 10 battery (the smallest commonly available hearing aid battery) is 5.8 mm x 3.6 mm. Two of these could be stacked to fit on a single actuator sized building block that spans two cells of the lattice (taking up a volume roughly 5 mm x 9 mm x 4 mm). This would provide approximately 200 mAh of capacity, enough to power a single actuator, which draws 100 mA (the 320-turn coil), for two hours. The four actuators of the stacked walking motor would conservatively last for at least 30 minutes with a single battery part.

Other part types may be useful such as a wireless communication part. This could simply act as a relay to connect the UART input of an integrated processor with an external controller attached to a computer. This part could be useful for the coordination and control of multiple assemblers acting simultaneously. An ATBTLC1000 chip, for example, is a bluetooth system-on-chip (SoC) that is available in a 2 mm x 2 mm WLCS package [143].

A pain point in the development of these circuitry capabilities was in achieving higher density routing connections between lattice sites. The in-lattice routing is remarkably robust for basic connectivity between electronic functions but extending beyond the in-lattice routing has been error prone and delicate. It may make sense to explore alternatives to individual connectors for each signal. For example, anisotropic conductive adhesives ("Z-tape") that are only conductive in the Z-axis but not the XY axes could be used to very simply attach planar parts through a patterned substrate [144]. There are likely also ways to create similar functionality through microstructure [63].

Given the overhead and complication of physical connections it may be possible to replace some

portion of these physical connections altogether with non-contact connections. In [145] inductive communication is used between modules by taking advantage of the windings of the electropermanent latches used to connect between modules. While well suited for this specific case, this is unlikely to be a space efficient solution for other designs as inductors are difficult to produce at small scales. Another alternative may be to use optical connections between parts. For example, an infrared emitter and detector pair may be used to send and receive signals, respectively. This technique has the advantage of the possibility for communication over distances greater than one lattice pitch. This could potentially be an efficient means of connecting parts that are within line of sight but relatively far geographically. On-chip optical communication, for example, is being pursued as a means to send signals more efficiently over longer distances on integrated circuit boards [146].

Chapter 10

Automation

While assembling assemblers is the ultimate aim of this work, intermediate off-ramps of automated assembly using table-top platforms could enable the translation of digital designs into physical machines without manual intervention.

The standardization of the interface between parts simplifies assembly automation. Rather than requiring a several degree-of-freedom arm in order to position parts in arbitrary orientations, the parts are designed to be assembled vertically. This makes the assembly process much more similar to the pick and place assembly used to manufacture printed circuit boards than the complex arms used in automotive assembly.

Here, I describe the implementation of two automated assembly systems that leverage this simplified assembly framework for two different digital material geometries. The first assembles electronic digital materials detailed in prior work and the second expands upon this prior work to assemble systems that incorporate structure, mechanism, and actuation.

10.1 Electronic Digital Material Stapler Assembler

10.2 Design Overview

I first automated the assembly of the electronic digital materials developed in previous work [61]. The design of the assembler largely resembles that of conventional fabrication machines. However, the assembler differs from other fabrication tools in that it takes advantage of the inherent qualities of digital material structures. Unlike conventional machine tools, the assembler can correct positioning errors within a tolerance by registering with the digital material lattice, enabling the assembly of structures more accurate than the assembler itself. To enable the toolhead of the machine to self-align with the digital material structure, intentional compliance between build platform and the toolhead was added through the use of an XY-flexure mechanism located on the Y-axis. This flexure allows the alignment fingers of the stapler toolheads to register to the negative space in the lattice, correcting for positioning errors up to 0.5 mm in X- and Y-axes.

Each toolhead features a part placement mechanism and a magazine of parts. The magazine, which contains up to 100 parts, is made to be easily removable from the rest of the toolhead. This is achieved through the use of a repeatable coupling mechanism. The tapered magazine is forced up

against two dowel pins by a conical point setscrew, which interfaces with a conical hole on the front of the stapler magazine. This constrains all 6-degrees of freedom of the stapler magazine in such a way that it can be removed and reinserted midway through a build without any loss of precision.

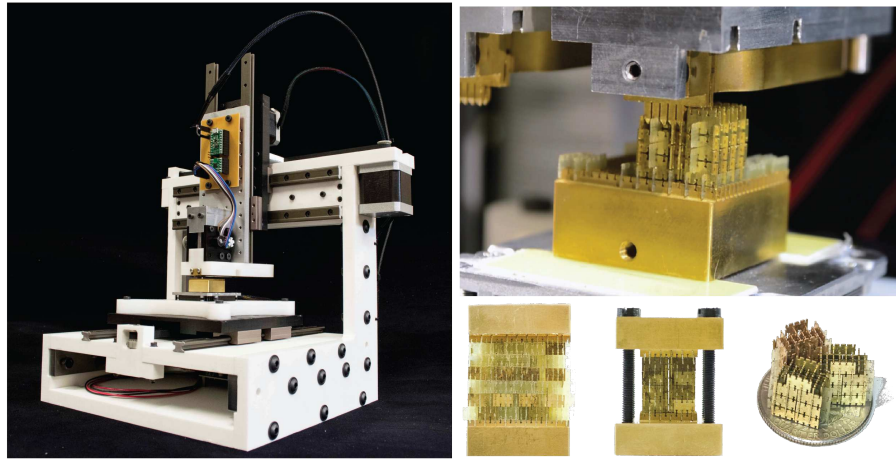


Figure 10-1: The stapler assembler builds electronic components from conductive and insulating parts.

10.2.1 Detailed Design

A 4-axis motion gantry is used to position two toolheads spatially with respect to the structure being built. The motion gantry is constructed from a steel reinforced HDPE frame. The frame is CNC milled to precisely position all holes and pockets. Precision ground steel is then bolted to the frame pieces to add rigidity and mass. The axes use polymer linear guideways for low friction motion in each axis. The axes are powered by high-torque NEMA-17 stepper motors and driven with GT2 timing belts. The motor and power transmission elements were specified to nominally provide a 1/16th microstep resolution of $5\ \mu\text{m}$ and a maximum operating speed of $50\ \text{mm/s}$ with a potential linear force delivery of $70\ \text{N}$ in each axis. Backlash in the timing belts was measured to be between $125\ \mu\text{m}$ and $250\ \mu\text{m}$ in the X- and Y-axes but can be compensated for by approaching part placement locations from the same direction. Doing so, enables a positioning repeatability better than $25\ \mu\text{m}$ in X- and Y-axes.

The part placement mechanism is driven by a 100:1 DC gear-motor through a worm gear. This mechanism produces roughly $32\ \text{N}$ of downward force for part-insertion, which is almost three times the expected $12\ \text{N}$ of force needed to insert a part. Using this mechanism, the maximum part deposition rate is $0.72\ \text{Hz}$.

10.2.2 Workflow and Characterization

The stapler assembler platform is able to assemble electronic components such as capacitors and inductors from conductive and insulating parts. The part placement speed for the assembler is approximately $0.2\ \text{Hz}$ (or 1 part every 5 seconds), enabling a volumetric build rate of $80\ \text{mm}^3/\text{min}$. This is on par with the build speed of commercial 3D printers, which take a few hours to build a one

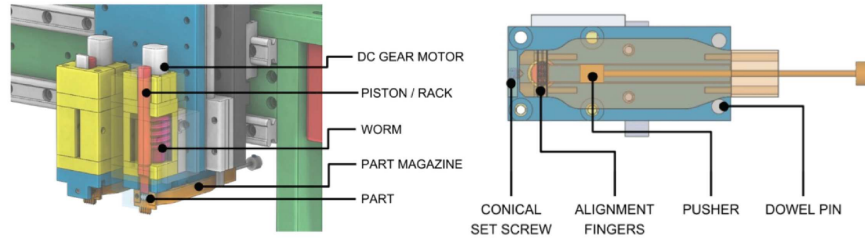


Figure 10-2: The stapler assembler features two toolheads (one for each part-type). The parts are deposited by a worm-rack mechanism powered by a DC gear motor. The part magazines are removable and interchangeable with quasi-kinematic coupling.

cubic inch structure. In the case of electronic functionality, this speed allows for the construction of two 5 pF capacitors in 20 minutes (including manual magazine refilling).

In order to generate designs and toolpaths for the assembler, a custom CAD/CAM workflow was developed and has been document in prior work [147]. The design tool enables the design, simulation, verification, toolpathing, and machine control within a single environment (Figure 10-3). This single environment greatly reduces the friction that is typically associated with converting a digital design into a physical object. Furthermore, design workflows like this lend support to the idea that assemblers can help lower barriers to the fabrication of integrated devices by empowering a single user to design, verify, and fabricate a device and go from building block parts to a functional device in an afternoon and on a desktop.

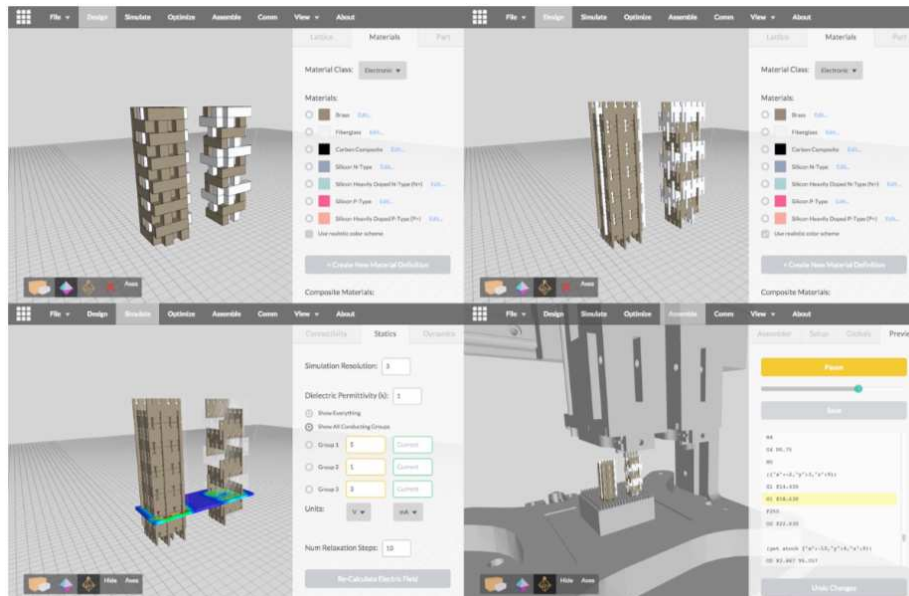


Figure 10-3: Reproduced from [147]. To control the assembler Ghassaei developed an integrated CAD/CAM workflow that enables design, simulation, toolpathing, and machine control within a single environment.

10.3 FABBR – Functional Assembler of Building Block Robots

10.3.1 Design Overview

Rather than use a stapler-type toolhead, I redesigned the placement heads for pick and place type operation. While this necessitates an extra traversal for each part placement, it significantly reduces the complexity of the toolhead and allows for much easier accommodation of larger or unusual parts like actuators or electropermanent feet.

Each toolhead actively grips the part. While requiring an extra degree of freedom and a more complex design, this eliminates the careful tuning of the various combinations of attachment forces that need to be considered between the part, toolhead, substrate, and assembly. This active gripper design lets the assembly machine vary the grip strength from approximately nothing when un-gripped to an order of magnitude stronger than the passive gripping elements of the substrate.

Three toolheads are required to support the assembly of machines integrating structure, mechanism, and actuation (Figure 10-5). A node toolhead places node parts. A strut toolhead places a pair of struts which can be rigid or variously flexible. An actuator toolhead places a coil and magnet part simultaneously.

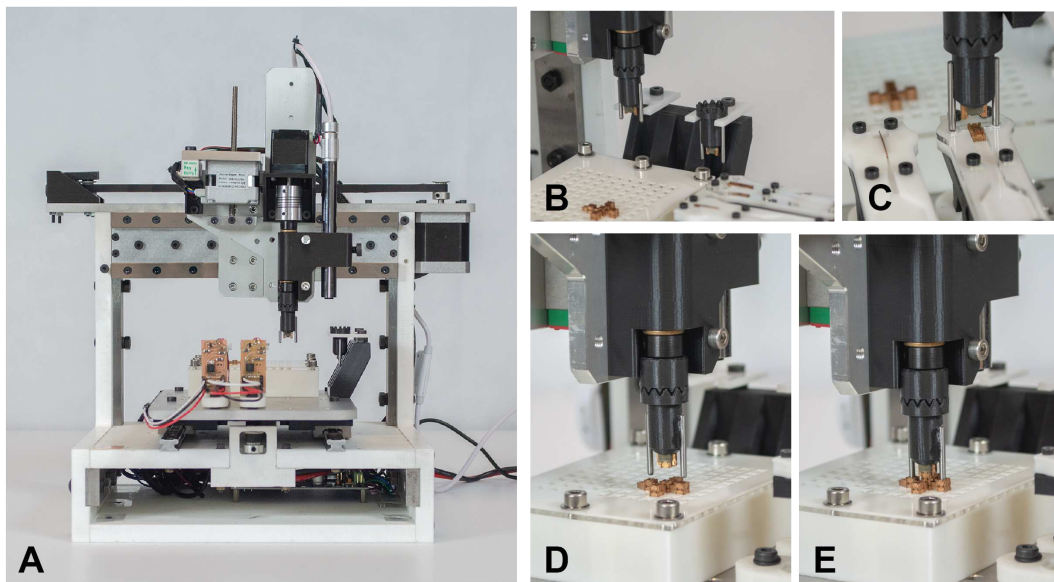


Figure 10-4: The upgraded assembler features an automatic tool-changer, a tool-mounted rotary axis, an on-tool microscope and a large 12x12 unit build substrate.

In developing the assembler I first attempted to automate the placement of individual (non-paired) struts. This proved challenging to do in a pick and place type operation since the size and aspect ratio of the struts necessitates precise and finely featured alignment jigs. The manipulation of a single strut is also challenging as they tend to act like playing cards; once stacked they are hard to unstack without active manipulation (like a feeder). I later decided to treat struts in pairs such that they are volumetric build elements. This allows the strut gripper design to much more closely resemble that of the node gripper and allows much larger features (and negative space) to be used for attachment and placement. In a future revision of the assembler it would certainly be

desirable to treat the struts as individual parts and could be accomplished by designing an actuated stapler-type magazine that automatically separates and presents the next part to be placed.

The struts are pre-assembled using orthogonal press-fit plates that set their spacing. This required a slight redesign of the strut parts to introduce a slot for this extra connection. For the flexible struts it also required shifting the hinge degree-of-freedom towards the center of the part. In the case of a pair of two degree-of-freedom struts this reduces the spacing between hinges and results in less range of motion and more parasitic error when used as a linear motion constraint. These tradeoffs were seen as necessary in order to develop the first version of the assembler but shouldn't be seen as limiting for future revisions.

10.3.2 Detailed Design

I updated the design of the stapler assembler for use with the mechanical part types (Figure 10-4). This involved a number of important upgrades. First, the HDPE panels supporting the X-axis rails were replaced with aluminum. The extra stiffness provided by the aluminum plate allows for much better tensioning of the timing belt, resulting in significantly reduced backlash. The Z-axis timing belt drive was replaced with a leadscrew transmission to enable much higher placement forces to be exerted. The rotary degree of freedom was moved to the toolhead rather than the build platform, significantly reducing the required precision of the rotary axis since the toolhead is much smaller than the build platform (and so the Abbe error is significantly reduced). The upgraded assembler features three main enhancements: the active gripper toolheads, the build substrate, and the control system.

Gripper Toolhead The gripper is actuated by a linear servo motor (Actuonix) that is housed on the Z-axis. The linear servo motor is composed of a small rotary DC motor and a small screw transmission that provides a 100:1 gear reduction. This enables the actuator to produce forces up to 35 N over a 20 mm stroke. The linear motor actuates the gripping mechanism through a thrust bearing that is magnetically coupled to the sliding part of the gripper toolhead. The thrust bearing is necessary to reduce the friction at the interface and allows the gripper to be rotated while actively gripping the part.

The sliding element of the gripper is used to actuate four gripping arms. The gripping arms are made of polyetherimide (Ultem). This material was chosen after a number of iterations because it machines very well, is relatively hard, but is not excessively stiff. This compliance allows a parallelogram flexural linkage to constrain the arms such that they can squeeze together to pick up a part while remaining stiff about the z-axis. A taper is used to couple the linear motion of the sliding element to the gripping action of the arms and provides mechanical advantage to amplify the gripping force.

The toolheads are able to be changed automatically during a build based on which part needs to be placed. The tool changing mechanism uses a magnet at the base of a tightly tolerance bore to attach and constrain the toolhead to the rotational axis. The toolheads are constrained and aligned about the rotational axis with a tab that interfaces with slot on the rotary axis. Picking up a tool simply involves moving to the appropriate X,Y location, driving the Z-axis down, and then moving sideways to pull the toolhead out of the flexural arms of the toolholder. Removing the tool is the same in reverse.

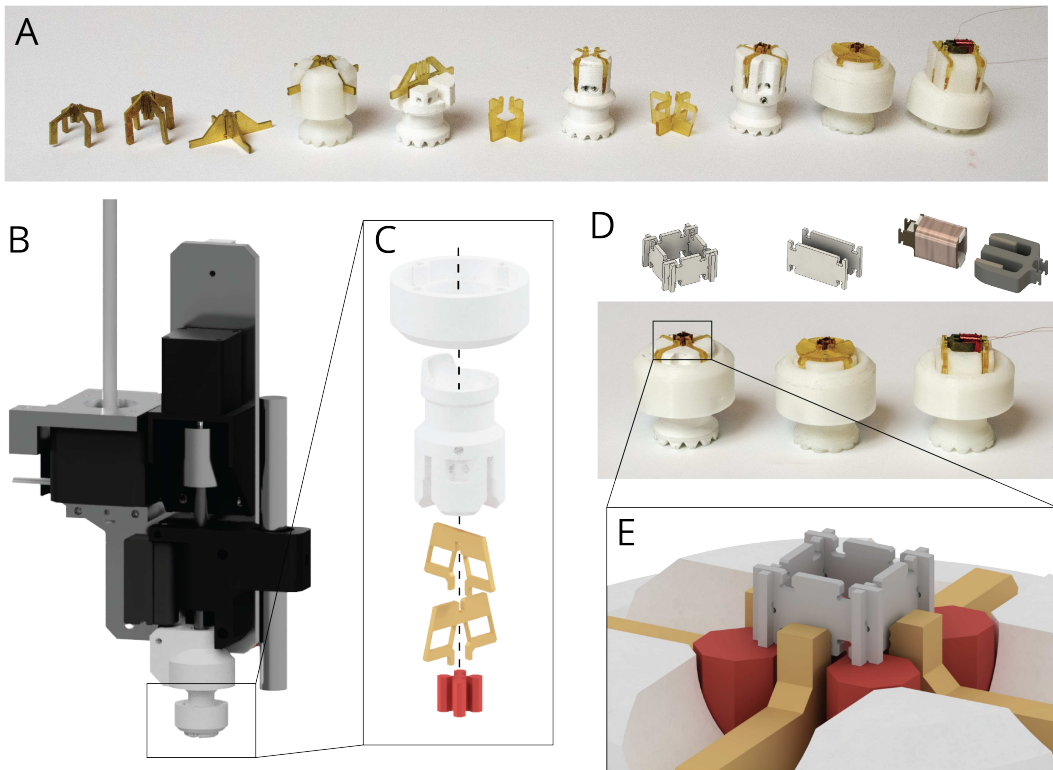


Figure 10-5: Development of the gripping toolhead required a number of iterations (A). The toolhead (B) integrates a linear servo to actuate the gripper (C) as well as a rotational degree of freedom. Three gripper toolheads are used and interchanged during assembly (D). The grippers feature machined Ultem flexures that grip the extents of the parts (E).

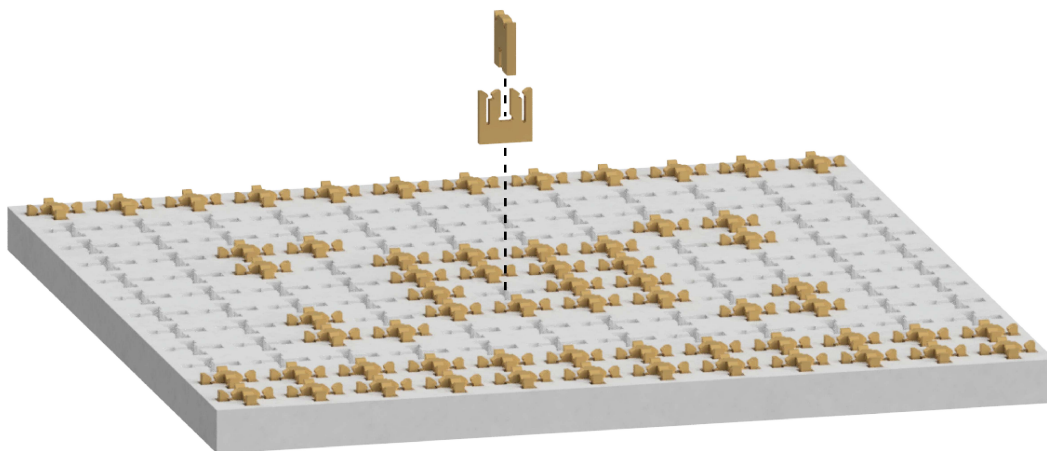


Figure 10-6: The build substrate is composed of individual flexural clips that are pressed into a plate with cutouts. The clips passively grip a specific part-type (node, strut, or actuator).

Build Substrate A build substrate is necessary to constrain the first layer of parts before they have been interlocked (Figure 10-6). For prototyping assembly, the build substrate is also used to position and constrain the feedstock of parts that are to be assembled. The substrate is composed of two parts: a flat plate with cutout features in X and Y axes spaced apart with the same pitch of the assembled lattice and individual clips for each part-type. The clips are designed to passively grip a certain part-type. They are cut using wire-EDM and are assembled to form an X-shape with flexurally preloaded tabs that hold a particular part in place. There are three different kinds of clips, one for nodes, one for struts, and one for actuators. The clips can be inserted or removed from the substrate in order to reconfigure the build area depending on what is being built.

Currently, when a build is finished, the assembly must be carefully removed from the bed of clips. A future version of the substrate may incorporate a single vertical degree of freedom mechanism that allows for all of the clips to be retracted simultaneously. This could simplify the removal process and reduce the chance of distorting the finished assembly.

Control System To run the assembler, I use an off the shelf controller (TinyG). This controller enables the simultaneous control of four stepper-motor driven axes (X,Y,Z,A) and supports G-code streaming and buffering to enable jerk-controlled motion. The additional functionality required for the active gripping of the toolheads and other peripheral functions is controlled through an external microcontroller (ATmega32u4) connected to the TinyG through the spindle and fan control ports.

The assembler is controlled by a browser-based custom developed software program. Communication with the TinyG happens through a USB-serial connection that communicates through a websocket to the browser. The browser console allows for command-line input to control the assembler but is also capable of running small macros or streaming whole G-code programs. For assembly automation, it's often beneficial to script the assembly tasks in javascript rather than writing a dedicated G-code program. Scripts have more flexibility to enable realtime control and automation (such as through the on-tool microscope camera) and programs that are able to call scripts and subroutines are more readable, modular, and reusable.

Each new toolhead needs to be calibrated for its X, Y, and Z coordinate offsets. To do this, the on-tool microscope is used to locate the assembler tool-axis directly over a building block part. The toolhead is lowered to just above the part, and is aligned to the part using fine-scale jog controls. The offset from the microscope center is recorded and stored in the javascript program. It is then recalled and used whenever the toolhead is active.

The geometry of the toolheads add some requirements to the order of assembly operations during a build. The actuator toolhead grips the actuator parts in a location that would interfere with other struts on that same layer. For this reason, the actuators must be the first objects placed after populating the node layer. Additionally, because of the vertical size of the actuators, the substrate node attachment point must be removed wherever an actuator is to be built on the first layer. Struts within the same layer can be placed in any order but it is often preferred to place the rigid struts first to ensure the node layer below is as rigid as possible before placing the flexible degrees of freedom.

10.3.3 Characterization

To demonstrate the capabilities of the assembler I assembled a walking motor. The motor is composed of 32 parts: 20 nodes, 6 rigid struts, 4 flexural struts, and 2 actuators. The assembly starts

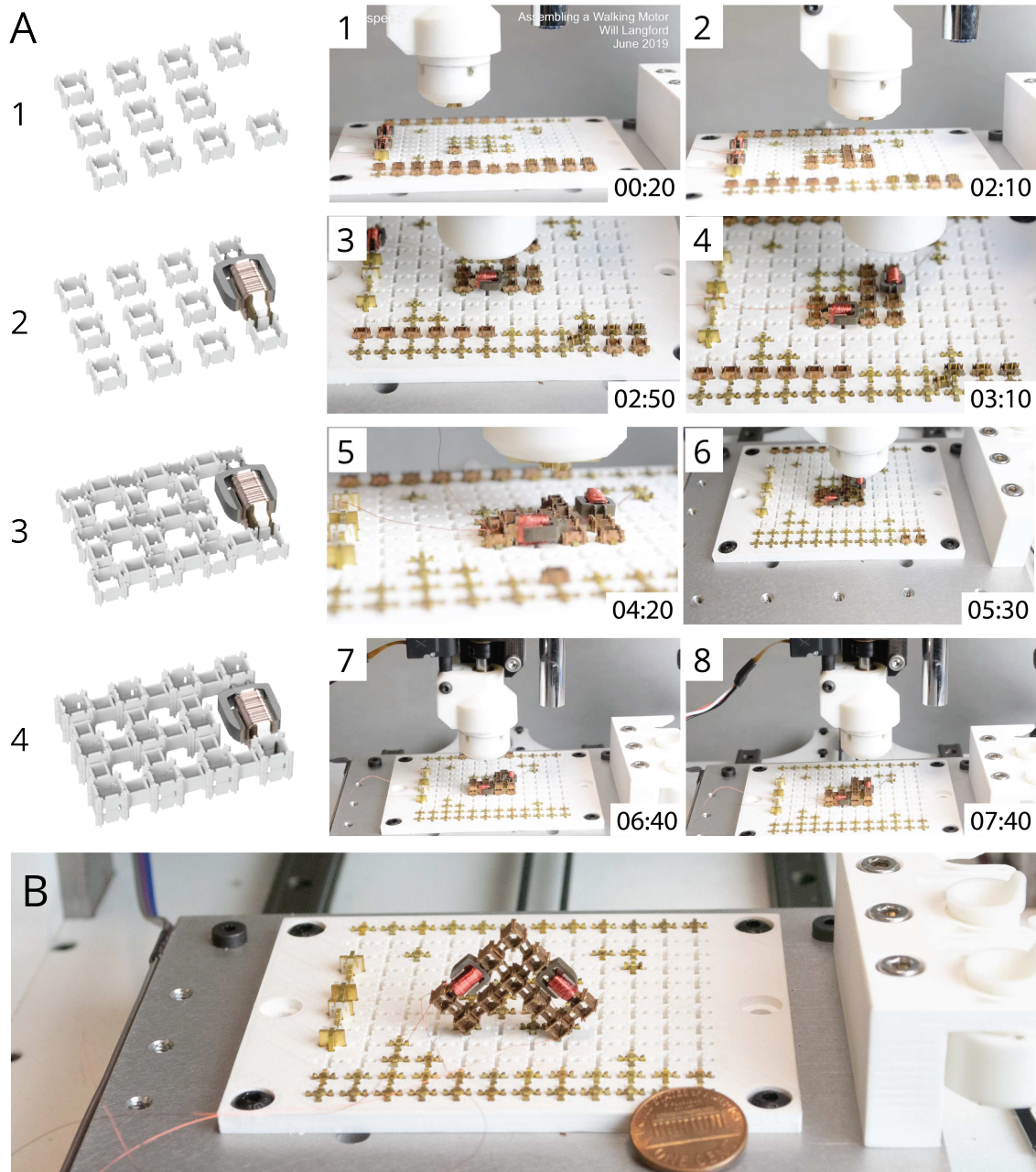


Figure 10-7: The assembly sequence (A) to build a walking motor (B). The assembly proceeds in stages with (1) the placement of nodes, then (2) the placement of actuators, then (3) the placement of rigid and flexible struts, and finally (4) the placement of the second node layer.

with a layer of 10 nodes. This is followed by the placement of the two actuators. The nodes are then connected by rigid and flexible struts and then finally capped off with another layer of nodes. The whole assembly process, including tool-changes, takes approximately 8 minutes (Figure 10-7). This is an equivalent rate of 15 seconds per part.

Much of the assembly time stems from the relative slowness of the actuated gripper and the z-axis. The z-axis is software limited to a maximum speed of 400 mm/min. Testing revealed that the z-axis is reliable up to approximately 800 mm/min, however, moving more slowly than this was found to be beneficial during early testing. Between picking and placing the assembler moves 13.5 mm above the pickup height. This move (both down and up), which happens four times per pick-and-place operation, accounts for 73.4% of the total time it takes to pick up a part and place it (Figure 10-8). This time could be drastically cut down by moving only the required distance for the picked part to clear the tallest point of the assembly (3 mm). This would cut the Z-move time from approximately 2.2 seconds to 0.48 seconds, and reduce the overall pick and place time by more than half, from 12 seconds to 5.12 seconds. The linear servo motor used in the gripping mechanism has a 100:1 internal gear reduction and so has a very high reflected inertia that must be overcome both to stop and start. As a result, a delay of one second after switching the gripper was found to be necessary for transients to settle to ensure that it is in the desired state before moving the toolhead. For a pick and place operation, this delay accounts for 16.6% of the time. Only 10% of the pick and place time is spent moving between XY locations.

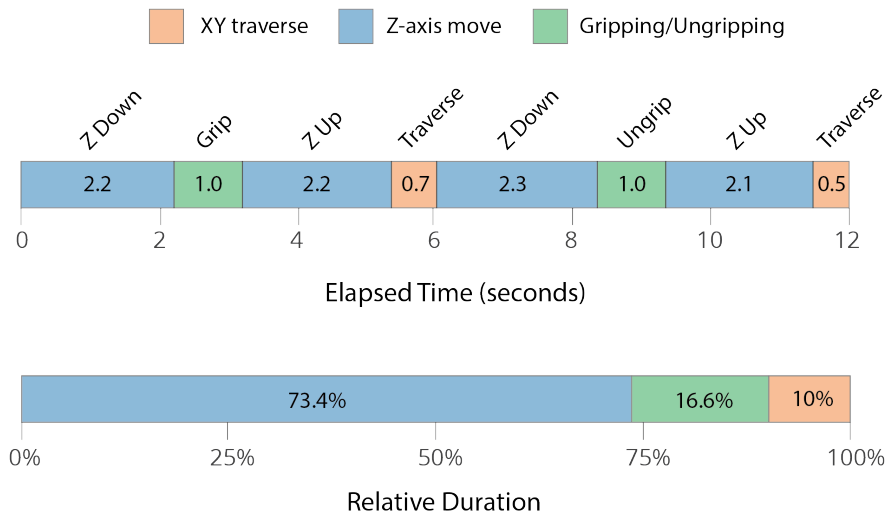


Figure 10-8: Analysis of the timeline during a single pick and place operation. Z-axis moves represent the majority of time spent.

10.3.4 Extensions

In the current embodiment of the assembler, the parts required for assembly must be pre-populated on the periphery of the build substrate. A future revision of the assembler would likely feature automated part feeders that each contain a particular part type and advance a new part as one

is picked up (Figure 10-9). This could be done using a variety of methods. I detailed the design of vibratory feeders for both nodes and individual struts. These feeders are capable of taking a randomly oriented bin of parts and feeding, orienting, and lining them up to be picked up at a given location. For node parts this involves a channel that is dimensioned to accept only a single node at a time in the preferred orientation. For individual strut parts it involves rotating the parts from their natural flat state into a vertically oriented channel.

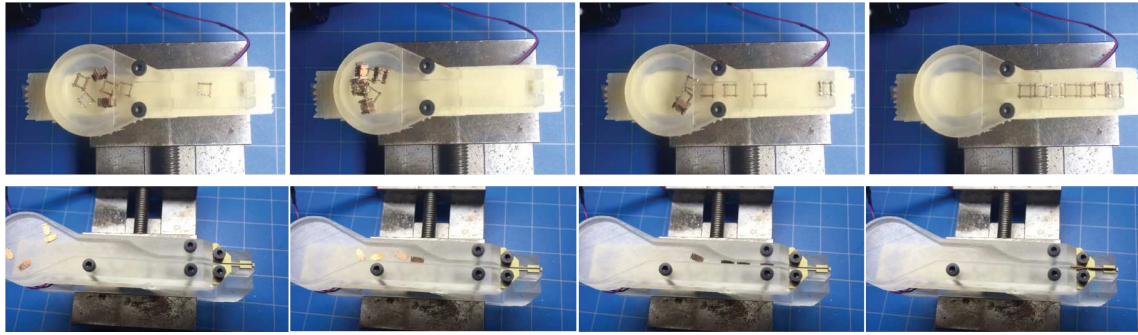


Figure 10-9: Vibratory part feeders can be used to align and feed parts to pickup locations.

Automated disassembly is desirable in addition to automated assembly. This would enable the rapid reconfiguration of systems and would mean that the parts wouldn't need to be single-use. While this is certainly possible to do in an automated way, the current toolheads and assembly machine do not support disassembly. This is because when pulling on a part on the topmost layer, there is no reason that the topmost part is removed and not a part on a lower layer with the same number of connections. Disassembly could be enabled with toolheads that apply downward force to neighboring parts while extracting the desired part. This could be accomplished with something as simple as a sprung ring that ensures that the removal force is directed at the specific part. Another way to accomplish disassembly would be use a different joint system. A joint system with an orthogonal clip for example, could enable a disassembly tool to unclip the part in question and then extract it.

10.4 Assembling Assemblers

Automated assembly systems like FABBR represent a way to go from a digital design file to an assembled machine. FABBR takes 8 minutes to assemble a walking motor composed of 32 parts. This is faster than an experienced human can manually assemble the same structure, but is far too slow if the goal is to assemble thousands, millions, or billions of parts.

Placing parts at the current rate, a billion element volume (a cube with one thousand parts on side) would take on the order of a human lifetime (80 years) to build. Even if the part deposition speed was sped up to 10 kHz (the speed of inkjet printing), it would take a full day to build the billion element volume.

Clearly it is important to find more parallel ways to assemble parts. Naturally, placing whole layers of the volume at once could be desirable. However, as the number of simultaneously assembled connections in a digital material is increased, there tends to be a corresponding increase in the error rate and assembly force [61]. As discussed in section 1.2.3, biology is able to scale manufacturing

throughput with the size of the manufacturing problem. It is able to do this because ribosomes can assemble ribosomes.

Inspired by the biological approach, this work has focused on parallelizing assembly by assembling assemblers. The range of functionality that can be assembled from the building blocks presented in this work lays the ground work for the assembly of machines that can move and manipulate their own parts. Assemblers need capabilities including locomotion, part manipulation, and integrated control.

- **Locomotion** While locomotion could be done in an unstructured environment with a conventionally designed walking robot, an assembling assembler needs motion to be aligned to a lattice or grid. This can be done, for example, with a grooved surface that registers imprecise local motions such that repeated steps are globally precise as long as each step falls within a certain tolerance. The walker demonstrated in Chapter 7 represents a basic step towards this locomotion capability. Walkers that are able to locomote in multiple directions may be made by combining two single degree-of-freedom walkers at a right angle to one another.
- **Part Manipulation** The assembled assemblers need to be able to pick up and place parts. This may be accomplished either with electropermanent latches or with mechanical grippers, as is demonstrated in Chapter 8.2.
- **Integrated Control** Each assembler will consist of a handful of degrees of freedom (≈ 7). In order to coordinate their actions, each assembler needs processors and control circuits on board in order to receive high level movement commands and translate them into controlled actuations.

In addition to these capabilities, the assemblers need to rely on a tailored environment. Just as ribosomes do not operate in a vacuum but rely on a supportive environment to deliver feedstock parts and energy, the assemblers built from these parts will need a supportive and structured environment in which to operate.

Between conventional pick-and-place style assemblers and assembled assemblers, are a family of machine configurations that may serve as stepping towards “true” self replicating machines. The concept pictured in Figure 10-10 depicts one of these. Mobile assemblers locomote on a lattice aligned grid in two axes (X and Y). This grid could be constructed in a number of different ways. The grid could be physically grooved to allow shaped feet to interlock. Or the grid could be defined based on spatially patterned permeability. For example, a permeable lattice with the pitch spacing of a single walker step would be physically flat but still allow the assembler to magnetically align itself on each step.

The assemblers are themselves built from the building block parts. They feature a gripper that is able to pickup parts and place them in the desired location. A conventional Z-axis serves two purposes: (1) it supplies the required force to press-fit an arranged part into place and (2) it moves up as the next layer needs to be placed.

Assembly would proceed as follows: (1) An assembler translates to a part pickup location on the lattice substrate. (2) The assembler picks up the part and translates to the target part location. (3) The part is placed, interfacing with grooves on the substrate to align to the build front. (4) The assembler moves out of the build envelope to pickup another part. (5) Once the assembler has exited

the build envelope, the Z-axis moves down to attach the placed part to the in-progress assembly. This process then repeats. Multiple assemblers could act simultaneously, each arranging a part on the substrate to be placed.

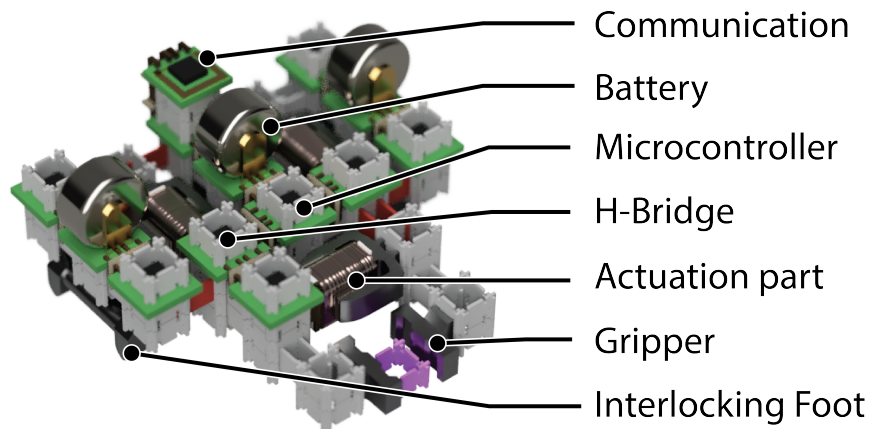
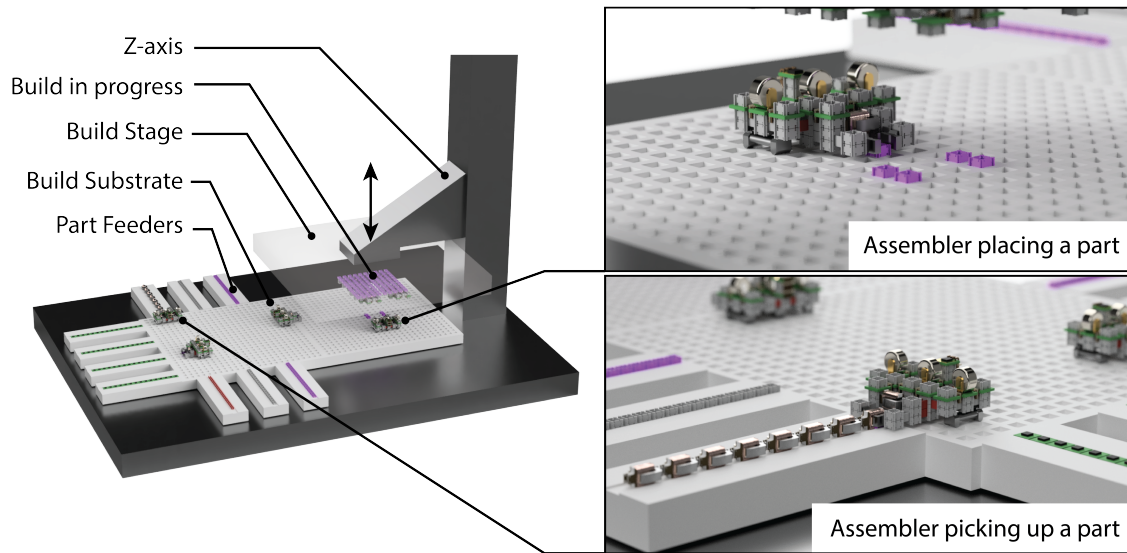


Figure 10-10: A stepping stone concept towards full self-replicating assembly. Mobile assemblers (bottom), assembled from building block parts, are able to locomote on a lattice-aligned grid, pick up and manipulate parts. Parts can be placed in parallel with multiple assemblers working simultaneously with the z-axis advanced as needed.

This concept encompasses the ability to assemble assemblers. However, it is limited in terms of throughput since the motion of the Z-axis needs to be coordinated with the displacement of the assemblers from the build envelope. To unlock the throughput benefits associated with assembling assemblers, the assemblers themselves need to be capable of placing parts without an external force-generating structure. In another embodiment, the assemblers could feature a yet-undeveloped capability of a high-force actuator. Even with an actuator capable of generating large-forces, the 2 N normal strength of the electropermanent feet would be unable to support the 50 N loads required to assemble a node. Based on this, it is clear that the part geometry and joint system may need to

be adapted in support of assembled assemblers.

Beyond the relatively conventional layout of the concept depicted in Figure 10-10, with a few additional degrees-of-freedom, the mobile assemblers could enable more unconventional machine tool configurations such as the concept depicted in Figure 10-11. In this concept, assemblers have an additional body hinge that allows the assembler to locomote on arbitrarily oriented surfaces and transition between horizontal locomotion and vertical locomotion. This could enable assemblers to operate simultaneously on many build fronts of a single object.

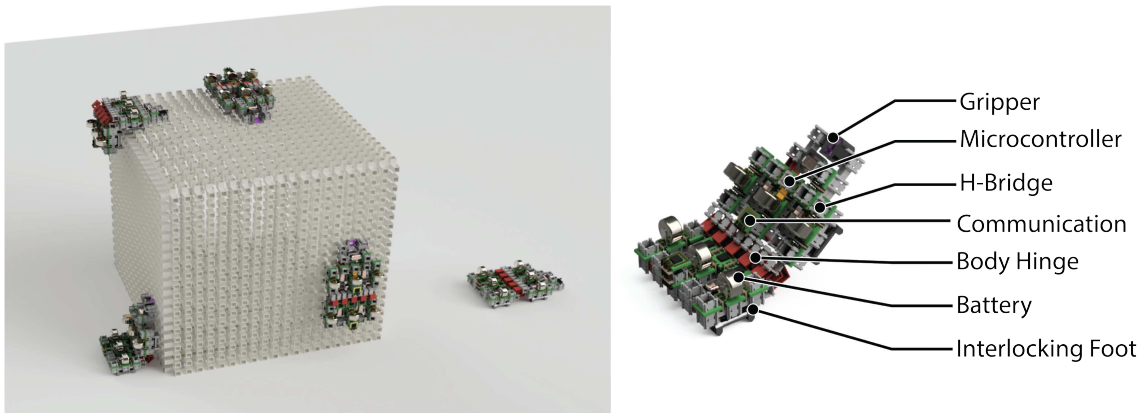


Figure 10-11: An extra degree-of-freedom hinge-joint could enable the assemblers to work on other surface orientations and allow for three-dimensional structures to be build without a conventional z-axis.

10.4.1 Current Limitations

A major question that has come up in this assembling assemblers work is, How can the assemblers generate the required force to attach a part? In the current embodiment of this work, force required to locomote (and the force that is generated by the actuator components) (50 mN) is three orders of magnitude less than the force required to insert a part (50 N).

One strategy to generate this force is could be to use force amplifying linkages. The maximum mechanical advantage created by a lever-arm linkage is often limited to on the order of 10:1 given spatial constraints. Generating a 1000:1 reduction would require three of these 10:1 stages and, as a result, seems impractical. Alternatively, a toggle-action linkage can generate considerable amounts of mechanical advantage but only over a very short stroke. These linkages may be built directly on the assemblers themselves, but space constraints may mean that it makes more sense to assemble linkages between mobile assemblers. In this envisioned concept a part may be placed by an assembler and then pressed into place by a pair of mobile assemblers that manipulate a toggle-action linkage between them.

Another strategy is to obviate the need to massive force amplification entirely by designing the parts to assemble with very low forces. As discussed in Section 2.3, there are a number of different joint systems that require a minimal amount of force to attach parts.

As is discussed in Chapter 7, this kind of mobile assembler concept hinges upon reliable open-loop positioning. An important next step for this work should be the development of a structured surface that constrains each step of the mobile assembler to a grid. This could enable precise open-

loop positioning over an arbitrarily sized build envelope and remove the usual inverse relationship between build envelope and precision that is common in conventional gantry-based machine tools [148].

Chapter 11

Scaling

While I have focused development at the millimeter-scale, other application domains may be possible by scaling the constituent parts and assemblies. For example, with smaller micro-scale building block parts, applications requiring finer-grain resolution can be explored such as ingestible medical robots [149] and dexterous microsurgical tools [150]. On the other hand, larger parts could be used to assemble architectural scale system that are not only structural but also functional.

In this chapter I will look at some of the opportunities and challenges in scaling this approach both down and up in length scale. I'll look at the methods to produce parts at a range of different sizes, the physics that determines the scaling of actuation, and the potential for the assembly process to be scaled both down and up.

11.1 Part Production

Because the parts used in this assembly method are two-dimensional and have a relatively simple geometric shape, they can be made using a range of different processes, in a range of different materials, and at a range of different length scales. As such, the choice of length-scale should be seen as a parameter that can be adjusted based on the application at hand.

For prototyping, I often started with centimeter-scale parts to begin exploring how certain part types could be composed to build useful mechanisms and machines. This allows for rapid fabrication and iteration using commercial lasercutters. The parts at this scale are 0.8 mm thick and just over 1 cm in their longest dimension. Acetal plastic (Delrin) works well at this scale for the purpose of prototyping. More robust parts can also be made by wire-cutting metal.

The millimeter parts, which are the parts predominately used in this work, are made using the wire-EDM with the 100 μm wire, which cuts with about a 150 μm kerf. The parts are 3.5 mm in the their longest dimension. Laser micromachining can also be used at this scale but it is much slower than wire-EDM and only useful for very rapid prototyping of one or a few parts.

Using laser micromachining allows for the fabrication of even smaller parts. Using a 532 nm diode-pumped solid state laser (Oxford Lasers Inc.), which has a kerf of about 20 μm , it is possible to make parts that are 75 μm thick and are 1 mm long in their longest dimension.

Even below this scale, a femtosecond machining laser (Pharos) is able to approach micron feature sizes. This is possible because the pulse lengths are so short that the peak power is high enough to

break atomic bonds without ablating the material, reducing or eliminating the heat affected zone [151].

Beyond scaling down in size, it is also worth thinking about how part production can be scaled up in throughput. Doing so for the basic rigid part types is relatively straightforward as the simple two dimensional geometry can be stamped with a single tool and die. To mass produce the flexural part types, roll to roll processes seem attractive. A web of the constituent materials (bronze and polyimide) would enter the machine and be tape cast with an adhesive film, stamped, and then pressed between heated rollers, and then singulated by another stamping press. Circuitry parts can leverage PCB fabrication capabilities but streamline the processes to only include the necessary steps. Actuators are likely the most difficult to produce in very large quantities. Coils and mandrels can likely use be made in roll-to-roll fashion with progressive stamping, bonding, and then automated coil winding. The magnetic cores may require a redesign in order to simplify their production at scale to eliminate the fine feature sizes in multiple orientations.

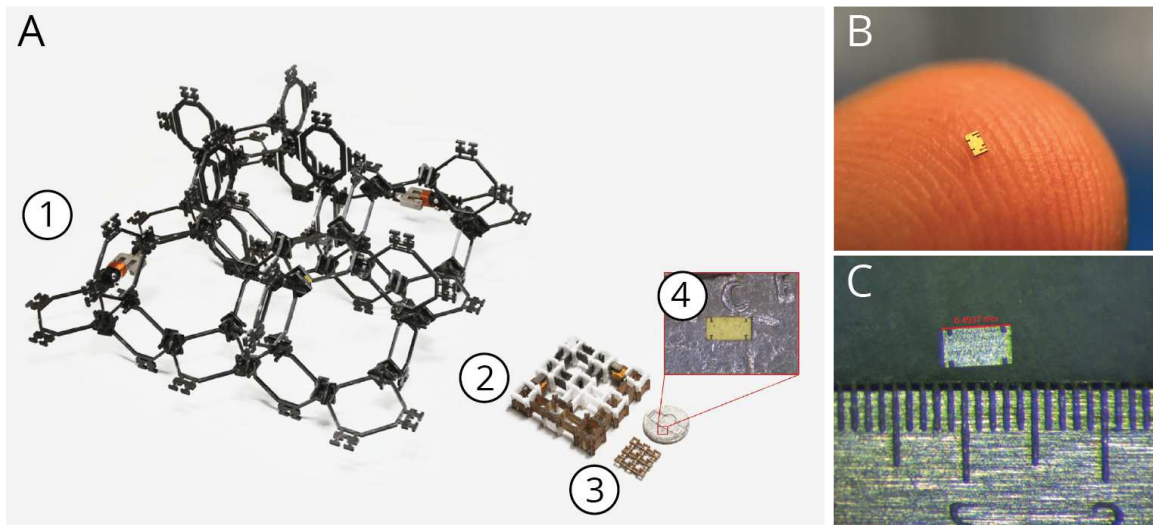


Figure 11-1: This assembly method is possible at a wide range of length-scales from decimeter (a) to centimeter (b) millimeter (c) and sub-millimeter (d).

11.2 Actuation

The discrete assembly approach is relatively scale agnostic. Colleagues and I have assembled walking motors, for example, at scales ranging from decimeters to millimeters (Figure 11-1). At the larger scale, Coplestone used a Kelvin lattice topology for its sparsity and ability to tile three-dimensional space. The same principles developed in this work at the millimeter scale are applicable at this larger scale, enabling structure, mechanism, and actuation to be combined.

Actuation is generally a challenge to scale since it often involves the most intensive fabrication and relies on a variety of physics working together (e.g. electricity and magnetism). It is possible to project the performance of the actuated assemblies developed in this work to other length scales through a proportionality scaling analysis (Table 11.1). The scale variable, s , is used to represent how a particular quantity scales, as is detailed in [108]. In this case, I assume that the actuation

current can scale with a constant temperature rise (s^1), rather than constant current density (s^2), because surface area scales favorably with respect to volume. Based on this assumption, both power and force (as well as their respective densities) scale favorably to smaller length-scales. Furthermore, bandwidth also scales favorably, proportionally increasing for every shrink in size. Efficiency, however, suffers at smaller length scales and decreases proportionally with scale.

Table 11.1: Scaling Laws for Voice Coil Actuation

Mass	s^3	Power	s^2
Current	s^1	Power Density	s^{-1}
Force	s^2	Force Density	s^{-1}
Bandwidth	s^{-1}	Efficiency	s^1
Energy Output	s^3	Energy Density	s^0

This points to the possibility of scaling this assembly approach down in length-scale. At some-point, however, the increase in bandwidth, force, and power density will be outweighed by the decrease in efficiency and will warrant a different type of actuation (for example, piezoelectric or electrostatic).

It can be instructive to look at the force density of an array of actuators to look at how these actuators stack up against larger commercial off-the-shelf (COTS) options. A representative commercial voice coil actuator [113] (25 mm diameter, 16.5 mm length, 58 g mass, 2.2 N blocked force) has a force density of 38 N/kg or 0.272 N/mm³. For comparison, densely packing the Lorentz force actuator components and neglecting any required wire routing or mechanical constraints results in a force density of approximately 82 N/kg or 0.114 N/mm³. Clearly the actuators developed in this work are much less force dense per volume but per mass, are more than two times stronger.

Ultimately the force per mass metric is likely more significant than the force per volume metric because, in the target applications, what usually matters is the ability to accelerate a mass, not overcome viscous forces. Furthermore, these actuators being much less dense than the COTS option is likely beneficial in terms of heat exchange with the environment. Since efficiency decreases as the actuators are scaled down, it becomes more and more important to efficiently remove heat from the coils.

This force density metric points to the possibility of replacing larger macroscopic actuators with arrays of these actuator components. By tiling the actuators in parallel, their force output can be increased. Furthermore, it is possible to arrange actuators in series as well, to increase displacement. This approach of assembling a large scale actuation from individual “micro-actuation” building blocks is likely not the most power dense or space-efficient because of the overhead of connectors between them, but enables the rapid production and extensibility of robotic systems.

Building up larger actuations from individual building blocks is exactly how biological muscles work. In fact, biological muscles demonstrate the feasibility of assembling very high force density actuators from individual building blocks. Muscle generates a specific actuation stress (N/m²/kg) of approximately 2000 kPa/kg [15], which is about 25 times the specific actuation stress possible with any kind of Lorentz force actuator.

Biological muscle force scales with the cross-sectional area of the muscle (s^2). They represent a remarkable design that is able to produce large macroscopic forces and strains based on the motion of billions of microscopic parts [15]. There are many different kinds of biological muscles. Skeletal

muscles, those muscles that we have conscious control over, are powered by the molecular motor protein, myosin II. Each of these molecular motors takes discrete steps approximately 5-10 nm in length along actin filaments, generating on the order of 5 pN of force. These filaments are arranged into segments called sarcomeres that expand and contract based on the motion of these individual proteins. These sarcomeres, each of which is a little over 2 μm in length, are the basic units of the higher order muscle fibers. Muscle fibers, each of which is a single cell, can span the full length of the muscle so a 20 cm long bicep, for example, may contain as many as $(20 * 10^{-2}) / (2 * 10^{-6}) = 10^5$ sarcomeres. Each sarcomere can expand and contract at a rate of approximately 10 $\mu\text{/s}$, with each of the 300 myosin heads per thick filament taking roughly 5 steps per second [152]. This remarkable feat serves as inspiration for how it might be possible to assemble fungible and extensible actuators from individual building blocks.

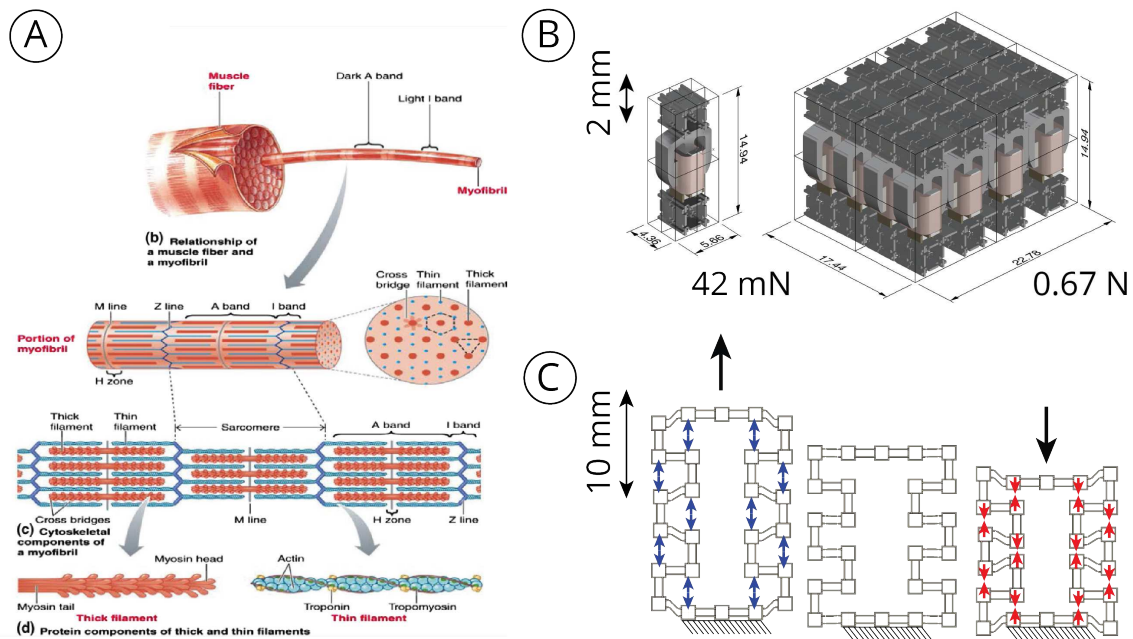


Figure 11-2: Biological muscles create macroscopic forces and displacements based on the motion of billions of microscopic parts arranged in hierarchical levels (A) [153]. The Lorentz force actuation components can be arranged in parallel to increase the force output (B) or in series to increase the displacement (C).

11.3 Assembly

Assembly at smaller length scales is often complicated by decreased positioning accuracy and difficulties in part manipulation because of the scaling of surface forces relative to inertial ones. I expect the discrete assembly method to be more amenable to high throughput assembly at small scales for a number of reasons.

- **Error Correction:** With the use of compliance in the toolhead, the assembler can take advantage of the interlocking nature of the parts. The shape of the interlocking slots enables

a degree of error correction and prior work has shown that the degree of positioning error tolerance can be as high as 39% of the part spacing [22].

- **Well-Defined Adhesion Forces:** Conventional micro-manipulation and micro-grasping often struggles with controlling the adhesion forces between the part and the tool and, in particular, it can be difficult to release parts at small scales because of surface forces. In this assembly framework the part-part interlocking forces can be made orders of magnitude stronger than the part-tool gripping force. Furthermore, with an actively driven gripping mechanism, the part-tool adhesion force can be modulated by more than an order of magnitude, enabling parts to be both picked from and placed into passive flexural bonding sites without the uncertainty of “sticking” parts.
- **Environment Agnostic:** Unlike many other micro-assembly strategies, which rely on liquid environments to suspend and manipulate parts, this one does not impose any constraints on the environment.

Chapter 12

Modeling

Commercial design and simulation tools struggle to model these kinds of discretely assembled structures that integrate a wide variety of functionality. While some multiphysics tools can model an actuated mechanism and structure (e.g. COMSOL), even these tools do not scale easily to encompass the dynamic range (maximum extents per feature size) of discretely assembled functional structures. Furthermore, no commercial tool exists to design control systems and circuitry embedded within the mechanical degrees of freedom that they control.

Instead, my colleagues and I decided to build our own tools to support end-to-end workflows for discrete assembly. One of these tools, DMDesign, developed by Amanda Ghassaei spans design, simulation, toolpathing, and machine control for electronic digital materials [147] [22]. Another tool, AMOEBA (also developed by Amanda Ghassaei), grew out of DMDesign to encompass a greater range of functionality including mechanisms, actuation, and control systems [147]. This tool enables users to build up integrated systems one building block at a time but also supports hierarchical representations, allowing users to abstract modular motifs that can be reused across a range of designs.

In this section I'll overview some approaches that have been used to model these kinds of integrated structures. I specifically focus on compliant mechanisms since the large displacement analysis of flexible structures offers the biggest challenge in modeling these systems efficiently. Furthermore, I detail a design tool developed to model and optimize discretely assembled compliant mechanisms.

12.1 Modeling Approaches

A number of different methods can be used for the simulation of mechanisms. Conventional mechanisms, which are typically made up of rigid links and revolute or prismatic degrees of freedom, are often simulated using rigid body models. While these are often analytical for mechanisms with only a handful of links and joints, numerical methods also exist. Automated analysis of arbitrary rigid body mechanisms is often complicated by the need to find closed kinematic loops to express the equations of motion. This approach is very accurate and efficient when the user has some knowledge of the mechanism being solved, but can be problematic with mechanisms of changing and various topologies. Singularities, for example, are a classic problem in kinematic analysis in which the mechanism locks up and has multiple equally possible trajectories [154]. Compliant mechanisms, on the other hand,

are often modeled using finite element methods. For mechanisms undergoing large displacements, this necessitates nonlinear finite element solvers [155]. A third approach, which is discussed by Jin et al., sits between these two approaches. Rather than modeling motion through the deflection of static elements, the authors describe a pseudo rigid body model in which virtual torsion springs are attached between each rigid bar. The problem of solving for the nonlinear kinematics of an arbitrary mechanism is then posed as an optimization which seeks to minimize the potential energy stored in the virtual springs [156]. Aviles et al. details a similar approach and does a more thorough treatment of the formulation with Lagrange multipliers to efficiently solve the static equilibrium problem [157].

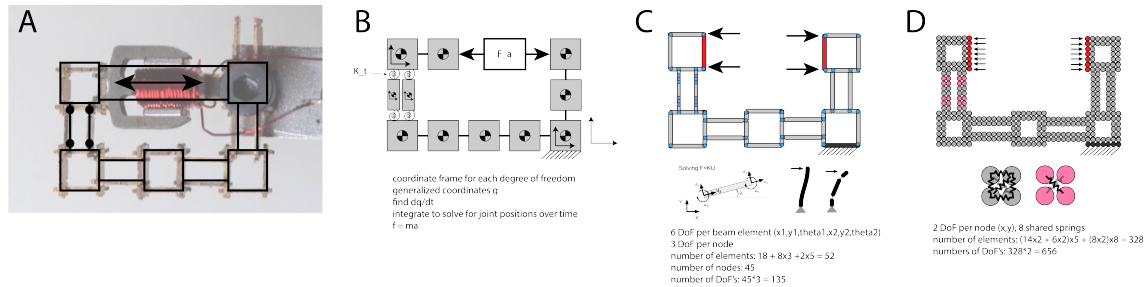


Figure 12-1: A number of modeling approaches can be used to model an actuated mechanism (A) including pseudo-rigid body models (B), plane-frame models (C), and discrete element models (D).

12.2 Optimization Approaches

Prior work in the topological optimization of compliant mechanisms has largely focused on two approaches: continuum-based methods and ground structure-based methods. Sigmund shows that the formulation of the compliant mechanism problem using these frameworks is very similar to the problem of optimizing for light, stiff structures. However, rather than simply minimizing compliance, the objective is to minimize compliance while effectively translating an input force or displacement into desired output work. In this case, Sigmund outlines an objective function based on mechanical advantage between the input and output force subject to constraints including the volume of material and the minimum and maximum densities each pixel can represent [158].

For the optimization of discrete-valued structures which aren't amenable to relaxing a continuum problem, heuristic methods like genetic algorithms are often used. Jin et al., for example, demonstrate a genetic algorithm implementation to find suitable mechanisms given bounding constraints for their pseudo rigid body models (in this case, a displacement inverting mechanism) [156].

12.3 Compliant Mechanism Simulation and Optimization

From a structural optimization perspective, discretely assembled mechanisms offer a unique advantage over conventionally fabricated devices. In contrast with prior topology optimization work, which has largely tried to approximate continuum materials with discrete voxels or ground structure elements, the discrete assembly approach enables a discrete-valued optimization of truly discrete materials; in essence, the physical parts are the finite elements themselves. I developed a nonlinear

finite element plane-frame solver capable of quickly simulating discrete mechanism problems. This solver is integrated in a browser based interface with interactive controls to aid in exploration of the discrete design space. Since the discrete design space is not well suited to traditional gradient based optimization methods, I developed an interactive heuristic for sequentially replacing parts to maximize displacement in a particular direction.

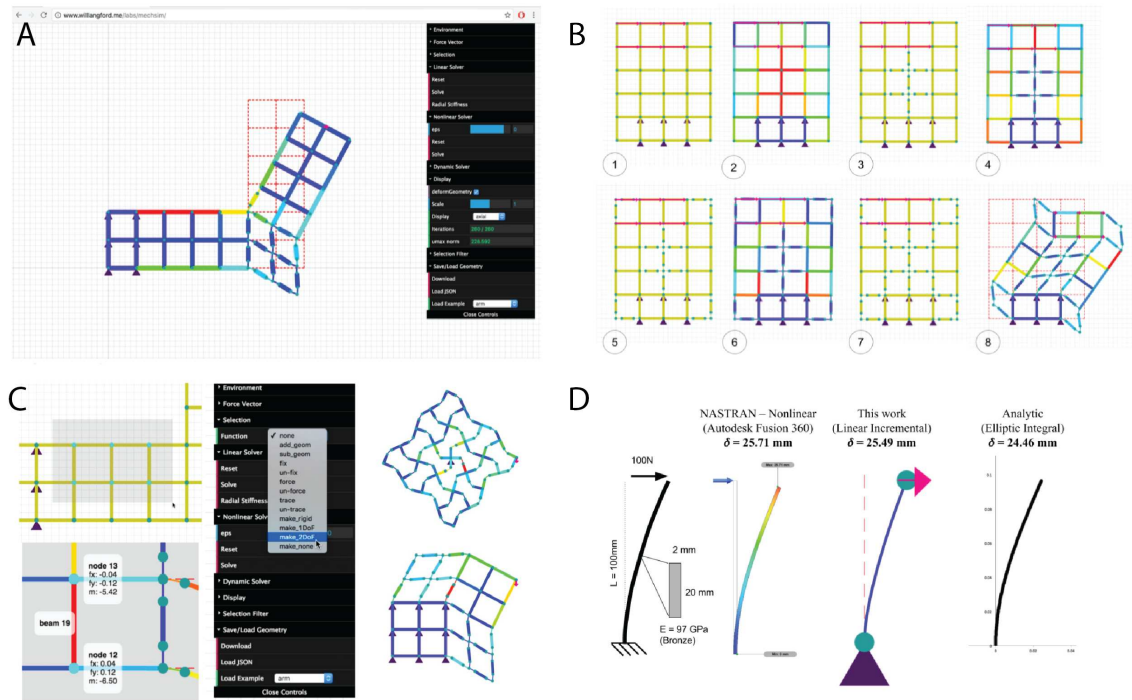


Figure 12-2: A browser based compliant mechanism design and simulation tool (A) can be used to interactively optimize the design of compliant mechanisms (B). Interactive features allow the visualization of forces and moments in the structure to inform the design (C). The simulation is physically meaningful, matching closely results from legacy finite element solvers and analytic solutions.

This tool is focused around planar mechanisms and so is purely two-dimensional. As such, each member has six degrees of freedom: two translational degrees of freedom and a rotational degree of freedom at each node. The design tool allows users to visualize the stiffness of the mechanism in all axes with the help of a radial stiffness plot. This helps give the user an intuition about the design space by allowing them to, for example, substitute rigid members with flexural parts and note the change in stiffness of the mechanism.

The two main computational expenses in solving the large-displacement problem are in assembling the system stiffness matrix and solving the system. The system stiffness matrix is inherently sparse and symmetric. This is especially certain in my case because of the topology of the discretely assembled mechanisms: there are no beam elements that span outside of their local neighborhood. This trait can be exploited to more efficiently assemble and solve the system by using sparse matrix data representations.

This software tool represents a design study of a simulation and optimization tool for compliant mechanisms. Future work should focus on extensions from 2D to 2.5D to 3D, integration of more

physics (e.g. electricity and magnetism), and optimization methods that allow users to specify desired outcomes and have the tool place individual parts.

Chapter 13

Applications and Extensions

Based on the work demonstrated in this thesis a number of applications and extensions of the work are currently being pursued.

13.1 Discrete Integrated Circuit Electronics (DICE)

One of extensions of the work being pursued is the assembly of reconfigurable high-performance computing. Much like the state of robot design and fabrication, the development of integrated circuits today often means choosing between the cost, expense, and long turn-time of an application specific integrated circuit (ASIC) or bulky and less performant (but quicker to develop) integration of existing integrated circuits (IC's). An assembly based approach for integrating heterogeneous "chipllets" could enable the configuration and re-configuration of compute hardware tailored to the computational problem to be solved (Figure 13-1). Potential benefits of this approach include reducing the development turn-time of a novel compute solution, rapidly reconfiguring systems to reflect changing workloads, on-demand production, and increasing system integration across the existing boundaries between chips, packages, boards, and interconnect.

A number of techniques have been proposed for ways to flexibly and densely integrate heterogeneous chipllets. In comparison with passive interposer approaches [159] [160], discrete assembly allows for reconfiguration and on-demand fabrication such that the routing between chips is not baked into hardware, but rather, can be incrementally built, modified, and extended upon. In comparison with approaches that use active interposers, or "switch fabrics" [161], discrete assembly offers the possibility of reconfiguration without the power and spatial overhead of crosspoint switches and FPGA's.

By scaling the size and complexity of the component parts, it is possible to balance the tradeoffs between the overhead of the connections and the refinement of the discretization. A number of components could be integrated within this framework including CPU's, GPU's, FPGA's, memory, analog, and input-output parts. Each of these component types come in a wide variety of capabilities and sizes. Looking at CPU's for example, the smallest commercial off the shelf (COTS) packaged microcontroller is the ATtiny20-UUR at just 1.4 mm by 1.55 mm. This 12-pin part is an 8-bit single cycle per instruction microcontroller that operates up to 12 MHz. One step up from that in complexity and in similarly small packages (< 2 mm x 2 mm) are microcontrollers like the Kinetis

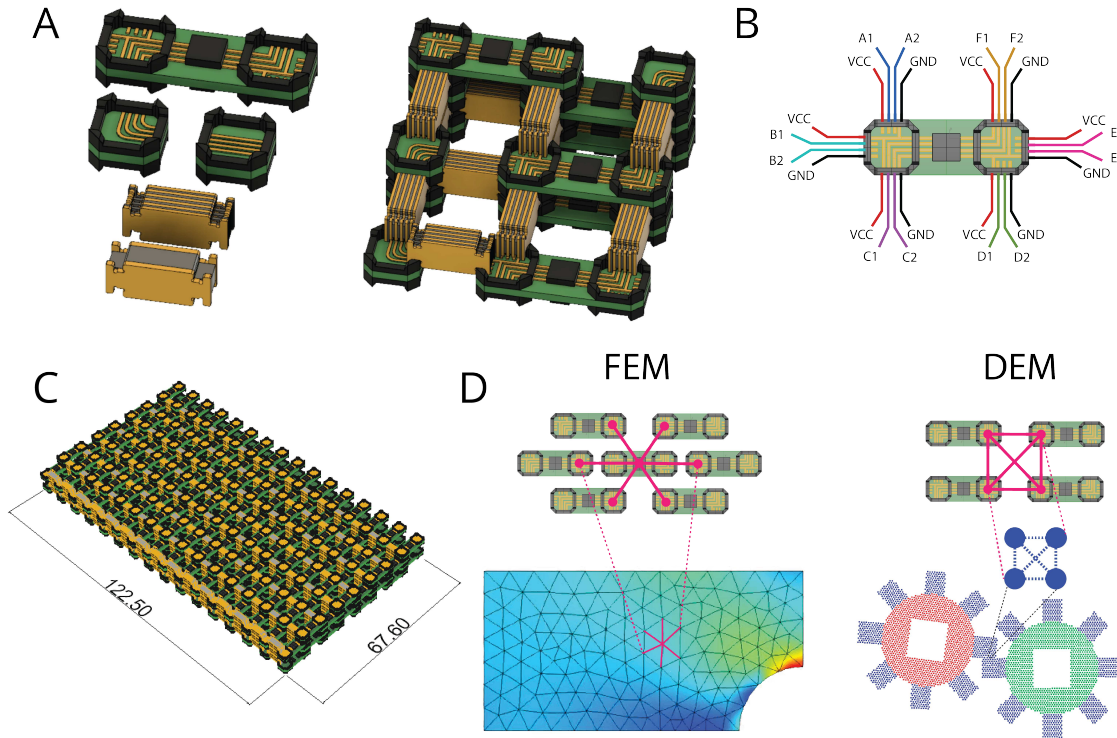


Figure 13-1: DICE application overview. (A) Discrete parts with embedded integrated circuits including microprocessors, FPGA's, analog peripherals, and memory. (B) The parts interlock with neighboring parts and have a number of input and output ports that can be connected to form a range of different topologies. (C) 256 microcontroller building blocks match the operations per second of a pentium processor. Configuring and reconfiguring to match the structure of the problem allows for potential speed ups from parallelization. (D) Reconfiguration could enable the physical architecture of the computer to mirror the computational structure of the problem being solved. This is particularly evident in problems like finite element analysis (FEA) and discrete element methods (DEM).

KL03 and Maxim MAX32660, an ARM Cortex-M0+ and ARM Cortex-M4F, respectively. These 32-bit processors are capable of running up to 96 MHz but have a 2 or 3 stage instruction pipeline. The Maxim part has an on-chip floating point unit which enables just 1-3 cycles per FLOP.

It is instructive to look at some very back-of-the-envelope numbers to get a sense of how many of these smaller CPU's are necessary to match the specifications for current state of the art computer processors. I take the 14-nm Intel i7-8700 Coffee Lake processor as the current state of the art. The base clock speed of 3.7GHz sells for \$360, consumes 95 W of power, and takes up a footprint of 37.5 mm x 37.5 mm x 4.4 mm. To achieve a similar instruction throughput with the 40-nm Maxim MAX32660 (neglecting bandwidth and latency constraints), one would need about 40 processors (3.7 GHz / 96 MHz). Mounting those processors on DICE parts with a 50% spatial overhead in each linear dimension results in an assembly that is approximately one quarter of the volume (12 mm x 12 mm x 4 mm) and one quarter of the cost (\$80) of the monolithic i7 processor. Furthermore, the power consumption of 40 MAX32660's (15 mW each) is less than 1 percent of the 95 W consumed by the Intel processor. While this number neglects real-world considerations such as available

bandwidth between processors and the intricacies of sharing memory, it represents the aim of this approach, which is to demonstrate the feasibility of assembling high performance computing from more basic constituent parts in a way that enables incremental extensibility and reconfiguration based on computing requirements.

A key driver for heterogeneous integration is the ability to combine parts made using dissimilar processes. For example, it is often beneficial to keep analog circuitry more spaced out while taking advantage of the ability to shrink the digital circuitry by using a more advanced process node. For this reason, DICE components will not just include microcontroller processors and other digital circuitry, but also analog-to-digital converters, GPIO expanders, and wireless components. While the aim of this work would be to eventually demonstrate integration of discrete chiplets designed specifically for this kind of discrete assembly, it is possible to demonstrate the feasibility of this approach using commercially available off the shelf components (Table 13.1).

Microcontroller	MAX32660	96 MHz	1.6 mm x 1.6 mm	14 IO	\$1.5
FPGA	MACHXO2	<400 MHz	2.5 mm x 2.5 mm	18 IO	\$5.2
Op-Amp	MAX4292	500 kHz GBP	1.5 mm x 1.5 mm	–	\$1.6
ADC	MAX19777	3 Msps	0.9 mm x 1.4 mm	2-ch	\$0.9
Memory	M95128	200 MHz	1.2 mm x 1.2 mm	–	\$0.45

Table 13.1: DICE parts that are being considered as starting points for the assembly and reconfiguration of high-performance computing systems.

This assembly methodology potentially opens up novel computer architectures that are not practical with existing methods. For example, the ability to assemble three-dimensional volumes of individual processors could enable the realization of much more parallel [162] [163] and defect tolerant [164] [165] computer architectures. Furthermore, because this discrete assembly method enables reconfiguration, the architecture can be reshaped based on the problem to be solved. Many compute-bound problems have a structure that can be exploited. Multiphysics simulations using finite element analysis or discrete element methods, for example, are governed by local interactions between neighboring vertices or nodes. By structuring the physical hardware to match this computational structure, the computation can be done almost entirely in parallel.

The hypothesis is that assembly of heterogeneous integrated circuits can be radically simplified by standardizing the the assembly interface between parts and allowing their interlocking geometry to dictate the precision of their placement. Evaluating the assembly automation of DICE parts will not so much prioritize throughput as it will the time it takes to go from idea to physical embodiment. Discretely assembling integrated electronics should enable users to go from idea to design to physical construction in hours, not months. In addition to this, the error-tolerance of the discrete assembly approach is critical to be able to scale down to the smallest pitch-densities that are desired (tens of microns).

13.2 Relaxing Constraints

This thesis details an approach to robotic construction that increases flexibility and lowers barriers to integrating functionality. This approach was largely developed within the confines of a number of strict constraints. These include, for example, the use of reversible mechanical connectors between

parts, the conformity to a regular rectangular lattice, and the limited part-set (with few exceptions). Implementing this approach relies on a relatively significant infrastructure. A cheap and accessible supply of building block parts is necessary. Additionally, an automated assembly tool is needed in order to realize the on-demand and direct-write fabrication possibilities. Not everyone reading this will have access to these kinds of materials and tools. As such, I think it is helpful to enumerate and elaborate on a number of possible relaxations of this work that make this work more generally implementable without the infrastructure requirements.

A modular design tool. In one instantiation, a design tool featuring discrete functional parts enables the design, simulation, and verification of a machine or system that incorporates structure, mechanism, and actuation. From this design, various physical instantiations of the machine could be “compiled.” An assembler could assemble the system from the building blocks described in this work. But there are other ways the device could be compiled including as monolithic or semi-monolithic digitally fabricated parts.

Mass-produced Actuator Components The actuator components developed in this work are the most fabrication intensive and require non-standardized processes to develop and fabricate. Getting a version of these actuators fabricated in mass quantities would not be a significant challenge using conventional manufacturing processes. These discrete actuator components could then enable the extensible assembly of robotic systems.

Monolithic compliant mechanisms. The design could be converted into a monolithic, single material representation that could be additively manufactured or laser cut (Figure 13-2). I actually employed this approach in testing some of my mechanism ideas. It allows for very rapid prototyping of structures and mechanisms that exhibit the same qualitative behaviors of the discretely assembled counterparts. This approach of monolithic construction doesn’t enable the same kind of heterogeneity as does the discrete assembly method and the mechanisms don’t have the same degree of anisotropy, but it makes accessible the modular approach developed in this thesis.

A ready supply of node parts. In another envisioned relaxation of this work, a mass produced node part type enables manual assembly integrated systems from laser-cut, 3D printed, or printed circuit board parts. This node part type could function as a “universal” connector that mechanically joins two dimensional parts made using these various processes.

In this concept, the nodes serve a purely mechanical role in connecting parts. Electrical connections would be made using PCB panels that interface directly with the nodes and other parts (Figure 13-3).

Given this supply of node parts, the construction of custom integrated robotic systems would begin with users designing their integrated system using modular building blocks in a digital design tool. The system could be simulated and verified for operation. Compilation of the design into a physical artifact could synthesize the design into elements that can be manufactured using commonly available tools (at least for a robotics lab) such as 3D printers, laser cutters, and PCB circuit designs. These parts would be cut, and then manually integrated through the use of the node connectors. Furthermore, a free parameter exists to determine the level of discretization. The design tool could output individual building block parts to be laser-cut, for example, or it could output a whole layer

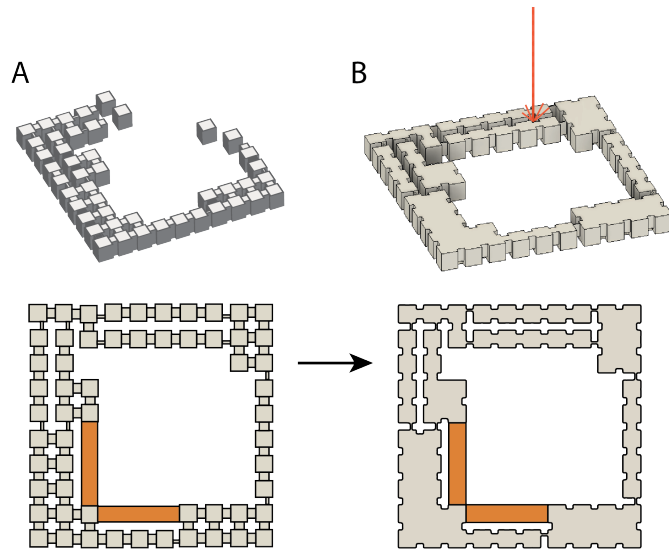


Figure 13-2: One possible relaxation of this approach involves compiling the discrete design (A) into a monolithic construction (B) that can be fabricated using 3D printers or laser-cutters.

of the device that features cutouts that interface with the node parts. This strategy allows for the integration of parts made using a variety of different processes while eliminating the need to assemble many individual parts where there is no need (Figure 13-3).

The nodes could serve purely mechanical role in connecting parts these various kinds of parts, or could be made using more advanced processes to incorporate electrical routing. The manufacturing of these more advanced node parts would likely be done in a similar way to how commercial electronic connectors are made, using stamped contacts and over-molded liquid crystal plastic bodies, for example. To encompass all of the possible routing degrees of freedom, a family of node parts would be necessary. Each of these having a particular routing arrangement such as passthrough, four-way, three-way, and no-connection.

These electrical nodes would enable the discretization of the electronic parts and allow connections to be made through layers of the assembly rather than remaining within a single plane.

Access to digital fabrication tools. At a larger scale than the millimeter parts developed in this work, these node parts could even be 3D printed, enabling very rapid prototyping of these kinds of assembled systems with commonly available digital fabrication tools. Custom node-parts could be developed to interface with off the shelf actuators and sensors.

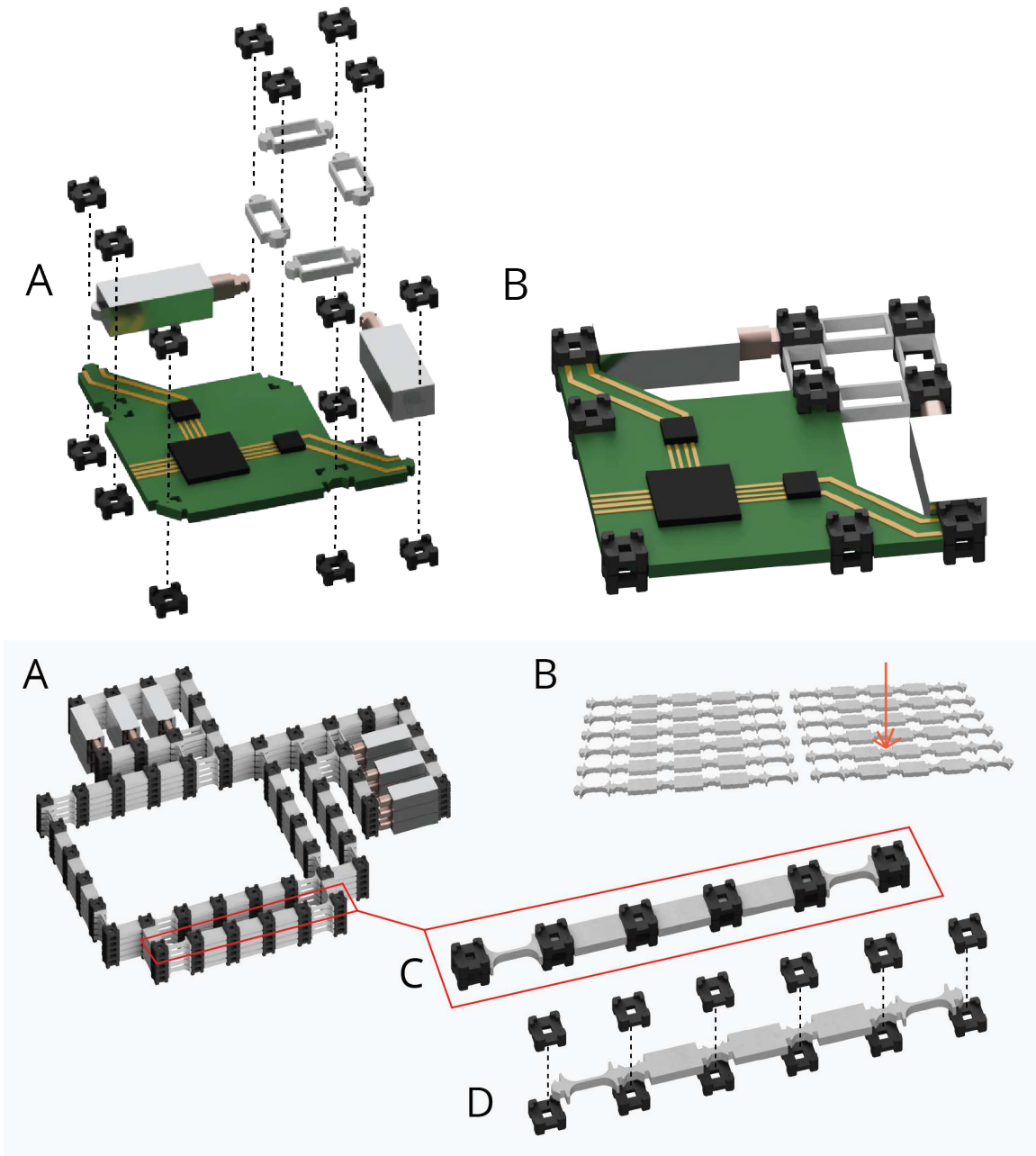


Figure 13-3: Another possible relaxation of this work enables the assembly of integrated machines from lasercut, 3D printed, and PCB parts using mass-produced nodes to build a walking motor (Top). These assemblies need not discretize at the finest level everywhere. The assembly can be broken down into sub-parts that still feature cutouts to interface with node parts to build a 2D positioner from semi-monolithic parts (Bottom).

Chapter 14

Conclusion

As we look to make devices that are more integrated and that combine more functionality through digital fabrication, current research has largely avoided assembly, preferring to try to integrate various functionalities within a single monolithic process. While doing so has extended what is possible and enabled new kinds of integrated robotic systems, I argue that it is ultimately limited by inherent constraints of each process and that no single monolithic process will be able to span the full range of desired functionality.

Instead, the approach introduced in this thesis represents a unified approach to robotic construction and a step towards on-demand robot fabrication. Rather than integrating functionality in a single process, it looks to enable integration through the standardization of assembly interfaces. Parts, with these assembly interfaces, can be produced using a wide variety of separate and dedicated processes, often enabling parts that are higher-performance and more functional than they could be in a monolithic process. This includes millimeter scale actuation components that have among the highest force density of any recently reported electromagnetic actuator as well as anisotropic compliant mechanisms that are more than two orders of magnitude stiffer off-axis as they are in the desired direction of motion.

Based on the capabilities developed in this work (structure, mechanism, actuation, circuitry, and control) a number of machines have been assembled that integrate these in various ways. A walking motor and walker, MOTILE, demonstrated two methods to convert small cyclic steps of discrete parts into long range motion. While this work has demonstrated the assembly of bidirectional linear motion, these systems can be thought of as modular primitives from which more powerful and complex degrees of freedom can be assembled.

The assembly process has been automated for structure, mechanism, and actuation part types, enabling a physical machine to be “compiled” directly from digital designs. The assembly platform has been shown to be able to take advantage of the interlocking joints of the discrete parts to build assemblies that are more precise than the machine itself. The speed of assembly currently exceeds that of manual assembly but requires time and effort to layout the feedstock of parts. Further developing the part production pipeline, going from raw materials to building block parts at a known pickup location on the assembler, would unlock the full potential of automated assembly.

This work interpolates between the field of modular robotics and digital fabrication, developing a set of relatively simple parts that can assemble relatively complex machines. In doing so, it lays

the groundwork for a viable path towards self-replicating machines by assembling assemblers. In this work, I demonstrated the basic capabilities that are necessary to do this including locomotion, part manipulation, and integrated control. In order to assemble assemblers, however, a few more challenges need to be overcome. First and foremost, control needs to be integrated within the same assembly as structure, mechanism, and actuation. Design studies and experiments have shown that this is nearly possible but higher-density electrical connectors between tiles need to be made more robust and reliable. Second, locomotion needs to register to a lattice. Currently, the exact step-size of the walker varies slightly from step to step. Assembling assemblers will critically rely on reliable open-loop positioning of machines by registering each step to a grid or lattice. Finally, the disparity between the force generated by the actuation components and the force required to place a part needs to be overcome. This likely warrants a redesign of the joints between parts to enable separate tuning of assembly and disassembly forces.

In the same way that computers and digital technology rest on the ability of a small family of gates to evaluate arbitrary logical expressions [166], this work points to a small family of building blocks that enable the construction of arbitrary robotic capabilities. While the design and fabrication of robots today often requires the integration of many diverse and custom parts, by standardizing the part set through the development of discrete assembly workflows, it is possible to take advantage of the same benefits inherent in computational universality and enable more flexible, inexpensive, and rapid design of robotic systems. The work developed here shows the utility of even a limited part set and the opportunity for future work to refine the part set to encompass a full range of robotic capabilities.

Appendix A

Lessons Learned

One of my favorite chapters in Ara Knaian's thesis is his chapter on lessons learned [58]. This chapter is very much inspired by that.

Here are some things that I've learned along the way:

- **Balance thinking with doing.** Even if you know an experiment is not going to work, you learn a lot in the process and often spark new ideas or directions.
- **Document early and often.** This means taking pictures and videos even when things aren't working perfectly. Often it's these work-in-progress photos/videos, which can feel like a waste of time in the moment, that end up becoming the things that encapsulate a whole project.
- **Don't be afraid to pivot when things aren't working.** I spent a while trying to build a transistor out of press-fit parts with very little progress. Eventually I decided to just put a transistor on a part and that spiraled into this thesis.
- **But also, don't give up an idea just because it gets hard.** It can be very tempting to switch gears to another project or problem when something gets hard. Sometimes this is good to do, but sometimes you end up bouncing between projects, not really making progress on any one in particular. Balancing these is a continual process.
- **Balance process development with end results.** It can be easy to get sucked into developing better processes and tools to make the thing you want to make faster, better, and cheaper. Developing better processes and workflows is great and makes results more reproducible and consistent. But spending too much time on it can detract from the whole point of developing the process in the first place.
- **Measure.** Test assumptions with experiments. Some of the most exciting moments of this research have been in performing an experiment only to find out that I was completely wrong about something.
- **Don't forget about books.** With the wealth of freely available research on the internet it can be easy to disregard books. But papers often dance over the core concepts and relationships in a particular area of research. Books represent a more curated set of knowledge that can help you establish a base of core principles from which you can project forward.

Additionally, throughout my research I've discovered some tools that have been enormously helpful in building these small scale systems:

- **Parallel Jaw Pliers.** I think I owe my PhD to this tool. Manual assembly without this is fraught with the possibility of damaging parts by applying force in the wrong direction. It's also great for grabbing pins and bolt-heads without marring them.
- **Micro-vises** like the Proxxon 24260 are essential for holding and manipulating small parts.
- **Pin-vises** can be used not just for holding small cylindrical parts, but also work great for precisely holding and using reamers, drills, and small taps.
- **Micro Spatulas** are more precise than syringe tips for applying very small amounts of adhesive.
- **EZ-Hook** electrical connectors are good for grabbing small wires and traces but contribute a non-trivial amount of resistance to the circuit.
- A **micro-ruler** on a stick is great for calibrating microscope measurements.
- **Gelpak** on a glass plate makes a great fixturing solution for laser micro-machining as well as all kinds of precise soldering and assembly work.
- I ended up using the **Analog Discovery 2** a great deal for things ranging from debugging serial bus issues, closing the loop on microcode, and even frequency response measurements.
- **Masking tape and superglue** makes for quick and reliable machining fixturing.
- Choosing the right endmill for the material makes a huge difference. Check out **single-flute super-O mills** for “grabby” plastics like HDPE. **Diamond-cut mills** work great on composites. **Straight-flute endmills** leave a nice finish on both the top and bottom sides of plywood. Avoid chatter by using the shortest, stubbiest endmill that you can for the job.

Bibliography

- [1] S. Tibbits, “From Automated to Autonomous Assembly,” *Architectural Design*, vol. 87, no. 4, pp. 6–15, 2017.
- [2] J. Paik, “Soft robot design methodology for ‘push-button’ manufacturing,” *Nature Reviews Materials*, pp. 1–3, 2018.
- [3] Z. Butler and A. Rizzi, “Distributed and Cellular Robots,” in *Springer Handbook of Robotics*, pp. 911–920, 2008.
- [4] T. Hornyak, “Be afraid: DARPA unveils Terminator-like Atlas robot.” <https://www.cnet.com/news/be-afraid-darpa-unveils-terminator-like-atlas-robot/>, jul.
- [5] “PETMAN (Protection Ensemble Test Mannequin) Humanoid Military Robot.” <https://www.army-technology.com/projects/petman/>.
- [6] Massachusetts Institute of Technology, “MIT Backflipping Mini Cheetah.” <https://youtu.be/xNeZWP5Mx9s>, 2019.
- [7] H. W. Park, P. M. Wensing, and S. Kim, “High-speed bounding with the MIT Cheetah 2: Control design and experiments,” *International Journal of Robotics Research*, vol. 36, no. 2, pp. 167–192, 2017.
- [8] J. P. Whitney, P. S. Sreetharan, K. Y. Ma, and R. J. Wood, “Pop-up book MEMS,” *Journal of Micromechanics and Microengineering*, vol. 21, no. 11, p. 115021, 2011.
- [9] C. Semini, M. Baker, K. Laxman, V. Chandan, T. Maruthiram, R. Morgan, M. Frigerio, V. Barasuol, D. G. Caldwell, and G. Rey, “A Brief Overview of a Novel, Highly-Integrated Hydraulic Servo Actuator with Additive-Manufactured Titanium Body,” *IROS Workshop 2016*, pp. 4–7, 2016.
- [10] M. Wehner, R. L. Truby, D. J. Fitzgerald, B. Mosadegh, G. M. Whitesides, J. A. Lewis, and R. J. Wood, “An integrated design and fabrication strategy for entirely soft, autonomous robots,” *Nature*, vol. 536, p. 451, aug 2016.
- [11] D. Barry, “Chromosome and Kinetochore.” <https://www.wehi.edu.au/wehi-tv/chromosome-and-kinetochore>, 2013.
- [12] A. J. Roberts, T. Kon, P. J. Knight, K. Sutoh, and S. A. Burgess, “Functions and mechanics of dynein motor proteins,” *Nature Reviews Molecular Cell Biology*, vol. 14, no. 11, pp. 713–726, 2013.

- [13] J. Lin and D. Nicastro, “Asymmetric distribution and spatial switching of dynein activity generates ciliary motility,” *Science*, vol. 360, no. 6387, 2018.
- [14] DNA Learning Center, “Transcription and Translation: Translation (Advanced).” <https://www.dnalc.org/resources/3d/16-translation-advanced.html>, 2010.
- [15] R. Milo and R. Phillips, “Cell Biology by the Numbers,” 2016.
- [16] Particle Sciences, “Protein Structure,” *Technical Brief 2009 vol. 8*, vol. 8, pp. 1–2, 2009.
- [17] BioNinja, “Amino Acids.” <https://ib.bioninja.com.au/standard-level/topic-2-molecular-biology/24-proteins/amino-acids.html>.
- [18] G. A. Popescu, T. Mahale, and N. A. Gershenfeld, “Digital materials for digital printing,” *NIP & Digital Fabrication Conference*, pp. 1–4, 2006.
- [19] J. D. Hiller and H. Lipson, “Fully Recyclable Multi-Material Printing,” *Solid Freeform Fabrication Symposium (SFF’09)*, 2009.
- [20] K. C. Cheung and N. Gershenfeld, “Reversibly Assembled Cellular Composite Materials,” *Science*, vol. 341, no. September, pp. 1219–1221, 2013.
- [21] B. Jenett, S. Calisch, D. Cellucci, N. Cramer, N. Gershenfeld, S. Sweil, and K. C. Cheung, “Digital Morphing Wing: Active Wing Shaping Concept Using Composite Lattice-Based Cellular Structures,” *Soft Robotics*, 2017.
- [22] W. Langford, A. Ghassaei, and N. Gershenfeld, “Automated Assembly of Electronic Digital Materials,” in *ASME MSEC*, (Blacksburg, VA), pp. 1–10, 2016.
- [23] R. MacCurdy, a. McNicoll, and H. Lipson, “Bitblox: Printable digital materials for electromechanical machines,” *The International Journal of Robotics Research*, jul 2014.
- [24] C. D. Onal, M. T. Tolley, R. J. Wood, and D. Rus, “Origami-Inspired Printed Robots,” *IEEE/ASME Transactions on Mechatronics*, vol. 20, no. 5, pp. 2214–2221, 2015.
- [25] A. Ion, J. Frohnhofen, L. Wall, R. Kovacs, M. Alistar, J. Lindsay, P. Lopes, H.-T. Chen, and P. Baudisch, “Metamaterial Mechanisms,” pp. 529–539, 2016.
- [26] N. Cramer, D. Cellucci, K. C. Cheung, S. Sweil, and M. Teodorescu, “Design and Testing of FERVOR: Flexible and Reconfigurable Voxel-based Robot,” *2017 IEEE/RSJ International Conference on Intelligent Robots and Systems (IROS)*, pp. 2730–2735, 2017.
- [27] D. M. Aukes, B. Goldberg, M. R. Cutkosky, and R. J. Wood, “An Analytic Framework for Developing Inherently-Manufacturable Pop-up Laminate Devices,”
- [28] A. T. Baisch and R. J. Wood, “Pop-up assembly of a quadrupedal ambulatory MicroRobot,” *IEEE International Conference on Intelligent Robots and Systems*, pp. 1518–1524, 2013.
- [29] M. Schaffner, J. A. Faber, L. Pianegonda, P. A. Rühs, F. Coulter, and A. R. Studart, “3D printing of robotic soft actuators with programmable bioinspired architectures,” *Nature Communications*, vol. 9, no. 1, 2018.

- [30] R. F. Shepherd, F. Ilievski, W. Choi, S. A. Morin, A. A. Stokes, A. D. Mazzeo, X. Chen, M. Wang, and G. M. Whitesides, “Multigait soft robot,” *Proceedings of the National Academy of Sciences*, 2011.
- [31] T. Ranzani, S. Russo, N. W. Bartlett, M. Wehner, and R. J. Wood, “Increasing the Dimensionality of Soft Microstructures through Injection-Induced Self-Folding,” *Advanced Materials*, vol. 1802739, p. 1802739, 2018.
- [32] E. MacDonald and R. Wicker, “Multiprocess 3D printing for increasing component functionality,” *Science*, vol. 353, no. 6307, 2016.
- [33] J. Hiller, “Digital Materials: Voxel Design, Rapid Assembly, Structural Properties, and Design Methods,” no. May, 2011.
- [34] W. Langford, A. Ghassaei, N. Gershenfeld, and B. Jenett, “Hierarchical assembly of a self-replicating spacecraft,” in *IEEE Aerospace Conference Proceedings2*, 2017.
- [35] A. W. Burks, “Von Neumann’s Self-Reproducing Automata,” Tech. Rep. June, The University of Michigan, 1969.
- [36] W. M. Stevens, *Self-Replication, Construction and Computation*. Doctor of philosophy, University of Kent, 2009.
- [37] A. Ellery, “Are Self-Replicating Machines Feasible?,” *Journal of Spacecraft and Rockets*, vol. 53, no. 2, pp. 317–327, 2016.
- [38] V. Zykov, E. Mytilinaios, M. Desnoyer, and H. Lipson, “Evolved and Designed Self-Reproducing Modular Robotics,” *IEEE Transactions on Robotics*, vol. 23, pp. 308–319, apr 2007.
- [39] M. Yim, W.-M. Shen, B. Salemi, D. Rus, M. Moll, H. Lipson, and E. Klavins, “Modular Self-reconfigurable Robot Systems: Challenges and Opportunities for the Future,” *IEEE Robotics & Automation Magazine*, vol. 14, no. 1, pp. 43–52, 2007.
- [40] A. N. Knaian, K. C. Cheung, M. B. Lobovsky, A. J. Oines, P. Schmidt-Neilsen, and N. A. Gershenfeld, “The Milli-Motein: A self-folding chain of programmable matter with a one centimeter module pitch,” *IEEE International Conference on Intelligent Robots and Systems*, pp. 1447–1453, 2012.
- [41] C. H. Belke and J. Paik, “Mori: A Modular Origami Robot,” *IEEE/ASME Transactions on Mechatronics*, vol. 22, no. 5, pp. 2153–2164, 2017.
- [42] K. Gilpin and D. Rus, “Modular Robot Systems From Self-Assembly to Self-Disassembly,” *IEEE Robotics & Automation Magazine*, pp. 38–55, 2010.
- [43] A. S. Howe, “Self-assembling modular robotic structures,” *IEEE Robotics and Automation Magazine*, vol. 14, no. 4, pp. 26–33, 2007.
- [44] T. Toth-Fejel, R. A. Freitas, and M. S. Moses, “Modeling Kinematic Cellular Automata Final Report,” tech. rep., NASA NIAC, 2004.

- [45] G. Chirikjian, “An architecture for self-replicating lunar factories,” *NIAC Phase I*, 2004.
- [46] M. S. Moses, H. Ma, K. C. Wolfe, and G. S. Chirikjian, “An architecture for universal construction via modular robotic components,” *Robotics and Autonomous Systems*, vol. 62, no. 7, pp. 945–965, 2014.
- [47] T. V. Karpinets, D. J. Greenwood, C. E. Sams, and J. T. Ammons, “RNA: Protein ratio of the unicellular organism as a characteristic of phosphorous and nitrogen stoichiometry and of the cellular requirement of ribosomes for protein synthesis,” *BMC Biology*, vol. 4, pp. 1–10, 2006.
- [48] Nanoscribe, “<https://www.nanoscribe.de/en/>,” tech. rep.
- [49] A. M. Pickering and K. J. A. Davies, “Degradation of damaged proteins: The main function of the 20S proteasome,” *Progress in Molecular Biology and Translational Science*, vol. 109, pp. 227–248, 2012.
- [50] M. Sprinzl, “Correction of errors during protein synthesis,” *Angewandte Chemie - International Edition*, vol. 48, no. 21, pp. 3738–3739, 2009.
- [51] L. Eshun-Wilson, R. Zhang, D. Portran, M. V. Nachury, D. B. Toso, T. Löhner, M. Vendruscolo, M. Bonomi, J. S. Fraser, and E. Nogales, “Effects of α -tubulin acetylation on microtubule structure and stability,” *Proceedings of the National Academy of Sciences*, vol. 116, no. 21, pp. 10366–10371, 2019.
- [52] J. Pelletier and S. Jun, “The Bacterial Nucleoid,” vol. 1624, pp. 311–322, 2017.
- [53] P. Mooney, T. Sulerud, J. F. Pelletier, M. R. Dilsaver, M. Tomschik, C. Geisler, and J. C. Gatlin, “Tau-based fluorescent protein fusions to visualize microtubules,” *Cytoskeleton*, vol. 74, no. 6, pp. 221–232, 2017.
- [54] M. C. Good, “Scaffold Proteins : Hubs for Controlling the Flow of Cellular Information,” vol. 680, no. 2011, pp. 680–687, 2012.
- [55] D. Rus and M. T. Tolley, “Design, fabrication and control of soft robots,” *Nature*, vol. 521, no. 7553, pp. 467–475, 2015.
- [56] D. Rus and M. T. Tolley, “Design, fabrication and control of origami robots,” *Nature Reviews Materials*, pp. 1–12, 2018.
- [57] J. Tocchio, “Exploded Views – Canon AE-1.” <https://www.casualphotophile.com/2015/03/26/exploded-views-canon-ae-1/>, 2015.
- [58] A. N. Knaian, *Electropermanent Magnetic Connectors and Actuators : Devices and Their Application in Programmable Matter*. Doctor of philosophy, Massachusetts Institute of Technology, 2010.
- [59] Cirris, “Connector Life Cycles.” <https://www.cirris.com/learning-center/product-articles/other-products/227-connector-life-cycles>.
- [60] P. V. Dijk, “Critical Aspects of Electrical Connector Contacts,” tech. rep.

- [61] W. K. Langford, *Electronic Digital Materials*. Master of science, Massachusetts Institute of Technology, 2014.
- [62] O. Tessmann, “Topological Interlocking Assemblies,” *Ecaade 30*, vol. 2, no. Lynn 2009, pp. 201–210, 2011.
- [63] A. G. Gillies and R. S. Fearing, “A micromolded connector for reconfigurable millirobots,” *Journal of Micromechanics and Microengineering*, vol. 20, p. 105011, oct 2010.
- [64] B. Jenett, N. Gershenfeld, and P. Guerrier, “Building Block-Based Assembly of Scalable Metallic Lattices,” *Proceedings of the 13th Manufacturing Science and Engineering Conference*, pp. 1–6, 2018.
- [65] B. Jenett, D. Cellucci, C. Gregg, and K. Cheung, “Meso-scale digital materials: modular, reconfigurable, lattice-based structures,” *Proceedings of the 2016 Manufacturing Science and Engineering Conference*, pp. 1–11, 2016.
- [66] G. Trinh, G. Copplesstone, M. O’Connor, S. Hu, S. Nowak, K. Cheung, B. Jenett, and D. Cellucci, “Robotically assembled aerospace structures: Digital material assembly using a gantry-type assembler,” *IEEE Aerospace Conference Proceedings*, pp. 1–7, 2017.
- [67] A. Hsu, A. Wong-Foy, B. McCoy, C. Cowan, J. Marlow, B. Chavez, T. Kobayashi, D. Shockey, and R. Pelrine, “Application of micro-robots for building carbon fiber trusses,” *2016 International Conference on Manipulation, Automation and Robotics at Small Scales, MARSS 2016*, pp. 1–6, 2016.
- [68] DuPont, “DuPont™ Pyralux® LF Sheet Adhesive,” tech. rep.
- [69] 3M, “3M™ XYZ / Isotropic Electrically Conductive Adhesive Transfer Tape 9709,” tech. rep., 2011.
- [70] J. Neubert and H. Lipson, “Soldercubes: a self-soldering self-reconfiguring modular robot system,” *Autonomous Robots*, jul 2015.
- [71] H. Lipson, “Rapid Assemblers for Voxel-Based VLSI Robotics,” tech. rep., 2015.
- [72] A. Miyachi America, “GENERAL PRINCIPLES Fundamentals of Small Parts Resistance Welding,”
- [73] T. A. Schaedler, A. J. Jacobsen, A. Torrents, A. E. Sorensen, J. Lian, J. R. Greer, L. Valdevit, and W. B. Carter, “Ultralight metallic microlattices,” *Science*, vol. 334, no. 6058, pp. 962–965, 2011.
- [74] NTopology, “nTopology.” <https://ntopology.com/>.
- [75] Autodesk, “Autodesk Within.” <http://www.withinlab.com/>.
- [76] Renishaw, “Metal Additive Manufacturing (3D printing).” <https://www.renishaw.com/en/metal-3d-printing-32084>.

- [77] N. B. Cramer, D. W. Cellucci, O. B. Formoso, C. E. Gregg, B. E. Jenett, J. H. Kim, M. Lendraitis, S. S. Sweit, G. T. Trinh, K. V. Trinh, and K. C. Cheung, “Elastic shape morphing of ultralight structures by programmable assembly,” *Smart Materials and Structures*, vol. 28, no. 5, 2019.
- [78] M. Mirkhalaf, A. Sunesara, B. Ashrafi, and F. Barthelat, “Toughness by segmentation: Fabrication, testing and micromechanics of architected ceramic panels for impact applications,” *International Journal of Solids and Structures*, vol. 0, pp. 1–14, 2018.
- [79] Y. Feng, T. Siegmund, E. Habtour, and J. Riddick, “Impact mechanics of topologically interlocked material assemblies,” *International Journal of Impact Engineering*, vol. 75, no. July 2016, pp. 140–149, 2015.
- [80] L. Djumas, A. Molotnikov, G. P. Simon, and Y. Estrin, “Enhanced Mechanical Performance of Bio-Inspired Hybrid Structures Utilising Topological Interlocking Geometry,” *Scientific Reports*, vol. 6, no. January, pp. 1–10, 2016.
- [81] X. Zheng, H. Lee, T. H. Weisgraber, M. Shusteff, J. DeOtte, E. B. Duoss, J. D. Kuntz, M. M. Biener, Q. Ge, J. a. Jackson, S. O. Kucheyev, N. X. Fang, and C. M. Spadaccini, “Ultralight, ultrastiff mechanical metamaterials,” *Science (New York, N.Y.)*, vol. 344, pp. 1373–7, jun 2014.
- [82] K. Cheung, *Digital cellular solids: reconfigurable composite materials*. Doctor of philosophy, Massachusetts Institute of Technology, 2012.
- [83] J. D. Hiller, J. Miller, and H. Lipson, “Microbricks for Three-Dimensional Reconfigurable Modular Microsystems,” *Journal of Microelectromechanical Systems*, vol. 20, pp. 1089–1097, oct 2011.
- [84] J. Hiller and H. Lipson, “Methods of Parallel Voxel Manipulation for 3D Digital Printing,” in *Proceedings of the 18th solid freeform fabrication symposium.*, p. 12, 2007.
- [85] J. Ward, *Additive assembly of digital materials*. Master of science in media arts and sciences, Massachusetts Institute of Technology, 2010.
- [86] J. Hiller and H. Lipson, “Design and analysis of digital materials for physical 3D voxel printing,” *Rapid Prototyping Journal*, vol. 15, no. 2, pp. 137–149, 2009.
- [87] R. J. Wood, “The challenge of manufacturing between macro and micro,” *American Scientist*, vol. 102, no. 2, pp. 124–131, 2014.
- [88] C. Conde and A. Cáceres, “Microtubule assembly, organization and dynamics in axons and dendrites,” *Nature reviews. Neuroscience*, vol. 10, pp. 319–32, may 2009.
- [89] S. P. Magleby, “Library of Compliant Mechanisms,” in *Handbook of Compliant Mechanisms*, pp. 147–153, 2013.
- [90] N. Meisel, A. Gaynor, C. Williams, and J. Guest, “Multiple-material topology optimization of compliant mechanisms created via polyjet 3D printing,” in *24th International SFF Symposium - An Additive Manufacturing Conference, SFF 2013*, 2013.

- [91] F. B., “Caress of the Gaze: A Gaze Actuated 3D Printed Body Architecture,” *Proceedings of Posthuman Frontiers: Acadia 2016*, pp. 352–361, 2016.
- [92] J. Gafford, Y. Ding, A. Harris, A. Moser, and C. Walsh, “Shape Deposition Manufacturing of a Soft , Atraumatic , Deployable Surgical Grasper,” no. 1, pp. 4–5.
- [93] R. J. Wood, S. Avadhanula, R. Sahai, E. Steltz, and R. S. Fearing, “Microrobot Design Using Fiber Reinforced Composites,” *Journal of Mechanical Design*, vol. 130, no. 5, p. 052304, 2008.
- [94] H. McClintock, F. Z. Temel, N. Doshi, J.-s. Koh, and R. J. Wood, “The milliDelta: A high-bandwidth, high-precision, millimeter-scale Delta robot,” *Science Robotics*, vol. 3, no. 14, p. eaar3018, 2018.
- [95] A. M. Hoover and R. S. Fearing, “Analysis of off-axis performance of compliant mechanisms with applications to mobile millirobot design,” *2009 IEEE/RSJ International Conference on Intelligent Robots and Systems, IROS 2009*, pp. 2770–2776, 2009.
- [96] B. P. Trease, Y.-M. Moon, and S. Kota, “Design of Large-Displacement Compliant Joints,” *Journal of Mechanical Design*, vol. 127, no. 4, p. 788, 2005.
- [97] R. M. Panas and J. B. Hopkins, “Eliminating Underconstraint in Double Parallelogram Flexure Mechanisms,” *Journal of Mechanical Design*, vol. 137, no. 9, p. 092301, 2015.
- [98] R. Malka, A. L. Desbiens, Y. Chen, and R. J. Wood, “Principles of microscale flexure hinge design for enhanced endurance,” *IEEE International Conference on Intelligent Robots and Systems*, no. Iros, pp. 2879–2885, 2014.
- [99] A. E. Guerinot, S. P. Magleby, L. L. Howell, and R. H. Todd, “Compliant Joint Design Principles for High Compressive Load Situations,” *Journal of Mechanical Design*, vol. 127, no. 4, p. 774, 2005.
- [100] R. Wood, E. Steltz, and R. Fearing, “Optimal energy density piezoelectric bending actuators,” *Sensors and Actuators A: Physical*, vol. 119, no. October 2004, pp. 476–488, 2005.
- [101] A. P. Gerratt, B. Balakrishnan, I. Penskiy, and S. Bergbreiter, “Dielectric elastomer actuators fabricated using a micro-molding process,” *Smart Materials and Structures*, vol. 23, p. 055004, may 2014.
- [102] N. J. Kohut, A. M. Hoover, K. Y. Ma, S. S. Baek, and R. S. Fearing, “MEDIC: A legged millirobot utilizing novel obstacle traversal,” *Proceedings - IEEE International Conference on Robotics and Automation*, pp. 802–808, 2011.
- [103] B. Goldberg, M. Karpelson, O. Ozcan, and R. J. Wood, “Planar fabrication of a mesoscale voice coil actuator,” *2014 IEEE International Conference on Robotics and Automation (ICRA)*, pp. 6319–6325, 2014.
- [104] R. Yeh, S. Hollar, and K. S. J. Pister, “Single mask, large force, and large displacement electrostatic linear inchworm motors,” *Journal of Microelectromechanical Systems*, vol. 11, no. 4, pp. 330–336, 2002.

- [105] Linear Technologies, “LTSpice.” <https://www.analog.com/en/design-center/design-tools-and-calculators/ltspice-simulator.html>.
- [106] K&J Magnetics Inc., “Temperature and Neodymium Magnets.” <https://www.kjmagnetics.com/blog.asp?p=temperature-and-neodymium-magnets>, 2016.
- [107] D. C. Hanselman, *Brushless permanent magnet motor design*. 2006.
- [108] W. S. N. Trimmer, “Microrobots and Micromechanical Systems,” *Sensors and Actuators*, vol. 19, no. 3, pp. 267–287, 1989.
- [109] Ingrid West Machinery Ltd., “Fully Automatic Hot Air Coil Winding Machine.” http://coilwindingmachines.eu/automatic_winding_machines/hot_air_coil_winding_machine.html.
- [110] C.-S. Liu and P. D. Lin, “Miniaturized auto-focusing VCM actuator with zero holding current,” *Optics Express*, vol. 17, no. 12, p. 9754, 2009.
- [111] M. Salerno, A. Firouzeh, and J. Paik, “A Low Profile Electromagnetic Actuator Design and Model for an Origami Parallel Platform,” *Journal of Mechanisms and Robotics*, vol. 9, no. 4, p. 041005, 2017.
- [112] B. H. Shin and S. Y. Lee, “Micro mobile robots using electromagnetic oscillatory actuator,” *Proceedings of the IEEE RAS and EMBS International Conference on Biomedical Robotics and Biomechatronics*, pp. 575–580, 2012.
- [113] H2W Technologies, “H2W NCC10-15-027-1RC.” <https://www.h2wtech.com/product/voice-coil-actuators/NCC10-15-027-1RC>.
- [114] Moticont, “LVCМ-010-013-01.” <http://moticont.com/voice-coil-motor.htm>.
- [115] P. A. York, S. Member, R. J. Wood, and S. Member, “A geometrically-amplified in-plane piezoelectric actuator for mesoscale robotic systems,” pp. 1263–1268, 2017.
- [116] E. W. Schaler, L. Jiang, C. Lee, and R. S. Fearing, “Bidirectional, Thin-Film Repulsive-/Attractive-Force Electrostatic Actuators for a Crawling Milli-Robot,” *MARSS 2018 (to appear)*, pp. 1–8, 2018.
- [117] J. E. Huber, N. a. Fleck, and M. F. Ashby, “The selection of mechanical actuators based on performance indices,” *Proceedings of the Royal Society A: Mathematical, Physical and Engineering Sciences*, vol. 453, no. 1965, pp. 2185–2205, 1997.
- [118] M. S. Tu, “Cardiac-like behavior of an insect flight muscle,” *Journal of Experimental Biology*, vol. 207, no. 14, pp. 2455–2464, 2004.
- [119] H. Iwamoto, “Structure, function and evolution of insect flight muscle,” *Biophysics*, vol. 7, pp. 21–28, 2011.
- [120] R. Merry, R. Van De Molengraft, and M. Steinbuch, “Modeling of a walking piezo actuator,” *Sensors and Actuators, A: Physical*, 2010.
- [121] Physikinstrumente, “Piezo Walk Piezo Motors.” <https://www.physikinstrumente.com/>, 2018.

- [122] K. Spanner and B. Koc, "Piezoelectric Motors, an Overview," *Actuators*, vol. 5, no. 1, p. 6, 2016.
- [123] J. B. Reese, S. L. Bober, M. B. Daly, C. Program, F. Chase, B. Sciences, P. Care, F. Chase, S. Behavior, and B. Neoplasms, "HHS Public Access," vol. 123, no. 24, pp. 4757–4763, 2018.
- [124] I. Penskiy and S. Bergbreiter, "Optimized electrostatic inchworm motors using a flexible driving arm," *Journal of Micromechanics and Microengineering*, vol. 23, no. 1, 2013.
- [125] Z. Bi, Y. Guan, S. Chen, H. Zhu, and H. Zhang, "A miniature biped wall-climbing robot for inspection of magnetic metal surfaces," *2012 IEEE International Conference on Robotics and Biomimetics, ROBIO 2012 - Conference Digest*, pp. 324–329, 2012.
- [126] X. Tang, D. Zhang, Z. Li, and J. Chen, "An omni-directional wall-climbing microrobot with magnetic wheels directly integrated with electromagnetic micromotors," *International Journal of Advanced Robotic Systems*, vol. 9, 2012.
- [127] M. Eich and T. V??gele, "Design and control of a lightweight magnetic climbing robot for vessel inspection," *2011 19th Mediterranean Conference on Control and Automation, MED 2011*, no. June, pp. 1200–1205, 2011.
- [128] G. Lee, G. Wu, J. Kim, and T. Seo, "High-payload climbing and transitioning by compliant locomotion with magnetic adhesion," *Robotics and Autonomous Systems*, vol. 60, no. 10, pp. 1308–1316, 2012.
- [129] J. Pinskiier, B. Shirinzadeh, and L. Clark, "Design & optimization of a compact, large amplification XY flexure-mechanism," *International Conference on Manipulation, Automation and Robotics at Small Scales, MARSS 2017 - Proceedings*, 2017.
- [130] M. N. M. Zubir, B. Shirinzadeh, Y. Tian, M. Nashrul, M. N. M. Zubir, B. Shirinzadeh, and Y. Tian, "Development of a novel flexure-based microgripper for high precision micro-object manipulation," *Sensors and Actuators A: Physical*, vol. 150, pp. 257–266, mar 2009.
- [131] A. M. Hoover, S. Avadhanula, R. E. Groff, and R. S. Fearing, "A rapidly prototyped 2-axis positioning stage for microassembly using large displacement compliant mechanisms," *Proceedings - IEEE International Conference on Robotics and Automation*, vol. 2006, pp. 289–295, 2006.
- [132] R. S. Fearing, R. Sahai, and A. Hoover, "Rapidly Prototyping Millirobots using Toolkits and Microassembly," tech. rep.
- [133] R. L. Henry, "Project Tinkertoy," *Journal of the Franklin Institute*, vol. 256, no. 6, pp. 598–599, 2003.
- [134] R. K. Jurgen, "Whatever happened to project tinkertoy?," *IEEE Spectrum*, vol. 24, no. 5, pp. 20–21, 1987.
- [135] A. Russo, B. Y. Ahn, J. J. Adams, E. B. Duoss, J. T. Bernhard, and J. A. Lewis, "Pen-on-Paper Flexible Electronics," *Advanced Materials*, vol. 23, no. 30, pp. 3426–3430, 2011.

- [136] D. Zhao, T. Liu, J. G. Park, M. Zhang, J.-m. M. Chen, B. Wang, J. Gyu, M. Zhang, J.-m. M. Chen, and B. Wang, “Conductivity enhancement of aerosol-jet printed electronics by using silver nanoparticles ink with carbon nanotubes,” *Microelectronic Engineering*, vol. 96, pp. 71–75, 2012.
- [137] K. Sun, T. S. Wei, B. Y. Ahn, J. Y. Seo, S. J. Dillon, and J. a. Lewis, “3D printing of interdigitated Li-ion microbattery architectures,” *Advanced Materials*, vol. 25, no. 33, pp. 4539–4543, 2013.
- [138] E. Malone, K. Rasa, D. Cohen, T. Isaacson, H. Lashley, and H. Lipson, “Freeform fabrication of zinc-air batteries and electromechanical assemblies,” *Rapid Prototyping Journal*, vol. 10, no. 1, pp. 58–69, 2004.
- [139] J. J. Adams, E. B. Duoss, T. F. Malkowski, M. J. Motala, B. Y. Ahn, R. G. Nuzzo, J. T. Bernhard, and J. a. Lewis, “Conformal printing of electrically small antennas on three-dimensional surfaces.,” *Advanced materials (Deerfield Beach, Fla.)*, vol. 23, pp. 1335–40, mar 2011.
- [140] S. Fuller, E. Wilhelm, and J. Jacobson, “Ink-jet printed nanoparticle microelectromechanical systems,” *Journal of Microelectromechanical Systems*, vol. 11, no. 1, pp. 54–60, 2002.
- [141] G. T. Trinh, D. Cellucci, W. Langford, S. Im, A. G. Luna, and K. C. Cheung, “Modular Rapidly Manufactured Small Satellite (MRMSS),” no. January, pp. 1–11, 2015.
- [142] Voxel8, “Voxel8.” <http://www.voxel8.co/>.
- [143] Microchip, “ATBTLC1000.” <https://www.microchip.com/wwwproducts/en/ATBTLC1000>.
- [144] V. R. Marinov, O. Swenson, Y. Atanasov, and N. Schneck, “Laser-assisted ultrathin bare die packaging: a route to a new class of microelectronic devices,” *Spie*, vol. 8608, pp. 86080L–86080L–19, 2013.
- [145] K. Gilpin, A. Knaian, and D. Rus, “Robot pebbles: One centimeter modules for programmable matter through self-disassembly,” *2010 IEEE International Conference on Robotics and Automation*, pp. 2485–2492, may 2010.
- [146] M. Haurylau, N. A. Nelson, D. H. Albonese, E. G. Friedman, P. M. Fauchet, G. Chen, H. Chen, and J. Zhang, “On-chip optical interconnect roadmap: Challenges and critical directions,” *IEEE Journal on Selected Topics in Quantum Electronics*, vol. 12, no. 6, pp. 1699–1704, 2006.
- [147] A. P. Ghassaei, *Rapid Design and Simulation of Functional Digital Materials by in partial fulfillment of the requirements for the degree of at the by*. Master of science, Massachusetts Institute of Technology, 2016.
- [148] M. Carney and B. Jenett, “Relative Robots: Scaling AUtomed Assembly of Discrete Cellular Lattices,” *Proceedings of the 2016 Manufacturing Science and Engineering Conference*, 2016.
- [149] M. Sitti, *Mobile Micro-Robotics*. Cambridge: MIT Press, 2017.
- [150] J. B. Gafford, S. Member, S. B. Kesner, R. J. Wood, and C. J. Walsh, “Force-Sensing Surgical Grasper Enabled by Pop-Up Book MEMS,” pp. 2552–2558, 2013.

- [151] J. Meijer, K. Du, a. Gillner, D. Hoffmann, V. Kovalenko, T. Masuzawa, a. Ostendorf, R. Poprawe, and W. Schulz, “Laser Machining by short and ultrashort pulses, state of the art and new opportunities in the age of the photons,” *CIRP Annals - Manufacturing Technology*, vol. 51, no. 2, pp. 531–550, 2002.
- [152] L. Harvey, B. Arnold, Z. S Lawrence, I. M. Pau, B. David, and D. James, *Molecular Cell Biology. 4th edition.* 2000.
- [153] W. R. Frontera and J. Ochala, “Skeletal Muscle: A Brief Review of Structure and Function,” *Behavior Genetics*, vol. 45, no. 2, pp. 183–195, 2015.
- [154] L. Cao, A. T. Dolovich, A. L. Schwab, J. L. Herder, and W. C. Zhang, “Toward a Unified Design Approach for Both Compliant Mechanisms and Rigid-Body Mechanisms: Module Optimization,” *Journal of Mechanical Design*, vol. 137, no. 12, p. 122301, 2015.
- [155] W. C. O. Mara, R. B. Herring, and L. P. Hunt, “Handbook of Compliant Mechanisms,”
- [156] M. Jin, X. Zhang, B. Zhu, and X. Z. Jin, Mohui, “A numerical method for static analysis of pseudo-rigid-body model of compliant mechanisms.,” *Proceedings of the Institution of Mechanical Engineers, Part C: Journal of Mechanical Engineering Science*, vol. 228, no. 228, pp. 3170–3177, 2014.
- [157] R. Avilés, M. Goizalde Ajuria, M. Victoria Hormaza, A. Hernández, F. Elements, I. N. Analysis, and A. N. D. Design, “A procedure based on finite elements for the solution of nonlinear problems in the kinematic analysis of mechanisms,” *Finite Elements in Analysis and Design*, vol. 22, no. 4, pp. 305–327, 1996.
- [158] O. Sigmund, “On the Design of Compliant Mechanisms Using Topology Optimization,” *Mechanics Based Design of Structures and Machines*, vol. 25, no. 4, pp. 493–524, 1997.
- [159] T. Lu, C. Ortega, J. Kulick, G. H. Bernstein, S. Ardisson, R. Engelhardt, P. Way, and P. O. Box, “Rapid SoC Prototyping Utilizing Quilt Packaging Technology For Modular Functional IC Partitioning,” *2016 International Symposium on Rapid System Prototyping (RSP)*, pp. 79–85, 2016.
- [160] J. H. Lau, *Fan-Out Wafer-Level Packaging*. Springer Nature Singapore, 2018.
- [161] ZGlue, “zGlue.” <https://www.zglue.com/>.
- [162] A. Olofsson, T. Nordström, and Z. Ul-Abdin, “Kickstarting high-performance energy-efficient manycore architectures with Epiphany,” *Conference Record - Asilomar Conference on Signals, Systems and Computers*, vol. 2015-April, no. May, pp. 1719–1726, 2015.
- [163] A. Olofsson, “Epiphany-V: A 1024 processor 64-bit RISC System-On-Chip,” pp. 1–15, 2016.
- [164] C. E. Leiserson, Z. S. Abuhamdeh, D. C. Douglas, C. R. Feynman, M. N. Ganmukhi, J. V. Hill, W. D. Hillis, B. C. Kuszmaul, M. A. Pierre, D. S. Wells, M. C. Wong-Chan, S. W. Yang, and R. Zak, “The network architecture of the connection machine CM-5,” *Journal of Parallel and Distributed Computing*, vol. 33, no. 2, pp. 145–158, 1996.

- [165] J. R. Heath, P. J. Kuekes, G. S. Snider, and R. S. Williams, "A Defect-Tolerant Computer Architecture : Opportunities for Nanotechnology," vol. 280, no. June, 1998.
- [166] C. E. Shannon, "A symbolic analysis of relay and switching circuits," 1938.